Electronic and Optical Properties of Functionalized Silicon Nanocrystals

by

Kelsey Deutsch

A thesis submitted in partial fulfillment of

the requirements for the degree of

Master of Science

Department of Chemistry

The University of Alberta

Abstract

Silicon nanocrystals (SiNCs) have unique properties manifested at nanometer dimensions. The optoelectronic properties of silicon nanocrystals depend on size and surface chemistry. Investigation into the electronic and optical nature of SiNCs can facilitate the synthesis of efficient optical and electronic devices. In studying the electronic nature of SiNCs, the functionalization of SiNCs with electroactive end groups is of interest. Successful functionalization of silicon nanocrystals with an electroactive ligand, ferrocene, was achieved and the resulting material was fully characterized. Electronic interaction between the SiNC and ferrocene occurs *via* an electron transfer mechanism. This is the first example of freestanding SiNCs functionalized with ferrocene.

Photostability of SiNC photoluminescence (PL) is a limitation in the development of efficient devices and bioimaging applications. The photostability of SiNCs with a series of surface ligands was studied due to strong influence of surface chemistry on SiNC optoelectronic properties. Investigation of a series of surface functionalized SiNCs under photobleaching condition revealed that the effect of oxygen has a greater influence on PL stability than the surface group functionalized.

Preface

This thesis is an original work by the author containing results from collaborative studies. STS and STM imaging studies where performed by Dr. Doron Azulay and Prof. Oded Millo. Samples SiNC-A, SiNC-B, SiNC-C and SiNC-D3 were synthesized by Dr. Md Hosnay Mobarok.

Dedication

To all of those who have helped me along the way.

Acknowledgements

I could not have completed this program without the support and encouragement from so many people along the way. My sincerest thank you to my supervisor Dr. Jon Veinot. Your constant guidance, support and patience made this all possible. The opportunities and freedom you provided me were unimaginable and I am continuously grateful. I wish to thank my supervisory committee, Dr. Arthur Mar and Dr. Micheal Serpe, have also provided valuable insight. Thank you to Prof. Millo Oded for your insight as well. Thank you to Dr. Al Meldrum for sharing your equipment and your expertise. As well, I would not have been able to complete my work without the technical and academic support from all the wonderful members of the Chemistry department.

I would like to thank all of the Veinot group members. All of you have helped me learn something new and my time with you has been unforgettable. Particularly, I would like to thank Dr. Hosnay Maborak and Dr. Tapas Purkait for their patience in answering so many of my questions. Christina and Regina, thank you both for your friendship and support.

To my family, my parents, Mom and Dad and Clayton and Pauline. You have all given me so much. Your love and support has been endless. Thank you. And lastly, to my husband Jared. You always believed in me.

Table of Contents

Table of Figures

List of Schemes

List of Tables

List of Symbols and Abbreviations

℃ – Degrees Celsius

AIBN – 2,2’-Azobis(2-methylpropionitrile)

atm – Atmospheric pressure

CDCl3 – chloroform-d

Cp – Cyclopentyldiene

CV – Cyclic voltammetry

DCM – Dichloromethane

DOS – Density of states

eV – Electron volts

EMA – Effective mass approximation

ESR – Electron spin resonance

FTIR – Fourier transform infrared spectroscopy

HSQ – Hydrogen silsesquioxane

HEBM – High energy ball milling

HF – Hydrofluoric acid

IR – Infrared

LED – Light emitting diode

NC – Nanocrystal

NMR – Nuclear magnetic resonance spectroscopy

PL – Photoluminescence

PTFE – Polytetrafluoroethylene

QD – Quantum dot

SiNC – Silicon nanocrystal

SiNC-A – Alkoxy functionalized silicon nanocrystals sample

SiNC-B – Perfluoro functionalized silicon nanocrystals sample

SiNC-C – Pentyl functionalized silicon nanocrystals sample

SiNC-D1 – Oxidized dodecyl functionalized silicon nanocrystals sample 1

SiNC-D2 – Partially oxidized dodecyl functionalized silicon nanocrystals sample 2

SiNC-D3 – Minimally oxidized dodecyl functionalized silicon nanocrystals sample 3

STM – Scanning tunneling microscopy

STS – Scanning tunneling spectroscopy

TBAHFP – Tetrabutylammonium hexafluorophospate

TEOS – Tetraethyl orthosilicate

TEM – Transmission electron microscopy

TGA – Thermogravimetric analysis

THF – Tetrahydrofuran

TMS – Tetramethylsilane

TOAB – Tetraoctylammonium bromide

TOPO – Trioctylphosphine oxide

UV – Ultraviolet

XPS – X-ray photoelectron spectroscopy

Chapter 1 Introduction to Nanomaterials and Quantum Dots

1.1 Nanomaterials

Over the last three decades, materials with nanometer size dimensions has gained attention because of their unique properties that arise by decreasing the dimensional size and are not exhibited by the bulk material of the same material type. Nanotechnology is the study of these properties and corresponding materials with at least one dimension smaller than 100 nm in size. Some of these properties include changes in optical,[1,2] electronic,[3,4] magnetic,[5] and mechanical properties.[6] Nanomaterials are potential candidates for use in numerous applications including optical and electronic devices[7,8] photovoltaics,[9] therapeutics,[10,11] and bio-imaging.[12]

1.2 Semiconductor Quantum Dots

Semiconductor nanoparticles, or quantum dots (QD) are an important class of nanomaterials because of their optical and electronic properties. QDs can be based upon numerous semiconductors. II-VI (e.g., CdSe),[13] III-V (e.g., GaAs, InP),[14,15] IV (e.g., Si, Ge),[16,17] IV-VI (e.g., SnS, PbSe)[18,19] and tertiary semiconductors (e.g., AlGaN, $AgInS_2$)[20,21] are among those that have been investigated. Potential applications of QDs cover a wide range from light-emitting diodes (LEDs),[7] photovoltaics,[22] field effect transitiors,[23] to bioimaging,[24] and sensing.[25] The optoelectronic properties of QDs can be controlled by designing the size and shape of the particle making them ideal candidates for the above mentioned applications.[26]

1.2.1 Quantum Dots and Quantum Confinement

Inorganic quantum dots were first discovered by Louis Brus.[27,28] The emergence of size-dependent photoluminescence (PL) in semiconductor crystallites such as CdSe, ZnO, and InSb, sparked immense interest in the application and understanding of these new materials. Fig 1.1 shows the dependence of PL on the particle size of CdSe QDs arising from quantum confinement effects.[26]

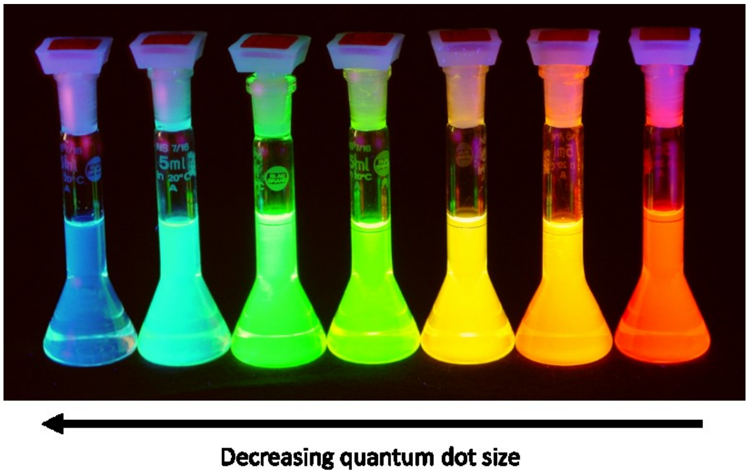

Fig 1.1 Size dependent PL from CdSe QDs. The size of the QD decreases right to left from 6 nm (orange) to 2 nm (blue). Reprinted with permission from Dr. Horst Weller.

Quantum confinement arises from the decrease in the dimensional size of a semiconducting material. Reduction of the particle dimensions close to the bulk exciton Bohr radius[i] confines electron and hole wave functions to an infinite potential well, increasing the probability of radiative emission.[28] As the size of the particle decreases, the removal of orbitals from the band edges creates discrete energy levels within the band structure of the quantum dot and increases the band gap.[29] Hence, the size of the QD controls the size of the band gap and the

---

[i] The exciton Bohr radius is the distance between an excited electron hole pair, or exciton.[175]

gap and the PL wavelength. The opening of the band gap as a function of dimensional size of a semiconductor is depicted in Fig 1.2. This discretized band structure has earned QDs the name "artificial atom" as QDs bridge the gap between atoms and bulk materials.

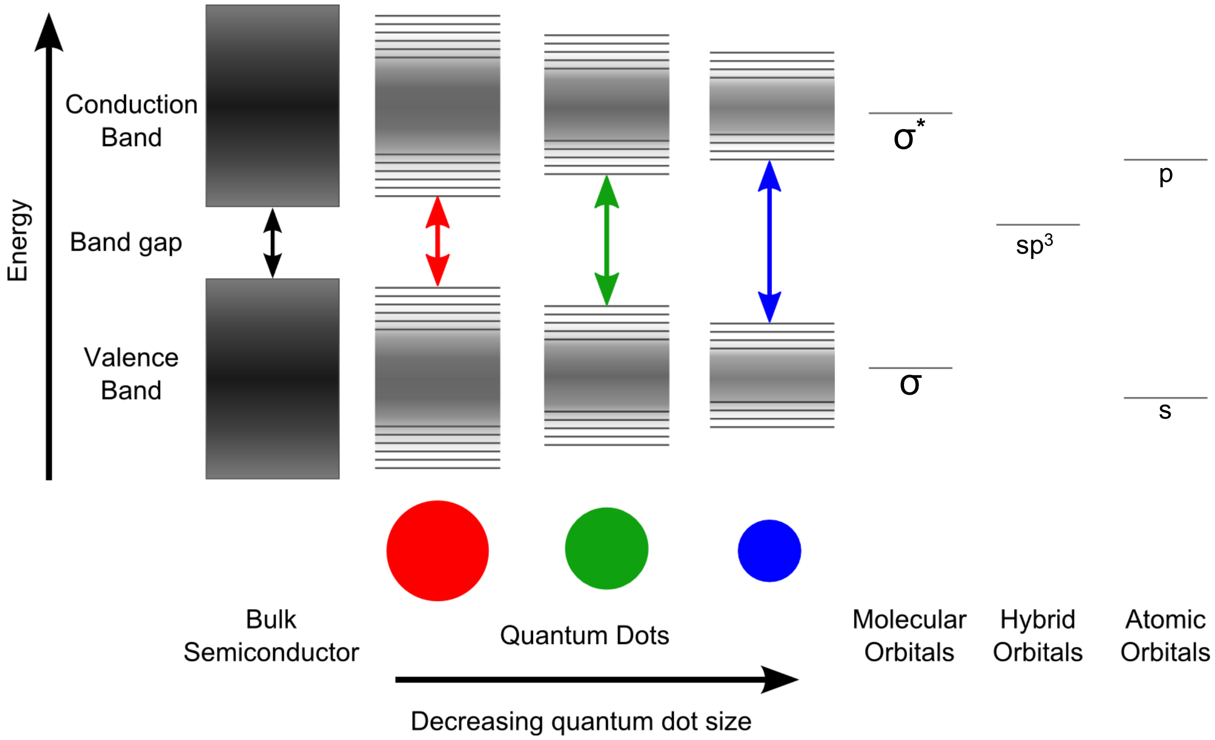

Fig 1.2. Schematic representation of the density of states (DOS) of semiconductors, QDs and molecular and atomic orbitals. Removal of orbitals discretizes the energy levels in the quantum dot and increases the band gap. Increasing the band gap in QDs results in emission of higher energy wavelengths.

1.2.2 The Effective Mass Approximation

Models have been introduced to further understand the phenomena associated with quantum confinement in QDs. Notably, the effective mass approximation (EMA) was first introduced by Efros to predict the opening of the band gap by reducing the size of semiconductor particles.[30] Further refinement of the EMA model provides a reasonable correlation between the size of the particle and the observed photoluminescence energy (E_n).[31,32] The EMA (Eq. 1.1) takes into account the confinement energy of the exciton, the exciton coulomb interaction energy, and the band gap of the bulk material, $E_{g.}$ The observed PL is inversely proportional to the square of the QD diameter (d^2). In Eqn 1.1, the effective masses of the electron and hole are m_e^* and are m_h^* respectively. The elementary charge is e and h is Planck's constant. In Eqn 1.2, m_0 is free electron mass, R is the Rydberg constant, ε is the dielectric constant of the semiconductor.

$$E_n = E_g + \frac{h^2\pi^2}{2d^2}\left(\frac{1}{m_e^*} + \frac{1}{m_h^*}\right) - \frac{1.786e^2}{\varepsilon R} + 0.284E_R \qquad \text{Eqn 1.1}$$

$$E_R = \frac{13.56\, m_0}{\varepsilon^2\left(\left(\frac{1}{m_e^*}\right)+\left(\frac{1}{m_e^*}\right)\right)}\ \text{eV} \qquad \text{Eqn 1.2}$$

1.3 Silicon Nanocrystals

Silicon is the most widely used semiconductor in the microelectronics industry and a promising material that can exhibit size dependent PL due to quantum confinement.[33,34] Silicon QDs, also referred to as silicon nanocrystals (SiNCs), offer an advantage over other QDs because of their biocompatibility.[35–37] The optoelectronic properties, facile tailoring of surface chemistry, and biocompatibility also make silicon QDs strong candidates for use in applications such as LEDs,[38–40] photovoltaics,[41] bioimaging,[37,42] and sensors,[43,44] among others.[45,46]

One of the earliest observations of luminescence in nanocrystalline silicon was reported in porous silicon wafers.[47] Electrochemical etching of silicon wafers with hydrofluoric acid (HF) resulted in a porous structure. Red PL was observed under ultraviolet (UV) illumination and the PL of the porous silicon shifted from the infrared (IR) to visible wavelengths with an increase in the etching time of the wafer.[47] Etching of the wafers retained the crystallinity of the bulk silicon but reduced size of the single crystalline domains within the silicon network.[48] Quantum confinement was proposed by the authors to be the mechanism of the observed shift in PL.

1.3.1 Quantum Confinement in Silicon Nanocrystals

Despite similarities between compound semiconductor (e.g., CdSe) and silicon QDs, SiNCs differ in that the band structure of silicon possesses an indirect band gap.[49] In direct band gap semiconductors such as CdSe, the lowest energy level of the conduction band lies directly above the highest energy level of the valence band in k-space (i.e., reciprocal space) as shown in Fig 1.3a. In the case of indirect band gap materials such as silicon, there is an offset in k-space between the lowest point of the conduction band and highest point of the valence band as shown in Fig 1.3b. In order for a vertical electronic transition to occur, momentum must be conserved. In bulk silicon, phonons are required to conserve electron momentum in excitation/relaxation transitions that result in radiative recombination.[50] The probability of a phonon assisted transition is low and as a result bulk silicon is an inefficient light emitter and has very limited photonic applications.

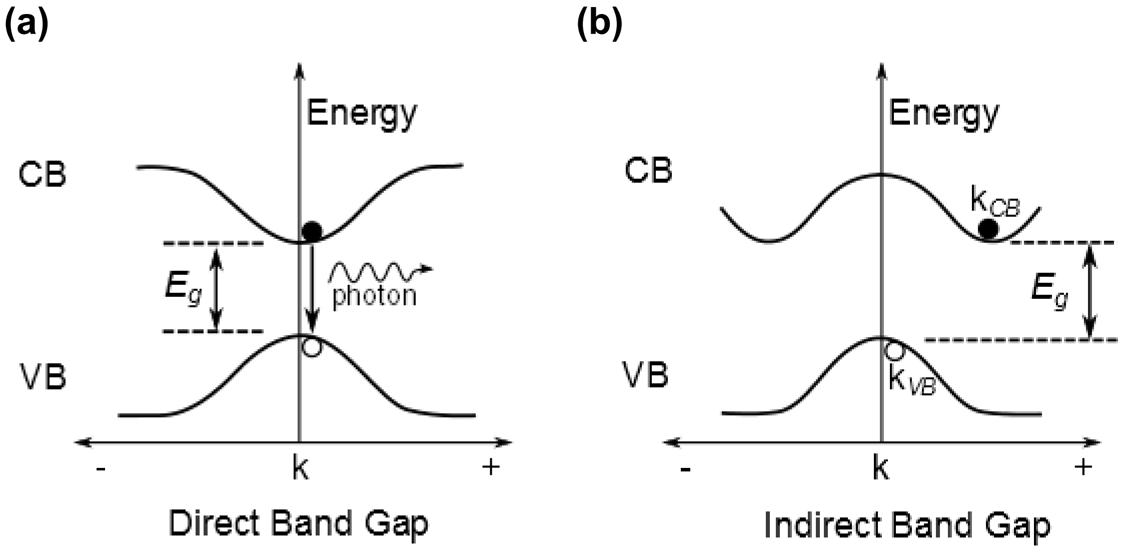

Fig 1.3. Band structure of (a) direct and (b) indirect semiconducting materials.

It has been proposed that in SiNCs the confinement of the wave functions occurs when particles approach the dimensions of the exciton Bohr radius in bulk silicon (i.e., 4.3 nm)[51] and it causes the superposition of the wave functions in a way otherwise not possible in the bulk material.[33] The probability of radiative recombination increases due to the overlap of the exciton wave function[40] and bright size-dependent photoluminescence is observed.[33] The band gap of the nanocrystal is also increased as a result of the decrease in particles size (Fig 1.4), consistent with other QDs.

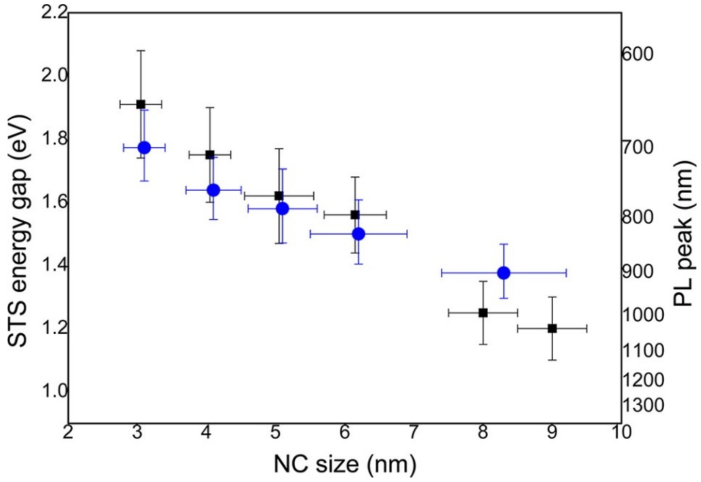

Fig 1.4 Scanning Tunneling Spectroscopy (STS) and PL measurements of SiNCs from approximately 9 nm to 3 nm. The blue circles correspond to the PL maxim while the black square correspond to the STS energy gap. The markers have been slightly offset for clarity. The STS band gap of the SiNC increases as the size decreases. Reprinted with permission from Nano Lett., 2013, 13, 2516. Copyright 2013 American Chemical Society.

1.3.2 Synthetic Approaches

Nanomaterial properties are strongly influenced by the size and shape of the material. As a result, synthetic methods that produced highly uniform shapes and monodisperse sizes are desired as these methods provide greater control over the resulting nanomaterial properties. The approaches to prepare nanomaterials generally fall into one of two broad categories: top-down or bottom-up. Top-down approaches rely on the reduction of the dimensions of a bulk material to nano-regime. In contrast, bottom-up methods start with molecular precursors and the size is incrementally increased to the target dimensions. Both top-down and bottom-up methods have been used to produce SiNCs. Electrochemical etching and high-energy ball milling (HEMB) of bulk silicon to produce nanocrystalline materials are examples of top down methods. Bottom-up methods include solution-based synthetic routes, gas phase decompositions and solid-state pyrolysis.

1.3.3 Synthesis of Silicon Nanocrystals from High Energy Ball Milling

Top-down synthesis of freestanding SiNCs has been demonstrated with HEMB of bulk silicon.[52] Bulk silicon fragments (ca. ~ 1 mm) were loaded into a vial with an alkyne and steel ball bearings. Subsequent HEMB reduces the silicon to nanoscale dimensions and functionalizes the particles in situ with the corresponding alkyne. No size distribution analysis was provided by the authors, but the resulting particles were 5-10 nm with the majority of the particles 4 nm in size.[52]

1.3.4 Synthesis of Silicon Nanocrystals by Electrochemical Etching

The electrochemical etching of silicon by Canham in the 1990s is an example of reducing the dimensions of bulk silicon to create particles of nanoscale lengths.[47] The interested reader is referred to a number of recent publications for further information.[53,54] However, electrochemical etching of silicon wafers followed by sonication produces freestanding particles.[55,56] This method often produced multiple nanocrystals embedded in an amorphous matrix.[55]

1.3.5 Solution Phase Syntheses of Silicon Nanocrystals

Solution-based syntheses of SiNCs are key examples of bottom-up preparations. The most notable solution based methods involve the reduction of silane precursors in various solvents using reactive reducing agents. In 1992, Heath demonstrated the reduction of silane precursors at high temperature (385℃) and pressure (> 100 atm) for several days to afford crystalline silicon (Scheme 1.1).[57] This method produced a large size distribution and the surface of the SiNCs was determined to be hydride, chloride and oxide terminated using IR spectroscopy. The conditions (i.e. high temperature and pressure) used by Heath were approximated via the localized heating in the sonochemical reduction of tetraethyl orthosilicate (TEOS) by colloidal sodium in toluene at -70℃.[58] The resulting product was annealed at 400℃ under inert atmosphere to produce ethoxy-terminated SiNCs between 2-5 nm with a PL maximum of 680 nm.

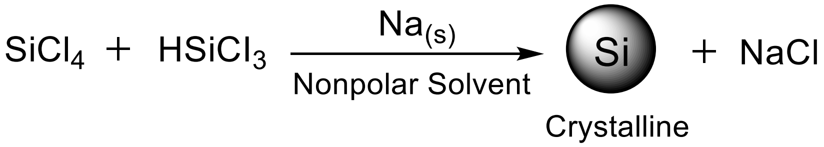

Scheme 1.1 Solution based synthesis of SiNCs used by Heath.

Various reducing agents have been investigated for solution phase methods. Sodium napthalide can also be used to reduce silicon tetrachloride ($SiCl_4$) in a dimethoxyethane (glyme) solution to produce SiNC with an average diameter of 5.2 ±1.9 nm.[59] The SiNCs produced from this method may be alkoxy terminated with further reaction with octanol. Variation of the solution based approach using inverse micelles as a templating agent for the reduction reaction offered greater control of the size distribution of nanocrystals (NCs) produced. Reduction of $SiCl_4$ using lithium aluminum hydride ($LiAlH_4$) with tetraoctylammonium bromide (TOAB) as a templating agent in toluene resulted in hydride terminated SiNCs with an average size of 1.8 nm and standard deviation of only 0.2 nm.[60]

Other modifications of solution-based methods include the use of reactive Zintl salts as the reducing agent of choice.[61,62] Group 1 or 2 elements combine with main group metals or metalloids to form Zintl salts. SiNCs produced *via* Zintl salts and $SiCl_4$ are presumed to be chloride terminated (Scheme 1.2a) and can be alkoxy terminated with further reaction with alcohols.[63] Other reactions of Zintl salts include the reaction of ammonium bromide with NaSi to afford hydride terminated SiNCs 4.91 ± 1.23 nm in diameter (Scheme 1.2b).[64] This method also afforded tens of milligram quantities (0.016 g) of SiNCs. Zintl salts offer a straightforward method of producing freestanding SiNCs. However SiNCs produced by Zintl salts and solution phase reduction reactions are characterized by large particle size distributions[59] and only show size-independent blue luminescence (vide infra).[65]

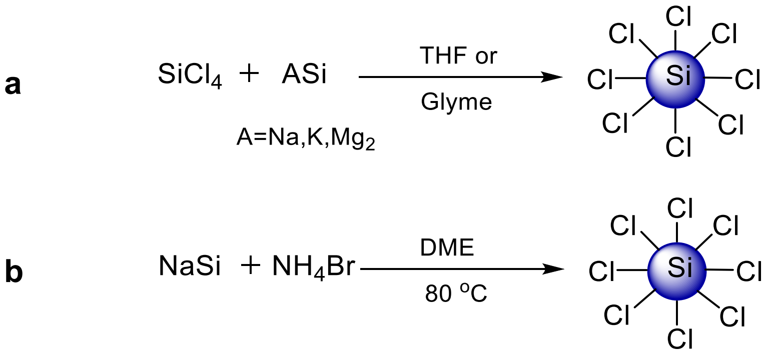

Scheme 1.2. Solution phase reduction of $SiCl_4$ with Zintl salts to produce chloride-terminated SiNCs.

An alternative approach to SiNCs involving solution phase thermal decomposition of silicon precursors was introduced by Holmes *et al*.[66] Decomposition of the diphenylsilane precursors in supercritical hexane with a capping agent above 500℃ and 345 bar was used to prepare SiNCs. The reaction is thought to proceed by a radical decomposition mechanism stabilized by the phenyl groups on the silicon, which are eventually replaced by the octanol capping ligand.[66] The size of particles could be varied by adjusting the octanol:diphenylsilane ratio in supercritical hexane but also resulted in a polydisperse size distribution. Monodisperse, *in situ* functionalized SiNCs of 1.5 nm diameter can be produced in pure supercritical octanol.[66]

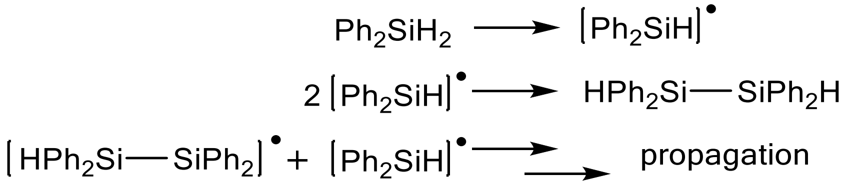

Scheme 1.3 Radical decomposition of diphenyl silane in supercritical solvent.

1.3.6 Gas Phase Decomposition Syntheses of Silicon Nanocrystals

Decomposition of silane precursors in the gas phase also produces SiNCs. The method was first demonstrated by Murthy *et al*. who observed 30 – 80 nm nanoparticles produced above 1100℃ with a critical silane concentration of 0.2 vol. %.[67] The particles were not uniform in shape showing octahedral, tetrahedral or truncated triangular bipyramidal shapes. Further modification showed that thermal gas phase decomposition of gaseous disilane can produce SiNCs with a highly uniform oxide shell.[68] Size selection methods can be used to produce monodisperse fractions of various sizes.[33] Other variations of gas phase synthesis include CO_2 laser induced pyrolysis of silane gas (Fig 1.5) followed by etching with HF to yield macroscopic quantities of luminescent SiNCs.[69]

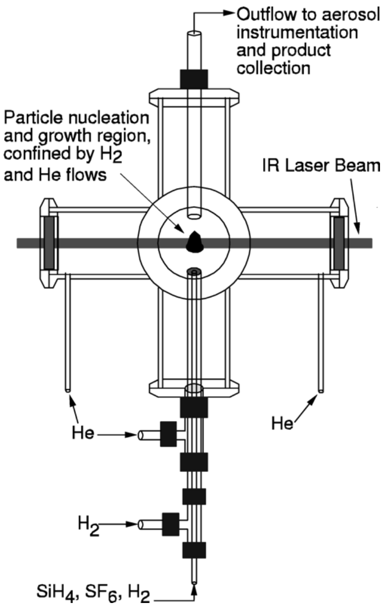

Fig 1.5 Schematic diagram of CO_2 laser pyrolysis experimental set up. SiF_6 is added as a photosensitizer in the pyrolysis reaction. Reprinted with permission from Langmuir, 2003, 19, 8490. Copyright 2003 American Chemical Society.

A low pressure non-thermal plasma variant has also been used to produce luminescent silicon nanoparticles via electron impact dissociation of silane gas.[70] Plasma produced SiNCs were shown to have a narrow size distribution and exhibited size dependent PL after exposure to air. This method could also produce large quantities of material in a relatively short time frame (up to 52 mg/hr). *In-situ* functionalization of the NCs can also be utilized with this method.[71]

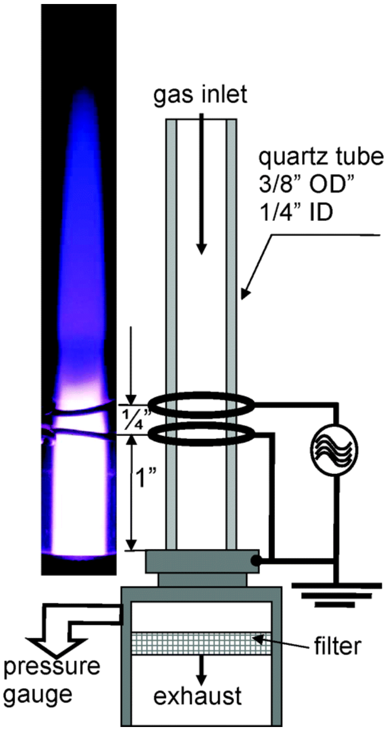

Fig 1.6 Schematic diagram experimental set up for plasma synthesis of SiNCs. NCs are formed in the plasma and collected on the exhaust filter. Reprinted with permission from Nano. Lett. 2005, 5, 655. Copyright 2005 American Chemical Society.

1.3.7 Synthesis of Silicon Nanocrystals by Solid Precursor Decomposition

A number of methods that rely on solid precursor decomposition have been developed as well. Thermal annealing of silicon rich oxides have resulted in the formation of crystalline silicon in a silicon-oxide matrix.[72] Notably, hydrogen silsesquioxane (HSQ) decomposition at 1100 ˚C in a reducing atmosphere results in SiNCs embedded in an oxide matrix (Scheme 1.4).[73] It is has been proposed that rearrangement of the HSQ cage structure is followed by loss and decomposition of silane ca. 450℃ to form amorphous silicon clusters.[74] Crystallization and growth of the silicon domains occurs at 1100℃. Etching with HF leads to the formation of freestanding, hydride-terminated SiNCs with size dependent PL. The size of the SiNCs, and therefore wavelength of PL, can be altered by adjusting the synthetic parameters (i.e., processing temperature,[74] and etching time,[73]; Fig 1.7).

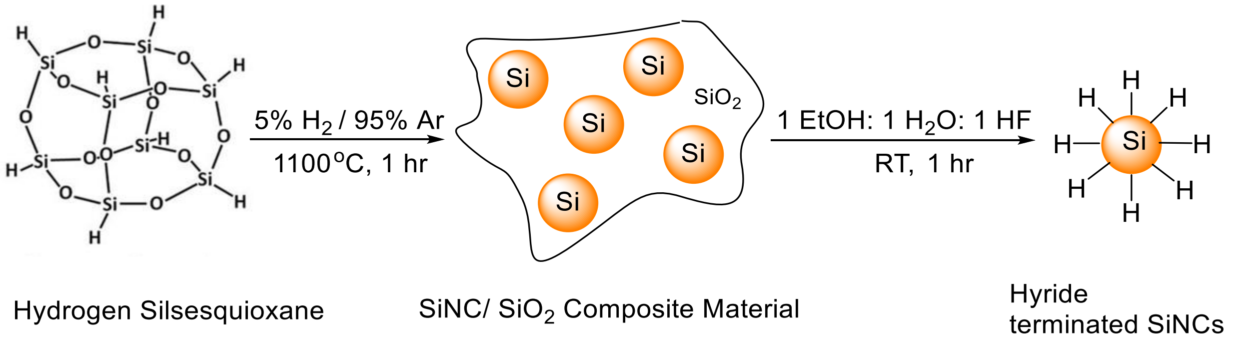

Scheme 1.4 Synthesis of SiNCs by thermal decomposition of HSQ followed by etching to produce freestanding hydride terminated photoluminescent SiNCs.

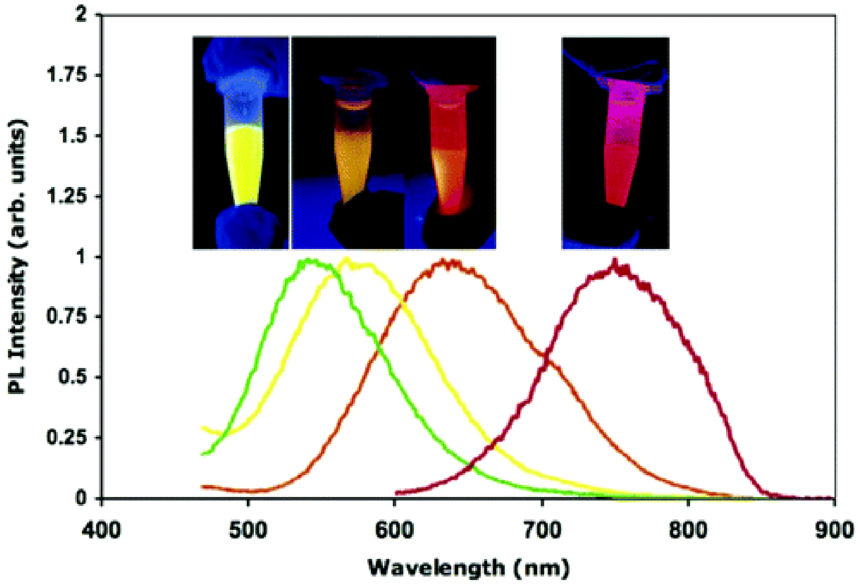

Fig 1.7 Effect of HF etching time of SiNC PL from HSQ. The etching time was increased from 50 minutes (red) to 135 minutes (green). Reprinted with permission from Chem. Mater. 2006, 18, 6139. Copyright 2006 American Chemical Society.

Similarly, co-sputtering of silicon and SiO_2 followed by grinding and annealing at 1150℃ can also produce freestanding SiNCs after HF etching.[75] The addition of phosphorous and boron during the co-sputtering procedure leads to co-doped SiNCs that are stable in methanol without further surface functionalization.[76] SiNCs with a mean diameter of 3.0 ± 0.9 nm can be obtained by the co-doping method. [77] SiNCs produced by the co-doping method emit in the near IR.

1.3.8 Silicon Nanocrystal Surface Chemistry

It is necessary to derivatize the surface of SiNCs to prevent unwanted reactions, agglomeration and degradation of optical properties that can occur.[78] A number of reviews have been published detailing the surface functionalization of SiNCs;[65,79,80] functionalization methods for SiNCs will be discussed briefly herein. The functionalization of silicon nanocrystals follows after the well-developed molecular and wafer chemistry and these are just a few of the many functionalization pathways for SiNCs.[80] Hydride-terminated surfaces can be modified with alkenes and alkynes via hydrosilylation reactions typical of silicon wafers and porous silicon (Scheme 1.5).[81] Thermal,[82] photochemical,[83] radical[84] and transition metal catalyst initiated[85] hydrosilylation reactions have been realized on nanocrystalline silicon. Room temperature hydrosilylation reactions initiated by Lewis acids[86] and diazonmiun salts[87] have also been demonstrated with SiNCs and can be relatively fast compared to thermal methods.

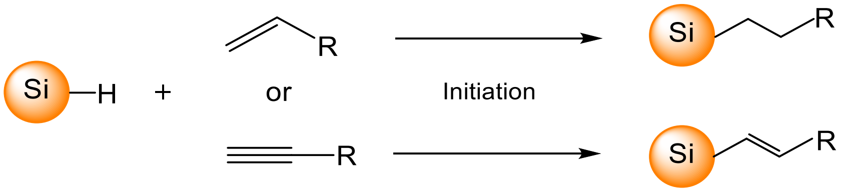

Scheme 1.5 Hydrosilylation of hydride terminated SiNCs with alkenes and alkyenes.

The reactivity of hydride-terminated surfaces can also allow for the direct reaction of surface ligands. Direct reaction of surface ligands to form Si-N bonds have been observed[88] as well as direct reaction with trioctylphosphine oxide (TOPO) and CO_2 under high pressure conditions.[89] Alkyllithium reagents have been shown to react with hydride-terminated SiNCs by breaking Si-Si surface bonds allowing for functionalization of aryl groups to the SiNC surface.[90] Because this method targets the Si-Si surface bond, mixed surfaces can be realized with additional hydrosilylation steps.

Halide-terminated surfaces can also be obtained by reaction of hydride surfaces with halogenating agents (Scheme 1.6). [91] Halide-terminated surfaces provide a convenient platform for further surface modification through alkyl lithium or Grignard reagents.[62] Alkoxy terminated surfaces have also been obtained from chloride terminated SiNC through direct reaction with alcohols as demonstrated by the Kauzalrich group.[61] Overall, the different SiNC surface chemistries (i.e. hydride-terminated or halide-terminated) and functionalization methods available has increased the accessibility of ligands and terminal SiNC surface chemistries that can be realized.

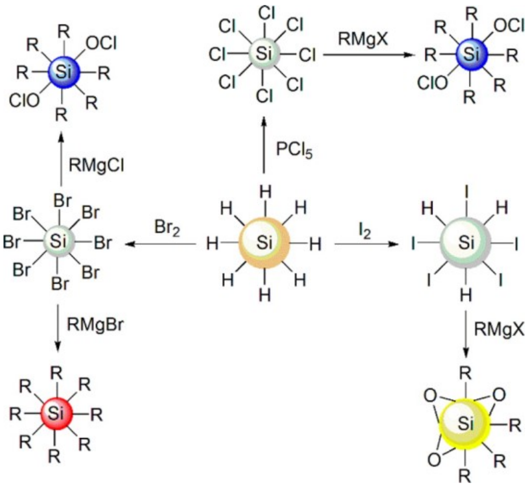

Scheme 1.6 Halide terminated surfaces derived from hydride terminated SiNCS followed by Grignard reactions. The colour of the SiNC also corresponds to the resulting PL reflecting the influence of the halide on SiNC optical properties. Reprinted with permission from Chem. Mater. 27, 2015, 1153. Copyright 2015 American Chemical Society.

1.3.9 Optical Properties of Silicon Nanocrystals

The tight binding model introduced by Delerue *et al.* provides a better correlation between the observed PL and the SiNC size than the EMA noted above.[92] The band gap emission is proportional to the inverse of the nanocrystal diameter (d) to the power of 1.39. The energy of the band gap is calculated for hydride-terminated SiNCs by Eq 1.3. The bulk silicon band gap is represented by E_g.

$$E_n = E_g + \frac{3.73}{d^{1.39}} \text{ eV} \qquad \text{Eq 1.3}$$

Despite agreement with theoretical models, the origin of PL from nanocrystalline silicon is not fully understood.[93] The onset of PL in SiNCs is still attributed to quantum confinement, but other observations of size independent PL from SiNCs do not follow theoretical predictions.[59] Interfacial regions and defects have been implicated as the dominant source of size independent SiNC PL.[94,95]

Size independent and temperature dependent PL has been attributed to an interfacial trapping state responsible for the SiNC PL.[94] A size independent emission of 1.65 eV was observed in SiO_2 embedded SiNC. It was proposed by the authors that the exciton is confined to a suboxide shell between the silicon core and an amorphous SiO_2 layer. Recombination of the exciton in the interfacial region accounted for the emission independent of SiNC core diameter.

Other interfacial surface states have also been suggested as the source of PL from porous silicon.[95] Surface states act as photoexcited carrier traps at energies between the formal bandgap of the SiNC. Emission could occur between both trapped carriers, between a trapped carrier and a free carrier, or between two free carriers. Blue PL from SiO_2 embedded SiNCs was attributed to recombination of two free carriers.

Experiments on porous silicon by Wolkin *et al.* provided insight into the role of surface oxide defects.[96] The authors proposed that oxygen created a surface state and would have one of three effects on the emission mechanism of SiNCs depending on the size of the particle. Larger particles would be largely unaffected and would emit via quantum confinement and free excitons depicted in zone I of Fig 1.8. Intermediate particles emission would be from a trapped electron and a free hole (zone II in Fig 1.8). For the smallest blue emitting particles, exposure to oxygen created a stabilized Si=O surface state that traps the exciton resulting in a red-shift of the initial PL (zone III, Fig 1.8). This remains to be a very a controversial proposal as silicon oxygen double bonds on SiNCs require large amounts of stabilization.[97] However, computational studies on hydride terminated SiNCs support double bonded species like Si=O being the predominate red-shifting source for the band gap.[98,99] Although the exact nature of the surface states on silicon nanoparticles has not been conclusively determined, oxidation of particles play a critical role in SiNC PL properties.

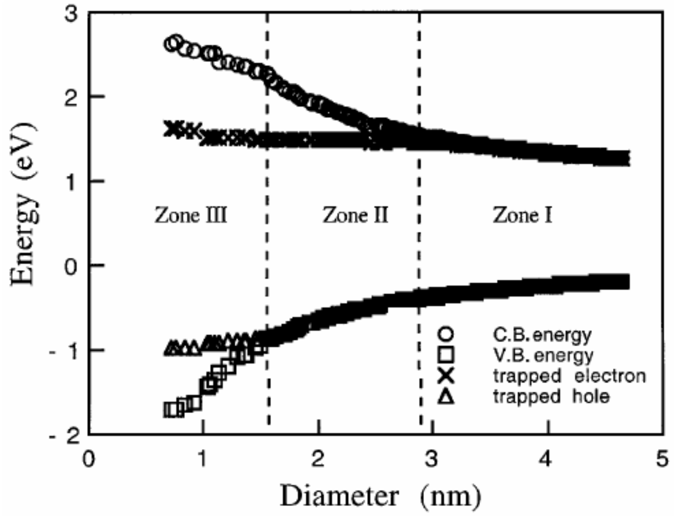

Fig 1.8. PL energy trap states for oxidized porous silicon of various sizes. The zones indicate the trapped carrier(s) and resulting band gap energy. Reprinted Fig 3 with permission from Wolkin, M. V.; Jorne, J.; Fauchet, P. M.; Allan, G.; Delerue, C. Phys. Rev. Lett. 82, 197, 1999. Copyright 1999 American Physical Society.

Surface ligands can also impact the resulting optoelectronic properties of SiNCs.[78,89,100,101] Dasog showed that the colour of the PL can be tuned via surface groups across the visible spectrum independent of the SiNC size.[89] Fig 1.9 displays the PL and surface groups of the SiNCs. Ligand-oxide surface species were implicated as the major source of size independent PL. This was determined to the origin of the size independent blue PL observed from SiNCs produced via solution phase synthesis.[88] Conjugated surface ligands can also induce "in gap" states within the band structure of the SiNCs.[102,103] Relaxation through the in gap states can cause shifting of the PL as demonstrated by the functionalization of phenylacetylene to SiNCs.[103] Surface chemistry no doubt plays a critical role in the complex optoelectronic properties of SiNCs.

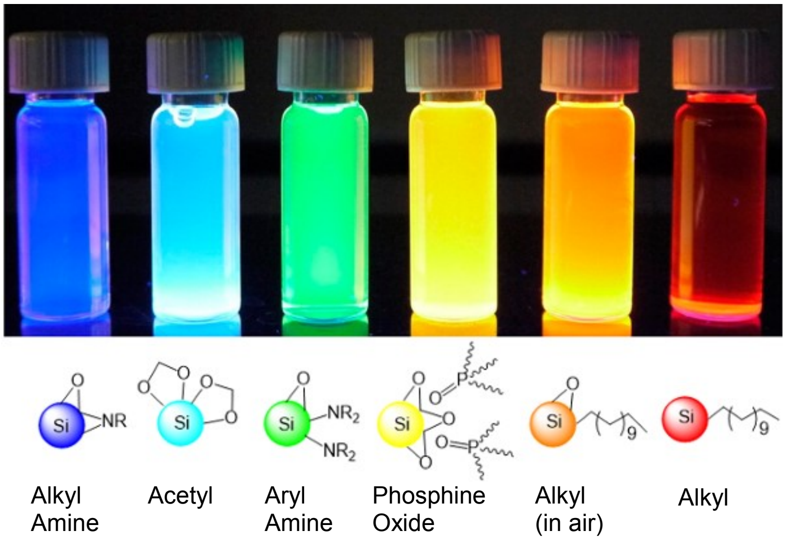

Fig 1.9. Size independent PL from functionalized SiNCs. Adapted with permission from ACS Nano, 2014, 8, 9636. Copyright 2014 American Chemical Society.

1.4 Functionalization of Nanomaterials with Electroactive End Groups

Surface passivation of SiNCs has so far focused mainly on “innocent” surface ligands despite the observation that the optoelectronic properties of SiNCs are sensitive to surface chemistry. Functionalization of bulk silicon with “non-innocent” ligands has been studied extensively, ferrocene being one of the most notable.[104,105] No reports of freestanding SiNCs functionalized with ferrocene exist, although a number of other nanomaterials have been functionalized with ferrocene. P-type porous silicon has been functionalized with ferrocene via thermal hydrosilylation.[82] Cyclic voltammetry (CV) measurements of the resulting materials showed an oxidation peak with a reduced cathodic peak for the ferrocene moiety functionalized to porous silicon. The authors propose that the oxidized ferrocene (ferrocenium ion) is able to inject holes into isolated silicon crystallites in the porous silicon thereby being reduced back to ferrocene and simultaneously oxidizing the silicon. Quenching of porous silicon PL by ferrocene, although not covalently bound, has been reported indicating electronic interaction between ferrocene and the nanocrystalline substrate.[106] CdSe/ZnS QDs were also functionalized with ferrocene via a ligand exchange reaction.[107] Comparison of the original QDs and ferrocene functionalized QDs via CV showed the evolution a new peak associated with the oxidation of ferrocene attached to functionalized particles. No reduction peak for ferrocene was reported. Other nanomaterials based on carbon nanoparticles and nanofibers have also been interfaced with ferrocene moieties via click reactions.[108,109]

1.5 Silicon Nanocrystal Photostability

Apart from SiNC surface chemistry, oxygen and UV exposure are known to impact SiNC optical properties. Photostability of SiNCs is crucial to the development of efficient optoelectronic devices.[110] Despite SiNCs superiority over fluorescent dyes in imaging applications, there are still limitations. SiNCs, for example, are susceptible to PL degradation because of oxidation as well as photobleaching under intense UV irradiation.

Oxidation in ambient conditions is most commonly associated with a decline in desirable PL properties of SiNCs. Alkyl functionalized SiNCs exposed to oxygen often show a decrease in absolute quantum yield that can be accompanied by a blue-shift of the PL maximum.[111] The blue shift is associated with a decrease in the crystalline core of the particles cause by surface oxidation.[112] Red shifting of the PL has also been attributed to creation of trap states due to oxidation of particles.[96] Electron spin resonance (ESR) studies indicate the oxidation of hydride terminated SiNCs in air can occur via the Cabrera-Mott mechanism (Fig 1.10).[113] In the Cabrera-Mott process, adsorption of water molecules to surface silanol bonds facilitates the breaking of Si-Si bonds accommodating the insertion of a negatively charged oxygen molecule to form two Si-O-Si bonds.[114]

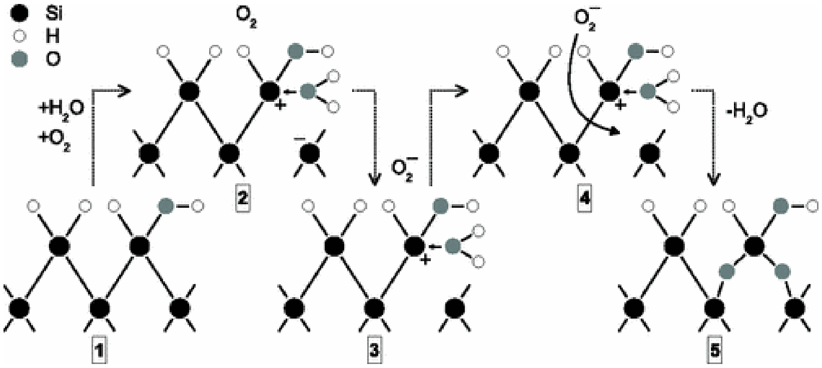

Fig 1.10 Cabrera Mott mechanism of silicon oxidation in the presence of water and oxygen molecules. Reprinted Fig 6 with permission from Pereira, R. N.; Rowe, D. J.; Anthony, R. J.; Kortshagen, U. Phys. Rev. B, 83, 155327, 2011. Copyright 2011, American Physical Society.

The oxidation process of nanocrystalline silicon can be enhanced under a number of conditions. Without stimulation, pure molecular oxygen showed no more effect than an initial PL intensity decrease from UV illumination under a nitrogen atmosphere.[115] However, UV illumination under an oxygen atmosphere showed a dramatic decrease in PL intensity of porous silicon.[115] High temperatures [101] and extended exposure[116] to oxygen can also accelerate the oxidative change and PL degeneration of nanocrystalline silicon.

Aside from oxidation, UV illumination has been shown to degrade the PL from SiNCs.[117,118] ESR experiments have indicated that extended UV irradiation can introduce surface defects capable of quenching of PL from passivated SiNCs.[119] These defects may arise from the breaking of unfunctionalized Si-Si bonds or Si-H bonds on surface passivated SiNCs resulting in non-radiative traps, also known as D defects, affecting the PL stability of the particles.[110] Si-H bonds are also homolytically cleaved during the photoactivation of silicon surfaces during light mediated hydrosilylation reactions.[120,121] Amorphous silicon properties are also affected by extended light exposure, known as the Staebler Wronski effect, which reduces conductivity of amorphous silicon but can be reversed with heat treatment.[122] Recently Wu and coworkers showed that the PL degradation due to photobleaching of alkyl functionalized SiNCs could be recovered with a second hydrosilylation period and no further photobleaching was observed under UV exposure.[110] This implies passivation of previously introduced radiative traps by the second hydrosilylation process and the subsequent shutting down of the photobleaching process caused by UV irradiation.

As the above discussion highlights, there a number of complex factors affecting SINC PL. It also highlights the complexity and dependence that the optical and electronic properties of silicon nanocrystals have on surface chemistry and induced surface states. These relationships and their effect on SiNC PL stability must be further understood for the efficient implementation of optical devices and theranostic technologies.

1.6 Thesis Outline

The present thesis focuses on the optoelectronic properties of SiNCs with functionalized surfaces. Chapter 2 focuses on functionalizing SiNCs with electroactive surface groups. Specifically, modification of the SiNC surface with ferrocene was used to diagnostically probe the electronic communication between the SiNC and surface group. Interactions between the SiNC and ferrocene surface group indicate electron transfer from the ferrocene to the SiNC. Chapter 3 focuses on the stability of optical properties of SiNCs with a series of different surface modifications. The photobleaching response of SiNCs with a series of surface functionalities was studied under atmosphere and inert conditions. In inert conditions, oxidation was determined to have the strongest influence on photobleaching response. Conclusions and future directions of the work presented here are outlined in Chapter 4.

1.7 References

(1) Daniel, M. C.; Astruc, D. *Chem. Rev.* **2004**, *104* (1), 293.
(2) Eustis, S.; El-Sayed, M. A. *Chem. Soc. Rev.* **2006**, *35* (3), 209.
(3) Thostenson, E. T.; Ren, Z.; Chou, T. *Compos. Sci. Technol.* **2001**, *61* (13), 1899.
(4) Baughman, R. H.; Zakhidov, A. A.; de Heer, W. A. *Science* **2002**, *297* (5582), 787.
(5) Lu, A.; Salabas, E. L.; Schüth, F. *Angew. Chem. Int. Ed.* **2007**, *46* (8), 1222.
(6) Lee, C.; Wei, X.; Kysar, J. W.; Hone, J. *Science* **2008**, *321* (5887), 385.
(7) Anikeeva, P. O.; Halpert, J. E.; Bawendi, M. G.; Bulović, V. *Nano Lett.* **2009**, *9* (7), 2532.
(8) Duan, X.; Niu, C.; Sahi, V.; Chen, J.; Parce, J. W.; Empedocles, S.; Goldman, J. L. *Nature* **2003**, *425* (6955), 274.
(9) Grätzel, M. *J. Photochem. Photobiol. A Chem.* **2004**, *164* (1), 3.
(10) West, J. L.; Halas, N. J. *Annu. Rev. Biomed. Eng.* **2003**, *5* (1), 285.
(11) Huang, X.; El-Sayed, I. H.; Qian, W.; El-Sayed, M. A. *J. Am. Chem. Soc.* **2006**, *128* (6), 2115.
(12) Alivisatos, A. P.; Gu, W.; Larabell, C. *Annu. Rev. Biomed. Eng.* **2005**, *7* (1), 55.
(13) Murray, C. B.; Norris, D. J.; Bawendi, M. G. *J. Am. Chem. Soc.* **1993**, *115* (19), 8706.
(14) Micic, O. I.; Curtis, C. J.; Jones, K. M.; Sprague, J. R.; Nozik, A. J. *J. Phys. Chem.* **1994**, *98* (19), 4966.
(15) Olshavsky, M. A.; Goldstein, A. N.; Alivisatos, A. P. *J. Am. Chem. Soc.* **1990**, *112* (25), 9438.
(16) Ishii, H.; Sugiyama, K.; Ito, E.; Seki, K. *Adv. Mater.* **1999**, *11* (8), 605.
(17) Hessel, C. M.; Reid, D.; Panthani, M. G.; Rasch, M. R.; Goodfellow, B. W.; Wei, J.; Fujii, H.; Akhavan, V.; Korgel, B. A. *Chem. Mater.* **2012**, *24* (2), 393.
(18) Murray, C. B.; Sun, S.; Gaschler, W.; Doyle, H.; Betley, T. A.; Kagan, C. R. *IBM J. Res. Dev.* **2001**, *45* (1), 47.
(19) Moreels, I.; Justo, Y.; De Geyter, B.; Haustraete, K.; Martins, J. C.; Hens, Z. *ACS Nano* **2012**, *5* (3), 2004.
(20) Hirayama, H.; Tanaka, S.; Ramvall, P.; Aoyagi, Y. *Appl. Phys. Lett.* **1998**, *72* (14), 1736.
(21) Uematsu, T.; Doi, T.; Torimoto, T.; Kuwabata, S. *J. Phys. Chem. Lett.* **2010**, *1* (22), 3283.
(22) Kamat, P. V. *J. Phys. Chem. C* **2008**, *112* (48), 18737.
(23) Talapin, D. V; Murray, C. B. *Science* **2005**, *310* (5745), 86.
(24) Chan, W. C. W.; Nie, S. *Science* **1998**, *281* (5385), 2016.
(25) Murphy, C. J. Anal. Chem. **2002**, 74 (19), 520 A.
(26) Alivisatos, A. P. *Science* **1996**, *271* (5251), 933.
(27) Brus, L. E. *J. Chem. Phys.* **1983**, *79* (11), 5566.
(28) Brus, L. E. *J. Chem. Phys.* **1984**, *80* (9), 4403.
(29) Alivisatos, A. P. *J. Phys. Chem.* **1996**, *100* (31), 13226.
(30) Ekimov, A. I.; Efros, A. L.; Onushchenko, A. A. *Solid State Commun.* **1985**, *56* (11), 921.
(31) Kayanuma, Y. *Phys. Rev. B* **1988**, *38* (14), 9797.
(32) Trwoga, P. F.; Kenyon, A. J.; Pitt, C. W. *J. Appl. Phys.* **1998**, *83* (7), 3789.
(33) Wilson, W. L.; Szajowski, P. F.; Brus, L. E. *Science* **1993**, *262* (5137), 1242.
(34) Ledoux, G.; Gong, J.; Huisken, F.; Guillois, O.; Reynaud, C. *Appl. Phys. Lett.* **2002**, *80* (25), 4834.
(35) Bayliss, S. C.; Heald, R.; Fletcher, D. I.; Buckberry, L. D. *Adv. Mater.* **1999**, *11* (4), 318.
(36) Stewart, M. P.; Buriak, J. M. *Adv. Mater.* **2000**, *12* (12), 859.

(37) Erogbogbo, F.; Yong, K.-T.; Roy, I.; Xu, G.; Prasad, P. N.; Swihart, M. T. *ACS Nano* **2008**, *2* (5), 873.
(38) Cheng, K.; Anthony, R.; Kortshagen, U. R.; Holmes, R. J. *Nano Lett.* **2011**, *11* (5), 1952.
(39) Lalic, N.; Linnros, J. *J. Lumin.* **1998**, *80* (1), 263.
(40) Puzzo, D. P.; Henderson, E. J.; Helander, M. G.; Wang, Z.; Ozin, G. A.; Lu, Z. *Nano Lett.* **2011**, *11* (4), 1585.
(41) Liu, C.; Holman, Z. C.; Kortshagen, U. R. *Nano Lett.* **2009**, *9* (1), 449.
(42) Park, J.-H.; Gu, L.; von Maltzahn, G.; Ruoslahti, E.; Bhatia, S. N.; Sailor, M. J. *Nat. Mater.* **2009**, *8* (4), 331.
(43) Content, S.; Trogler, W. C.; Sailor, M. J. *Chem. - A Eur. J.* **2000**, *6* (12), 2205.
(44) Germanenko, I. N.; Li, S.; El-Shall, M. S. *J. Phys. Chem. B* **2001**, *105* (1), 59.
(45) Graetz, J.; Ahn, C. C.; Yazami, R.; Fultz, B. *Electrochem. Solid-State Lett.* **2003**, *6* (9), A194.
(46) Islam, M. A.; Purkait, T. K.; Veinot, J. G. C. *J. Am. Chem. Soc.* **2014**, *136* (43), 15130.
(47) Canham, L. T. *Appl. Phys. Lett.* **1990**, *57* (10), 1046.
(48) Cullis, A. G.; Canham, L. T. *Nature* **1991**, *353* (6342), 335.
(49) Fahlman, B. D. *Materials Chemistry*; Springer Netherlands: Dordrecht, 2011.
(50) Kasap, S. O. *Optoelectronics and photonics : principles and practices*; Prentice Hall, 2013.
(51) Yoffe, A. D. *Adv. Phys.* **1993**, *42* (2), 173.
(52) Heintz, B. A. S.; Fink, M. J.; Mitchell, B. S. *Adv. Mater.* **2007**, *19* (22), 3984.
(53) Sailor, M. J. *Porous silicon in practice preparation, characterization and applications*; Weinheim :, 2012.
(54) Long, Y.; Zhao, Q.; Zhang, Z.; Tian, Z.; Pang, D. *Analyst* **2012**, *137* (4), 805.
(55) Heinrich, J. L.; Curtis, C. L.; Credo, G. M.; Kavanagh, K. L.; Sailor, M. J. *Science* **1992**, *255* (5040), 66.
(56) Bley, R. A.; Kauzlarich, S. M.; Davis, J. E.; Lee, H. W. H. *Chem. Mater.* **1996**, *8* (8), 1881.
(57) Heath, J. R. *Science* **1992**, *258* (5085), 1131.
(58) Arul Dhas, N.; Raj, C. P.; Gedanken, A. *Chem. Mater.* **1998**, *10* (11), 3278.
(59) Baldwin, R. K.; Pettigrew, K. A.; Ratai, E.; Augustine, M. P.; Kauzlarich, S. M. *Chem. Commun.* **2002**, *23* (17), 1822.
(60) Tilley, R. D.; Warner, J. H.; Yamamoto, K.; Matsui, I.; Fujimori, H. *Chem. Commun.* **2005**, *115* (14), 1833.
(61) Bley, R. A.; Kauzlarich, S. M. *J. Am. Chem. Soc.* **1996**, *118* (49), 12461.
(62) Yang, C.; Bley, R. A.; Kauzlarich, S. M.; Lee, H. W. H.; Delgado, G. R. *J. Am. Chem. Soc.* **1999**, *121* (22), 5191.
(63) Pettigrew, K. A.; Liu, Q.; Power, P. P.; Kauzlarich, S. M. *Chem. Mater.* **2003**, *15* (21), 4005.
(64) Neiner, D.; Chiu, H. W.; Kauzlarich, S. M. *J. Am. Chem. Soc.* **2006**, *128* (34), 11016.
(65) Cheng, X.; Lowe, S. B.; Reece, P. J.; Gooding, J. J. *Chem. Soc. Rev.* **2014**, *43* (8), 2680.
(66) Holmes, J. D.; Ziegler, K. J.; Doty, R. C.; Pell, L. E.; Johnston, K. P.; Korgel, B. A. *J. Am. Chem. Soc.* **2001**, *123* (16), 3743.
(67) Murthy, T. U. M. S.; Miyamoto, N.; Shimbo, M.; Nishizawa, J. *J. Cryst. Growth* **1976**, *33* (1), 1.
(68) Littau, K. A.; Szajowski, P. J.; Muller, A. J.; Kortan, A. R.; Brus, L. E. *J. Phys. Chem.*

1993, *97* (6), 1224.
(69) Li, X.; He, Y.; Talukdar, S. S.; Swihart, M. T. *Langmuir* **2003**, *19* (20), 8490.
(70) Mangolini, L.; Thimsen, E.; Kortshagen, U. *Nano Lett.* **2005**, *5* (4), 655.
(71) Mangolini, L.; Kortshagen, U. *Adv. Mater.* **2007**, *19* (18), 2513.
(72) Liu, S.-M.; Sato, S.; Kimura, K. *Langmuir* **2005**, *21* (14), 6324.
(73) Hessel, C. M.; Henderson, E. J.; Veinot, J. G. C. *Chem. Mater.* **2006**, *18* (138), 36139.
(74) Hessel, C. M.; Henderson, E. J.; Veinot, J. G. C. *J. Phys. Chem. C* **2007**, *111* (19), 6956.
(75) Fujii, M.; Yamaguchi, Y.; Takase, Y.; Ninomiya, K.; Hayashi, S. *Appl. Phys. Lett.* **2004**, *85* (7), 1158.
(76) Fukuda, M.; Fujii, M.; Sugimoto, H.; Imakita, K.; Hayashi, S. *Opt. Lett.* **2011**, *36* (20), 4026.
(77) Sugimoto, H.; Fujii, M.; Imakita, K.; Hayashi, S.; Akamatsu, K. **2012**, *116* (33), 17969.
(78) Gupta, A.; Swihart, M. T.; Wiggers, H. *Adv. Funct. Mater.* **2009**, *19* (5), 696.
(79) Veinot, J. G. C. *Chem. Commun.* **2006**, No. 40, 4160.
(80) Dasog, M.; Kehrle, J.; Rieger, B.; Veinot, J. G. C. *Angew. Chem. Int. Ed.* **2016**, *55* (7), 2322.
(81) Buriak, J. M. *Chem. Rev.* **2002**, *102* (5), 1271.
(82) Bateman, J. E.; Eagling, R. D.; Worrall, D. R.; Horrocks, B. R.; Houlton, A. *Angew. Chem. Int. Ed.* **1998**, *37* (19), 2683.
(83) Hua, F.; Swihart, M. T.; Ruckenstein, E. *Langmuir* **2005**, *21* (13), 6054.
(84) J. M. Schmeltzer; Lon A. Porter, J.; Michael P. Stewart; Buriak, J. M. **2002**, *18* (8), 2971.
(85) Warner, J. H.; Hoshino, A.; Yamamoto, K.; Tilley, R. D. *Angew. Chemie* **2005**, *117* (29), 4626.
(86) Purkait, T. K.; Iqbal, M.; Wahl, M. H.; Gottschling, K.; Gonzalez, C. M.; Islam, M. A.; Veinot, J. G. C. *J. Am. Chem. Soc.* **2014**, *136* (52), 17914.
(87) Höhlein, I. M. D.; Kehrle, J.; Helbich, T.; Yang, Z.; Veinot, J. G. C.; Rieger, B. *Chem. - A Eur. J.* **2014**, *20* (15), 4212.
(88) Dasog, M.; Yang, Z.; Regli, S.; Atkins, T. M.; Faramus, A.; Singh, M. P.; Muthuswamy, E.; Kauzlarich, S. M.; Tilley, R. D.; Veinot, J. G. C. *ACS Nano* **2013**, *7* (3), 2676.
(89) Dasog, M.; De los Reyes, G. B.; Titova, L. V; Hegmann, F. A.; Veinot, J. G. C. *ACS Nano* **2014**, *8* (9), 9636.
(90) Höhlein, I. M. D.; Angı, A.; Sinelnikov, R.; Veinot, J. G. C.; Rieger, B. *Chem. - A Eur. J.* **2015**, *21* (7), 2755.
(91) Dasog, M.; Bader, K.; Veinot, J. G. C. *Chem. Mater.* **2015**, *27* (4), 1153.
(92) Delerue, C.; Allan, G.; Lannoo, M. *Phys. Rev. B* **1993**, *48* (15), 11024.
(93) Rodríguez, J. A.; Vásquez-Agustín, M. A.; Morales-Sánchez, A.; Aceves-Mijares, M. *J. Nanomater.* **2014**, *2014*, 1.
(94) Kanemitsu, Y.; Ogawa, T.; Shiraishi, K.; Takeda, K. *Phys. Rev. B* **1993**, *48* (7), 4883.
(95) Koch, F.; Petrova-Koch, V.; Muschik, T. *J. Lumin.* **1993**, *57* (1), 271.
(96) Wolkin, M. V.; Jorne, J.; Fauchet, P. M.; Allan, G.; Delerue, C. *Phys. Rev. Lett.* **1999**, *82* (1), 197.
(97) Filippou, A. C.; Baars, B.; Chernov, O.; Lebedev, Y. N.; Schnakenburg, G. *Angew. Chem. Int. Ed.* **2014**, *53* (2), 565.
(98) Puzder, A.; Williamson, A. J.; Grossman, J. C.; Galli, G. *Phys. Rev. Lett.* **2002**, *88* (9), 097401.
(99) Kocevski, V.; Eriksson, O.; Rusz, J. *Phys. Rev. B* **2015**, *91* (12), 125402.

(100) Pi, X. D.; Liptak, R. W.; Deneen Nowak, J.; Wells, N. P.; Carter, C. B.; Campbell, S. A.; Kortshagen, U. R. *Nanotechnology* **2008**, *19* (24), 245603.
(101) Hua, F.; Erogbogbo, F.; Swihart, M. T.; Ruckenstein, E. *Langmuir* **2006**, *22* (9), 4363.
(102) Islam, M. A.; Purkait, T. K.; Mobarok, M. H.; Hoehlein, I. M. D.; Sinelnikov, R.; Iqbal, M.; Azulay, D.; Balberg, I.; Millo, O.; Rieger, B.; Veinot, J. G. C. *Angew. Chemie Int. Ed.* **2016**, *55* (26), 7393.
(103) Angı, A.; Sinelnikov, R.; Meldrum, A.; Veinot, J. G. C.; Balberg, I.; Azulay, D.; Millo, O.; Rieger, B. *Nanoscale* **2016**, *8* (15), 7849.
(104) Fabre, B. *Chem. Rev.* **2016**, *116* (8), 4808.
(105) Fabre, B. *Acc. Chem. Res.* **2010**, *43* (12), 1509.
(106) Rehm, J. M.; McLendon, G. L.; Fauchet, P. M. *J. Am. Chem. Soc.* **1996**, *118* (18), 4490.
(107) Dorokhin, D.; Tomczak, N.; Reinhoudt, D. N.; Velders, A. H.; Vancso, G. J. *Nanotechnology* **2010**, *21* (28), 285703.
(108) Song, Y.; Kang, X.; Zuckerman, N. B.; Phebus, B.; Konopelski, J. P.; Chen, S. *Nanoscale* **2011**, *3* (5), 1984.
(109) Guldi, D. M.; Marcaccio, M.; Paolucci, D.; Paolucci, F.; Tagmatarchis, N.; Tasis, D.; Vázquez, E.; Prato, M. *Angew. Chemie* **2003**, *115* (35), 4338.
(110) Wu, J. J.; Kortshagen, U. R. *RSC Adv.* **2015**, *5* (126), 103822.
(111) Jurbergs, D.; Rogojina, E.; Mangolini, L.; Kortshagen, U. *Appl. Phys. Lett.* **2006**, *88* (23), 233116.
(112) Ledoux, G.; Guillois, O.; Porterat, D.; Reynaud, C.; Huisken, F.; Kohn, B.; Paillard, V. *Phys. Rev. B* **2000**, *62* (23), 15942.
(113) Pereira, R. N.; Rowe, D. J.; Anthony, R. J.; Kortshagen, U. *Phys. Rev. B* **2011**, *83* (15), 155327.
(114) Cerofolini, G. F.; Mascolo, D.; Vlad, M. O. *J. Appl. Phys.* **2006**, *100* (5), 054308.
(115) Tischler, M. A.; Collins, R. T.; Stathis, J. H.; Tsang, J. C. *Appl. Phys. Lett.* **1992**, *60* (5), 639.
(116) Harper, J.; Sailor, M. J. *Langmuir* **1997**, *13* (17), 4652.
(117) Yang, J.; Liptak, R.; Rowe, D.; Wu, J.; Casey, J.; Witker, D.; Campbell, S. A.; Kortshagen, U. *Appl. Surf. Sci.* **2014**, *323*, 54.
(118) English, D. S.; Pell, L. E.; Yu, Z.; Barbara, P. F.; Korgel, B. A. *Nano Lett.* **2002**, *2* (7), 681.
(119) Godefroo, S.; Hayne, M.; Jivanescu, M.; Stesmans, A.; Zacharias, M.; Lebedev, O. I.; Van Tendeloo, G.; Moshchalkov, V. V. *Nat. Nanotechnol.* **2008**, *3* (3), 174.
(120) Buriak, J. M. *Chem. Mater.* **2014**, *26* (1), 763.
(121) Huck, L. A.; Buriak, J. M. *Langmuir* **2012**, *28* (47), 16285.
(122) Staebler, D. L.; Wronski, C. R. *Appl. Phys. Lett.* **1977**, *31* (4), 292.
(123) Wolfe, J. P. *Phys. Today* **1982**, *35* (3), 46.

Chapter 2 Functionalization of Silicon Nanocrystals with an Electroactive End Group and their Electrochemical Response

2.1 Introduction to Ferrocene Modified Surfaces

SiNCs are of interest for a variety of optical and electronic applications including memory devices,[1] field effect transistors,[2] photovoltaics,[3] and light emitting diodes.[4–6] Surface chemistry has a strong influence on the optoelectronic properties of QDs.[2,7,8] Control over the optoelectronic properties of SiNCs is necessary if efficient and tailorable devices are to be realized. To date, most investigations have focused on "innocent" (i.e., non-electroactive) surface groups. Further investigation into the interaction of "non-innocent" surface groups and resulting electronic properties of functionalized SiNCs will no doubt be beneficial to furthering the development of new silicon quantum dot-based technologies.

Ferrocene was identified as an ideal first candidate to study the electronic interactions between the silicon particle and surface groups. Ferrocene is a metallocene complex consisting of two cyclopentyldiene rings sandwiching an iron center.[9,10] It can exist in one of two stable oxidation states[11] and possesses fast electron transfer kinetics[12,13] making it an ideal candidate for use in molecular switches,[14] sensors,[15] as well as charge storage devices.[16] Deviations from the well-developed electrochemistry of ferrocene are a useful diagnostic tool in determining the electronic character and interactions of the ferrocenyl iron center[17] and are expected to provide insight into the SiNC-surface group electronic interactions.

The electrochemistry of ferrocene has been studied on a number of surfaces including gold,[12,18] bulk silicon,[16,19–22] as well as nanoscale materials such as porous silicon,[23] carbon nanotubes,[24] and other quantum dots.[25,26] The intent of these studies was to interrogate surface-substrate interactions. To our knowledge there are no reports of ferrocene on freestanding silicon quantum dots.

2.2 Experimental

2.2.1 Reagents and Materials

HSQ was purchased as Fox 18 from DOW Corning. The solvent was removed to give a white solid. Electronics grade 48-50% hydrofluoric acid was purchased from Fisher. Toluene (99.9% HPLC grade, anhydrous dried over columns), methanol (99.8% Reagent grade), dichloromethane (DCM) (99.9% HPLC grade, dried using a solvent system) and acetonitrile (anhydrous) were purchased from Sigma Aldrich. Ethanol was reagent grade (95%). Vinylferrocene (97%), 2,2'-Azobis(2-methylpropionitrile) (98%, AIBN), tetrabutylammonium hexafluorophosphate (≥99.0%) (TBAHFP) were purchased from Sigma Aldrich and used as received. 1-dodecene (95%) and ferrocene (98%) were also ordered from Sigma Aldrich. 1-Dodecene was passed over activated alumina prior to use. Ferrocene was sublimed prior to use as a standard in electrochemistry experiments. Nuclear magnetic resonance (NMR) solvents chloroform-d ($CDCl_3$) and chloroform-d containing 0.03% tetramethylsilane (TMS) by volume were purchased from Sigma Aldrich. Silver nitrate was from Basi Analytical and used as received.

2.2.2 Hydride Terminated Freestanding 3 nm Silicon Nanocrystals

HSQ (3.0 g) was transferred to a quartz boat and heated to 1100 ˚C at a heating rate of 18 ˚C/min where it was maintained for one hour. All thermal processing was performed under a 5 %/ 95 % hydrogen/ argon atmosphere. After cooling to room temperature, the resulting brown black solid was transferred to an agate mortar and pestle and ground until a fine brown powder was obtained. This powder was shaken mechanically with silica beads for approximately 15 hours after which the powder was suspended in ethanol and transferred to a filter. After filtration, the solid was allowed to dry in air. The composite was briefly ground again in an agate mortar and pestle to break up large pieces of material prior to etching.

The composite (0.15 g) was placed in a Teflon beaker. Equal volumes of deionized water, ethanol and HF were added and the mixture was stirred for one hour at room temperature. The cloudy, pale yellow mixture was extracted three times with 15 mL toluene. The toluene extract containing hydride terminated SiNCs was centrifuged for 10 minutes at 3000 rpm to give an orange solid and clear colourless supernatant. The supernatant was discarded and the solid was used in the functionalization procedures noted below.

2.2.3 Ferrocenyl-dodecyl Terminated Silicon Nanocrystals (FcD-SiNC)

Hydride terminated silicon nanoparticles (d ~ 3 nm) obtained from etching 0.15 g of composite were re-dispersed in 5 mL of 1-dodecene. The mixture was mixed over molecular sieves to remove moisture and transferred to a Schlenk flask filled with argon. 0.05 g of vinylferrocene was added and the flask was evacuated to remove any residual toluene. The flask was then degassed and refilled with argon in triplicate. AIBN (0.017 g) was added and the flask was heated overnight with stirring at 65 ˚C. The resulting clear orange solution was transferred to two 40 mL polytetrafluoroethylene (PTFE) centrifuge tubes with 7 mL toluene each. 5 mL ethanol and 20 mL methanol were added to each tubes. Centrifugation at 12 000 rpm was performed and the supernatant discarded. The orange solid residue in each tube was redispersed in 7 mL toluene and 25 mL methanol was added. Centrifugation was repeated for three additional cycles. The final residue was redispersed in toluene and filtered through a 0.45 μm PTFE filter into a vial.

2.3 Materials Characterization

2.3.1 Fourier Transform Infrared Spectroscopy

Fourier Transform Infrared Spectroscopy (FTIR) was performed using a Thermo Nicolet Magna 750 FTIR Spectrometer. Samples where drop cast as a thin film from solution onto a KBr plate.

2.3.2 Nuclear Magnet Resonance Spectroscopy

^{1}H NMR was recorder on a Varian Inova four-channel 500 MHz spectrometer with an autoxdb probe. Spectra were recorded at room temperature for a total of 16 scans. Samples were dried in a small vail under nitrogen then dissolved in $CDCl_3$ or $CDCl_3$ with 0.3% TMS standard.

2.3.3 X-ray Photoelectron Spectroscopy

X-ray photoelectron spectroscopy (XPS) experiments were performed at room temperature using a Kratos Axis spectrometer with monochromatized Al Kα (hυ = 1486.71 eV). The pressure of the chamber was maintained at or below 5×10^{-10} Torr. Samples were drop cast from solution onto a copper foil. A hemispherical electron-energy analyzer working at the pass energy of 20 eV was used to collect core-level spectra. Survey spectra within a range of binding energies from 0 to 1100 eV were collected at an analyzer pass energy of 160 eV. Calibration to the carbon 1s peak at 284.8 eV was used to correct for charging effects for all spectra. Fitting of the components was done using CasaXPS software. A Shirley type background was used and all full width half maxima were maintained below 1.

2.3.4 Transmission Electron Microscopy

Transmission electron microscopy (TEM) images were taken with a JOEL2011TEM equipped with a LaB_6 filament using an accelerating voltage of 200 kV. TEM samples were prepared by depositing a droplet of dilute functionalized SiNC suspensions in toluene onto a holey carbon coated copper grid and the solvent was removed under vacuum. The size distribution of the particles was determined on a sample of over 200 particles.

High resolution images were recorded with a JEOL2200FS transmission electron microscope with an operating voltage of 200 kV.

2.3.5 Thermogravimetric Analysis

Thermogravimetric analysis (TGA) was performed using a Perkin Elmer Pyris 1 TGA with a platinum pan. Samples were freeze-dried from benzene prior to submission. A heating rate of 10 ˚C/minute was maintained from room temperature to 900 ˚C in an argon atmosphere.

2.3.6 Scanning Tunneling Microscopy and Scanning Tunneling Spectroscopy

Scanning tunneling microscopy (STM) and scanning tunneling spectroscopy (STS) analysis were performed by Dr. Doron Azulay and Prof. Oded Millo of the Racah Institute of Physics, at the Hebrew University of Jerusalem. The sample was deposited onto a gold substrate. A tip-to-sample bias of 1.6 eV and 0.2 nA was used to record STM images of the particles. The bias was lowered to 1.3 eV without adjustment of the current prior to STS measurements to increase spectral resolution.

2.3.7 Cyclic Voltammetry

CV experiments were carried out with a Basi Epsilon Potentiostat. A non-aqueous 0.01 M Ag/$AgNO_3$ in acetonitrile reference electrode was used for all reported experiments. A platinum working electrode was used. Prior to each cyclic voltammetry experiment the working electrode was polished to a 0.05 micron finish with alumina and sonicated in Millipure DI water, then ethanol. The counter electrode was a platinum coil. TBAHFP was dissolved in 5 mL of dry DCM to make a 0.1 M electrolyte solution. The electrolyte solution was purged with argon and measured via CV to ensure no contamination. Particles dried under a nitrogen stream were subsequently added to the electrochemical cell (approximately 1 mg/mL) and measured. At the end of each experiment a small amount of sublimed ferrocene was added to each solution as an internal standard.[27]

2.4 Results

2.4.1 Synthesis of Ferrocene Functionalized Silicon Nanoparticles

A number of methods were explored to bond ferrocene to the surface of the hydride terminated SiNCs. This included a number of direct hydrosilylation reactions with ethynylferrocene or vinylferrocene. Reactions with only the ethynylferrocene or vinylferrocene ligand present yielded a product with limited solubility in organic solvents. A soluble product was obtained with a radical initiated reaction of a mixture of vinylferrocene and 1-dodecene in the presence of hydride terminated SiNC as summarized in Scheme 2.1. The product was readily soluble in organic solvents such as toluene and DCM. The product displayed no detectable visible photoluminescence upon excitation at 365 nm consistent with an interaction between the vinylferrocene and the SiNC.

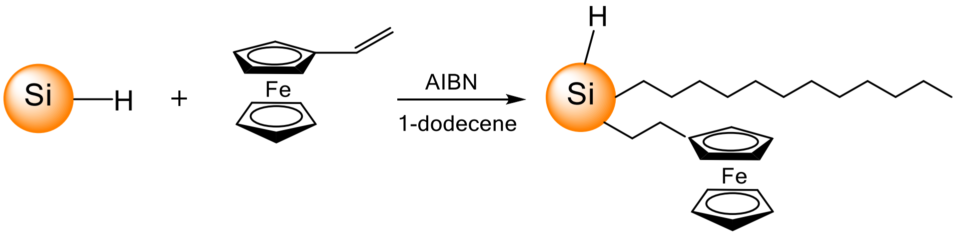

Scheme 2.1 Synthesis of organic solvent soluble, mixed surface ferrocenyl-dodecyl functionalized SiNCs.

The same synthetic method used to produce the FcD-SiNCs was repeated with ferrocene instead of vinylferrocene as depicted in Scheme 2.2. The initial addition of the ferrocene quenched the PL of the hydride terminated nanoparticles. However, upon extended reaction (i.e., 16 h), a soluble product displaying red photoluminescence was obtained. This provided qualitative evidence that the vinyl functionality of vinylferrocene is necessary in stabilizing the interaction between the ferrocene and the SiNC. Further characterization of the hybrid particles supports the presence of a ferrocene moiety on the surface of the SiNC as discussed below.

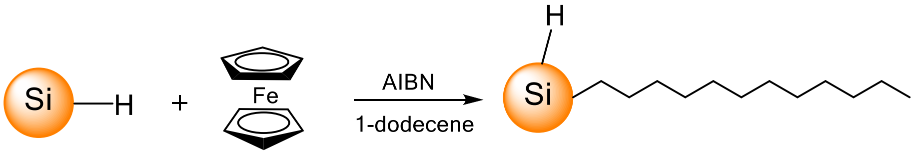

Scheme 2.2 Reaction of silicon nanoparticles with ferrocene in neat 1-dodecene. This product is photoluminescence indicating the PL quenching of the nanoparticles by ferrocene is reversible in absence of the vinyl group present.

2.4.2 Nanocrystal Characterization

FTIR spectroscopy reveals the surface functionality of silicon nanocrystals through characteristic vibrational modes of surface groups on the nanocrystal. The FTIR spectrum obtained for FcD-SiNC (Fig 2.1a) shows characteristics peaks of both the ferrocene moiety, dodecyl functionality and residual hydride of the silicon nanoparticles. The sharp peak at 3095 cm^{-1} is characteristic of the C-H stretching of the cyclopentyldiene (Cp) rings of vinylferrocene.[23] The FTIR spectra of vinylferrocene is shown in Fig 2.2. Dominant alkane C-H stretches reside between 2853 and 2956 cm^{-1} for the functionalized particles. This stretching is likely a mixture of the functionalized alkyl-ferrocene and dodecyl C-H stretches, but is expected to be predominantly due to the long chain dodecyl moiety. Residual hydride on the silicon surface is evident by the peak at 2085 cm^{-1}. This also indicates incomplete surface passivation that can result in further oxidation of the silicon surface. Oxidation of the silicon surface is indicated by the broad peak at approximately 1040 cm^{-1} which is likely Si-O.[28]

Fig 2.1b shows the spectrum of the product from the reaction of ferrocene and SiNCs in neat 1-dodecene (Scheme 2.2). The spectrum indicates the product is dodecyl functionalized without evidence of ferrocene on the surface of the SiNCs following purification. Similar C-H, Si-H and Si-O vibrational modes are observed, but the C-H stretch attributed to the ferrocene rings are absent. The residual hydride absorption is less intense compared to vinyl ferrocene functionalized particles. Disruption of the alkyl chain packing due to the steric bulk of the ferrocene moiety may result in less efficient surface passivation of the FcD-SiNCs as indicated by larger Si-H absorption peak.

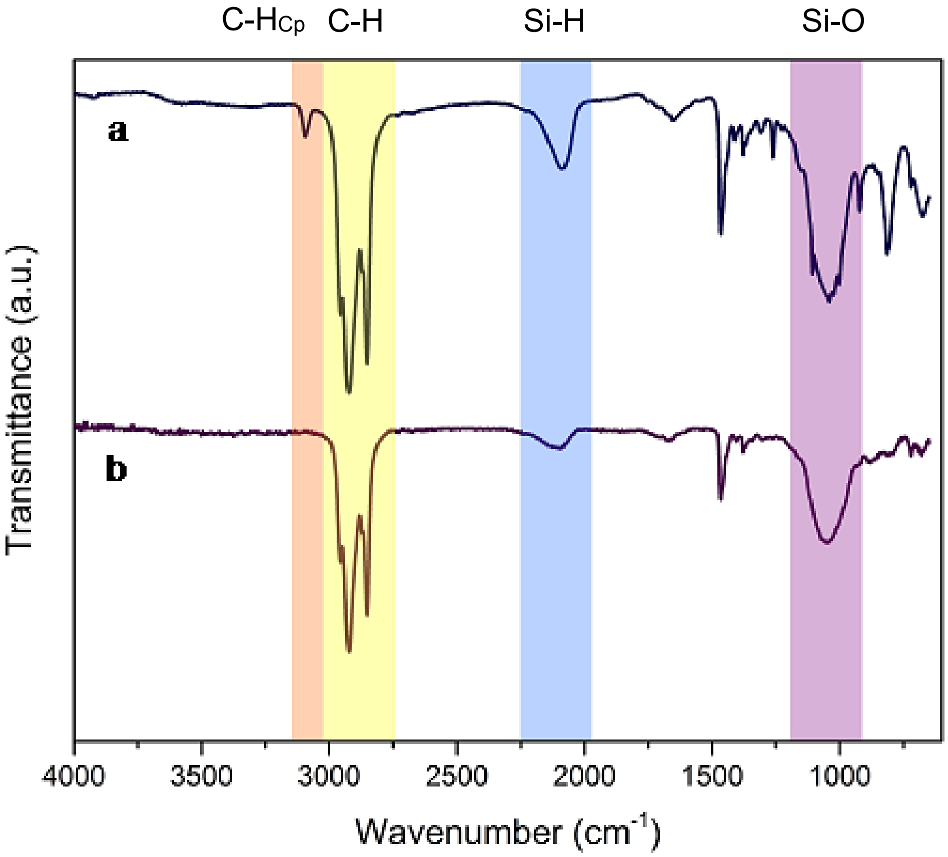

Fig 2.1 FTIR of (a) FcD-SiNCs and (b) SiNCs reacted with ferrocene in neat 1-dodecene (Scheme 2.2).

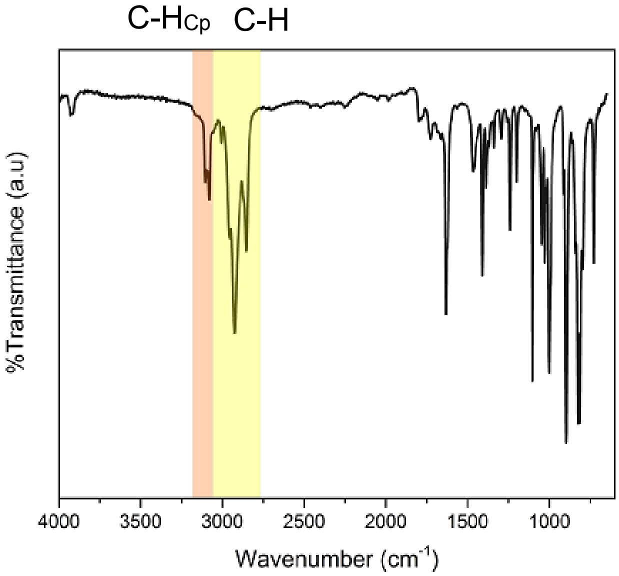

Fig 2.2 FTIR of the starting material vinylferrocene.

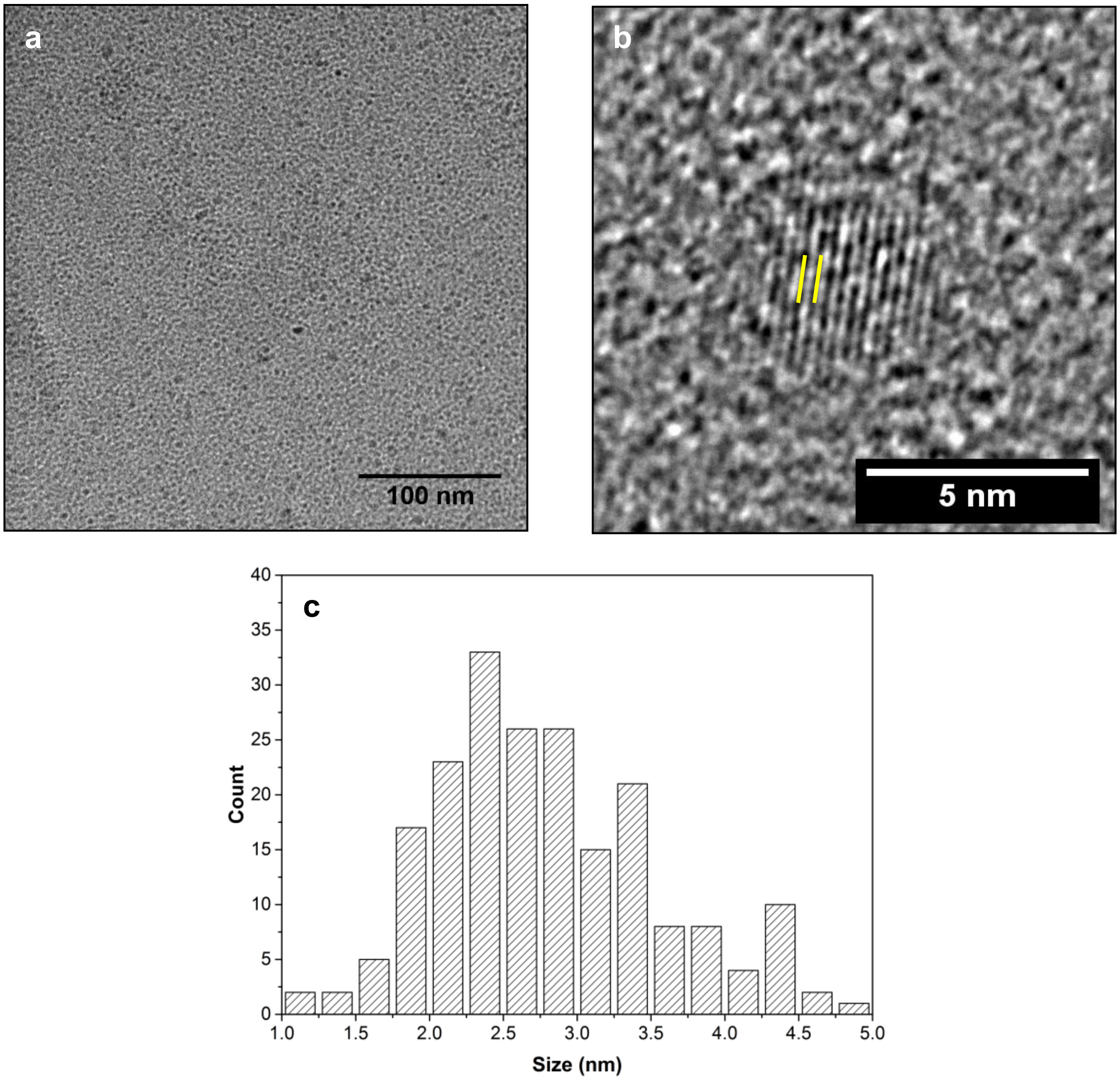

Fig 2.3 (a) TEM image of FcD-SiNCs and a high resolution image (b) of FcD-SiNCs showing the lattice fringes of the particles. The lattice spacing was determined to be 0.30 nm consistent with the (111) planes of silicon. The size distribution of the particles is shown in (c).

TEM images (Fig 2.3a) confirm the presence of particles in the sample after reaction with vinylferrocene. The mean size distribution was determined to be 2.9 ± 0.7 nm as shown in Fig 2.3c. There is a large size distribution of the particles. High resolution images of the particles, Fig 2.3b show that the particles retain a crystalline Si core. The d-spacing was determined to be 0.30 nm, consistent with the spacing of (111) planes of silicon.[29]

^{1}H NMR of the soluble mixed surface nanocrystals indicates the presence of a ferrocene moiety as well as dodecyl protons. A broad peak at approximately 4 ppm in the spectrum for the FcD-SiNC, shown in Fig 2.4, is attributed to the protons of the Cp rings of the ferrocene functionality. Peaks attributed to the dodecyl ligands are observed at 1.26 and 0.9 ppm.[30] The broadening of the proton peaks in the NMR spectrum is attributed to longer relaxation times combined with the restricted motion of surface bonded moeities.[31] The broadening of the ferrocene peak seen the spectrum is consistent with the ferrocene being bonded to the particle. The NMR spectrum presented here is consistent with previous reports of ferrocene functionalized CdSe/Zn nanoparticles.[32]

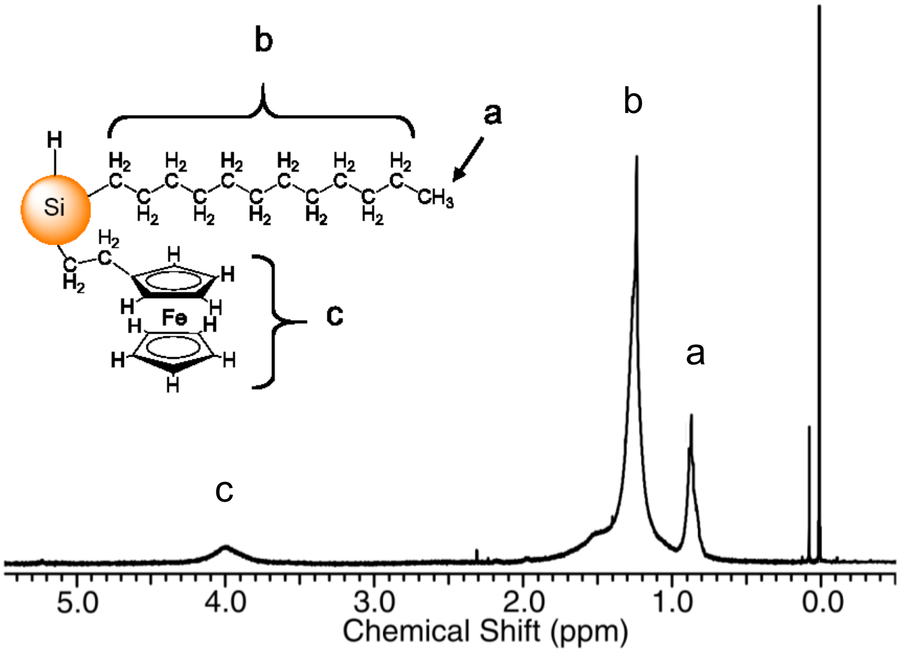

Fig 2.4 ^1H NMR of FcD-SiNCs in $CDCl_3$ with 0.3 % TMS. Broadening of the peaks is attributed to the restricted motion of ligand groups anchored to the surface of the nanoparticle.

An estimation of the total surface coverage was obtained from NMR samples containing TMS as an internal standard using a method modified from Purkait *et al.*[30] and Mobarok *et al.*[33] This provides an approximation of the total number of surface bound ligands and total surface coverage. The surface coverage was determined to be approximately 50 % assuming a 2.8 nm silicon nanocrystal with a total of 600 silicon atoms and 200 terminal hydrides.[34] It was estimated that there is approximately 36 ferrocenyl ligands and 63 dodecyl ligands per Si nanocrystal. Details of the calculation can be found in Appendix I.1.

Thermogravimetric analysis was also used to estimate the degree of surface coverage of functionalized nanoparticles.[35] For nanoparticle analysis, the weight loss in TGA is attributed to complete removal of ligands from the particle surface. A total percent weight loss of 49.3 % was recorded for the FcD-SiNCs. The ratio of the ferrocene and dodecyl peaks obtained in the NMR was used as the mole ratio in the TGA surface coverage calculation. The weight loss was calculated to correspond to the surface coverage of approximately 44 %. Appendix I.2 contains the surface calculation from the TGA analysis. There is approximately a 6 % difference in surface coverage between the two calculations. The difference between the NMR and TGA calculations may be due to the volatility of the TMS reference standard. A decrease in the reference standard volume would overestimate the number of ligands relative to the TMS signal in the NMR calculation.

X-ray photoelectron spectroscopy reveals the elemental composition of functionalized nanocrystals and provided further confirmation of functionalization of a ferrocene moiety to the SiNCs. The XP survey spectrum of a freshly prepared sample of FcD-SiNC is shown in Fig 2.5a. The Si $2p_{3/2}$ region shows the samples retained a Si (0) core as indicated by the peak at 99.5 eV. There is oxidation of silicon as evidenced by the higher binding energy components: Si (I), Si (III) and Si (IV) at 100.7, 102.1, and 102.9 eV, respectively. The higher binding energies are due to the presence of the surface groups as well as oxygen on the silicon surface resulting the formation of silicon suboxides.[36] The presence of surface oxide is supported by the FTIR results.

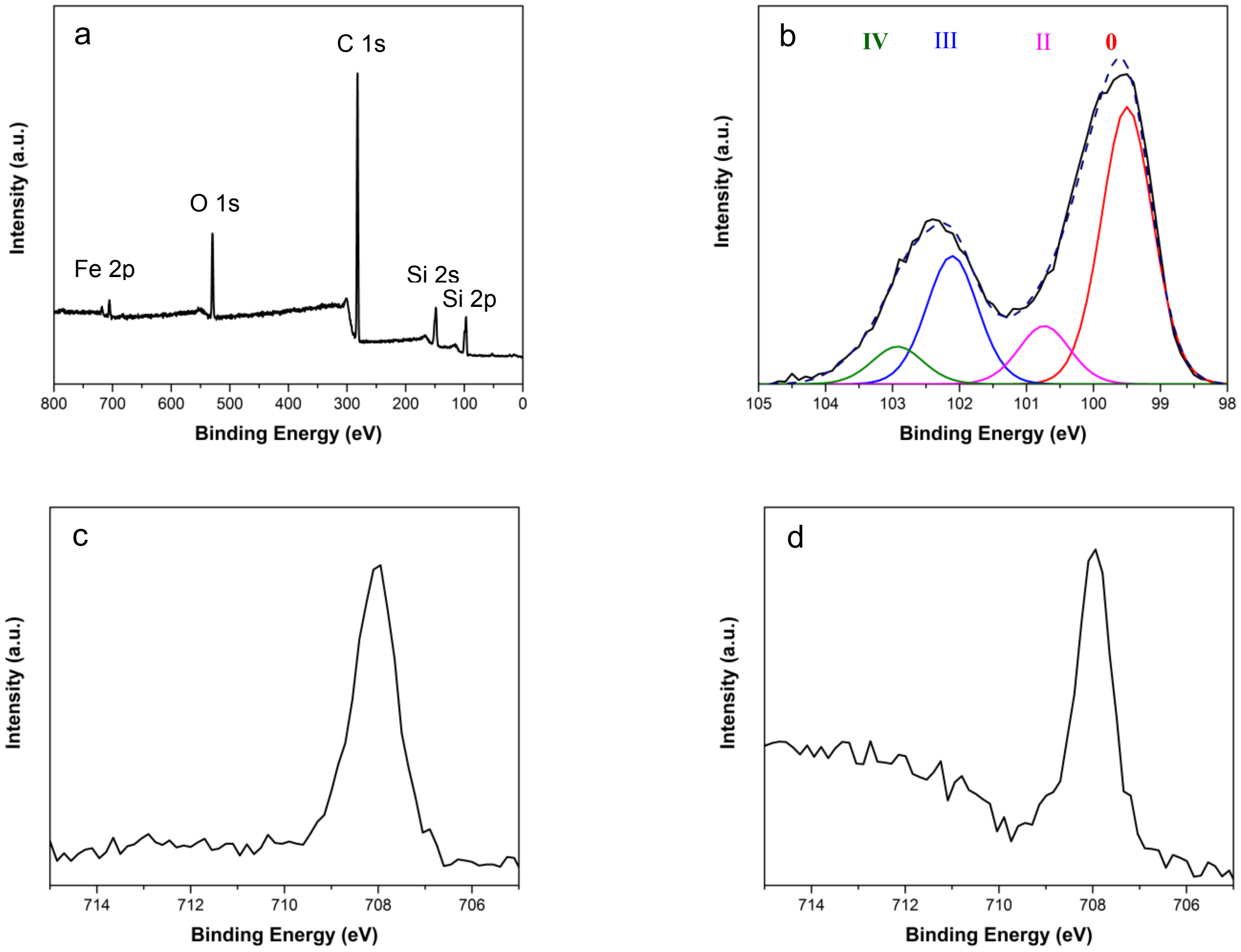

Fig 2.5 (a) Survey scan of FcD-SiNC and the (b) high resolution XP spectra of the Si 2p region. The dashed line is the envelope of the fit. The oxidation states of silicon correspond to the colored roman numerals. The Si $2p_{1/2}$ peaks are omitted for clarity. (c) Fe 2p region of FcD-SiNC and (d) Fe 2p region of vinyl ferrocene.

The XPS survey scan also shows a weak iron (Fe) peak for the functionalized NCs in Fig 2.5a. The Fe $2p_{3/2}$ spectrum is shown alongside the Fe $2p_{3/2}$ of vinylferrocene in Fig 2.5c and Fig 2.5d respectively. The Fe $2p_{3/2}$ for the vinyl ferrocene is centered at 707.96 eV consistent with previous measurements of ferrocene on bulk surfaces. [19,37] The Fe $2p_{3/2}$ peak for FcD-SiNC was centered at 708.04 eV indicating the iron on the nanocrystals is likely in a similar oxidation environment to the free vinyl ferrocene environment. The iron XPS peaks were not deconvoluted.

Investigation of the electronic properties of the iron center was also conducted using CV measurements. CV experiments provide a measure of an electroactive species reduction and oxidation potentials. The electrochemical response of 1 mM vinylferrocene is seen in Fig 2.6. In practice the formal reduction potential or $E_{1/2}$ (see Eqn 2.1) of the cathode and anode peaks is typically reported due to the scan rate dependence of the peak positions; $E_{1/2}$ is independent of scan rate.[17] In dichloromethane the $E_{1/2}$ of vinylferrocene was measured to 252 mV vs. an $Ag/AgNO_3$ reference electrode. Ferrocene had a similar $E_{1/2}$ of 238 mV vs. $Ag/AgNO_3$ (not shown).

$$E_{1/2} = \frac{E_c + E_a}{2} \qquad \text{Eqn 2.1}$$

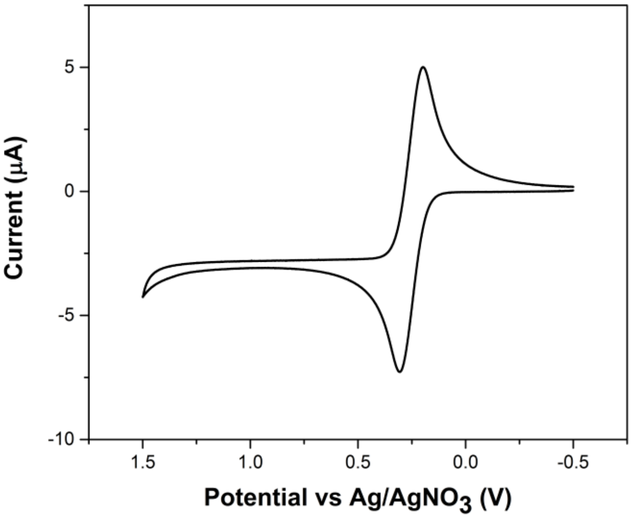

Fig 2.6 CV of vinylferrocene in 0.1 M TBAHFP in DCM vs. an Ag/AgNO$_3$ reference electrode at a scan rate of 100 mV/s.

The CV of the ferrocene functionalized nanocrystals (Fig 2.7) differs significantly from that of the typical CV of ferrocene or vinylferrocene. The potential was scanned from negative to positive and subsequently reversed. No oxidation peak appears in the potential window of the experiment. However, there is a cathodic peak that appears during the reverse scan. It should be noted that neither Si-H terminated nor purely dodecyl functionalized SiNC show an electrochemical response under the same experimental conditions investigated.

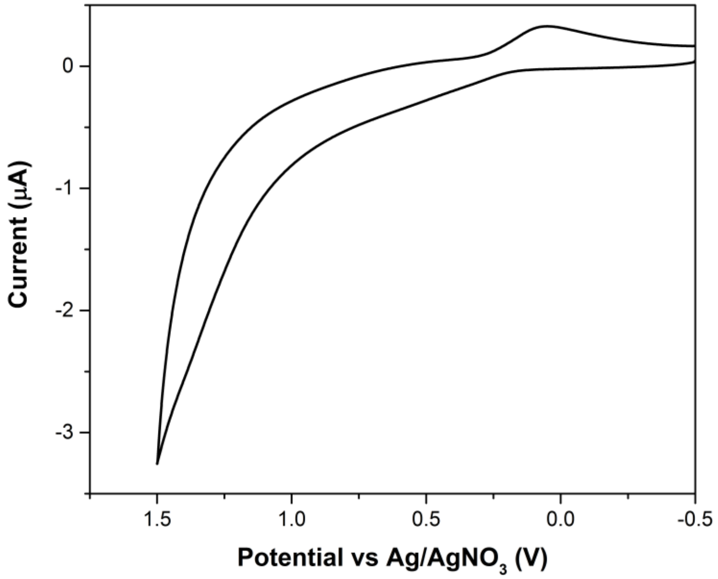

Fig 2.7 CV of FcD-SiNCs in 0.1 M TBAHFP in DCM vs Ag/AgNO$_3$ reference electrode at a scan rate of 100 mV/s.

The deviation from the normal vinylferrocene CV curve supports the hypothesis of interaction between the surface ligand and the silicon nanocrystal. The electrochemistry of the ferrocene group is no longer reversible (within the potential range investigated) as indicated by the absence of the oxidation peak. It is proposed that oxidation of the ferrocene moiety is likely caused by electron transfer to the silicon nanocrystal - behavior consistent with previous reports of quenching of porous silicon by molecular ferrocene.[38] Buriak and Lindsay also reported reduced functionalization efficiencies of porous Si likely due to ferrocene quenching a white light induced excitonic functionalization mechanism.[39] Reports of quenching of CdSe/ZnS QDs with ferrocene is hypothesized to occur through the same mechanism.[26,32]

The cathodic peak observed for the FcD-SiNCs varied in potential from 53mV to 169mV vs Ag/AgNO$_3$. This variance between measurements is attributed to a number of factors. The broad nature of cathodic peak makes it difficult to precisely assign a potential value and is a likely source of error between measurements. Oxidation of the particle surfaces may also contribute to the shift in peak potential and also influence the overall shape of the voltammogram as discussed below.

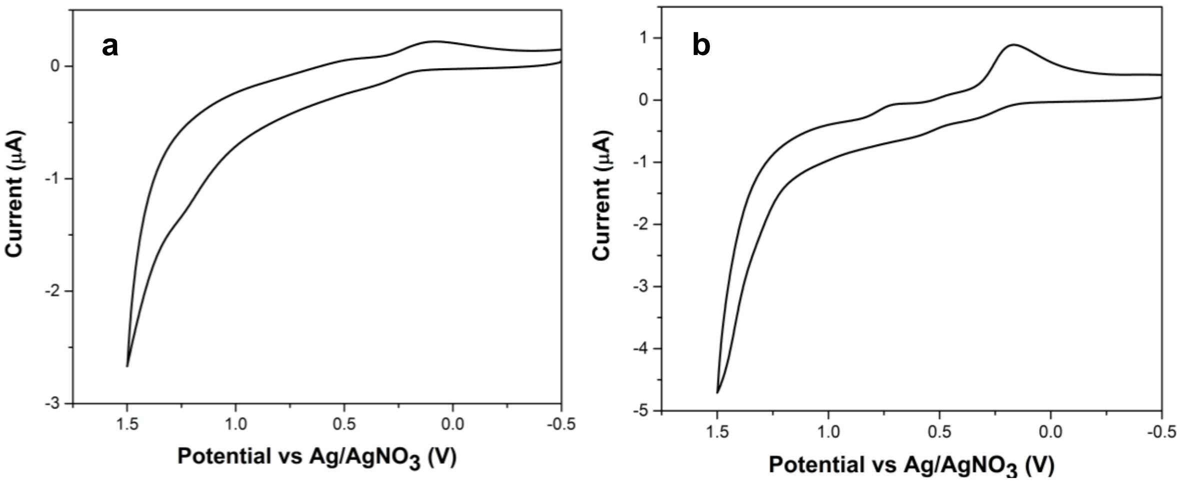

Fig 2.8 CV of FcD-SiNC (a) recorded one week after initial CV and (b) after bubbling with oxygen for 60 minutes. Both voltamagrams where recorded in 0.1 M TBAHPF in DCM at a scan rate of 100 mV/s.

The CV response of the FcD-SiNCs were investigated after deliberate oxidation of the samples. Fig 2.8a shows the same sample as in Fig 2.7 but is recorded several days after the initial CV in Fig 2.7. There is a shift of the cathodic peak from 53 mV to 96 mV from Fig 2.7 to 2.8a respectively. Further oxidation of the sample by bubbling with oxygen prior to CV analysis increased the shift to 169mV as seen in Fig 2.8b and induced additional cathodic and anodic peaks also seen. This oxidation may provide an insulating layer reducing the effectiveness of the electron transfer to the silicon nanoparticle.

STM imaging and STS are complementary methods to CV and PL, and reveal insight into the topography in correlation with the electronic level structure of at the nanoscale.[40] Unlike PL, which provides information on optical transition between electronic levels from which the excitonic band-gap can be extracted, in STS the valence and conduction bands (VB and CB) levels are monitored separately. Specifically, the electronic DOS is proportional to the measured dI/dV-V tunneling spectra, from which the fundamental (single-particle) band gap can be determined, rather than the excitonic band-gap measured by PL.[41,42]

STM topographic measurements confirm that the nanocrystals are within the size regime of 3-5 nm, as expected from TEM (Fig 2.9b). Measurements performed on FcD-SiNC showed a band gap close to that of alkyl functionalized SiNCs of similar size.[8] The STS (fundamental) band gap of the FcD-SiNCs was extracted from the dI/dV-V curves, Fig 2.9a, and determined to be approximately 2.30 eV. The band gap was determined from the separation between the midpoint of the DOS onset and the maximum DOS at both the conductance and valence band voltages. Fig 2.9 also clearly shows that the Fermi level (V=0) is positioned closer to the CB edge, an effect that was not observed for the dodecyl functionalized SiNCs.[8] This behavior is indicative of n-type surface doping of the nanocrystals and is consistent with the CV measurements. Oxidation of the ferrocene through an electron transfer mechanism to the silicon particle would account for the n-type doping of the nanocrystals by increasing the fermi level closer to the conduction band of the particle.

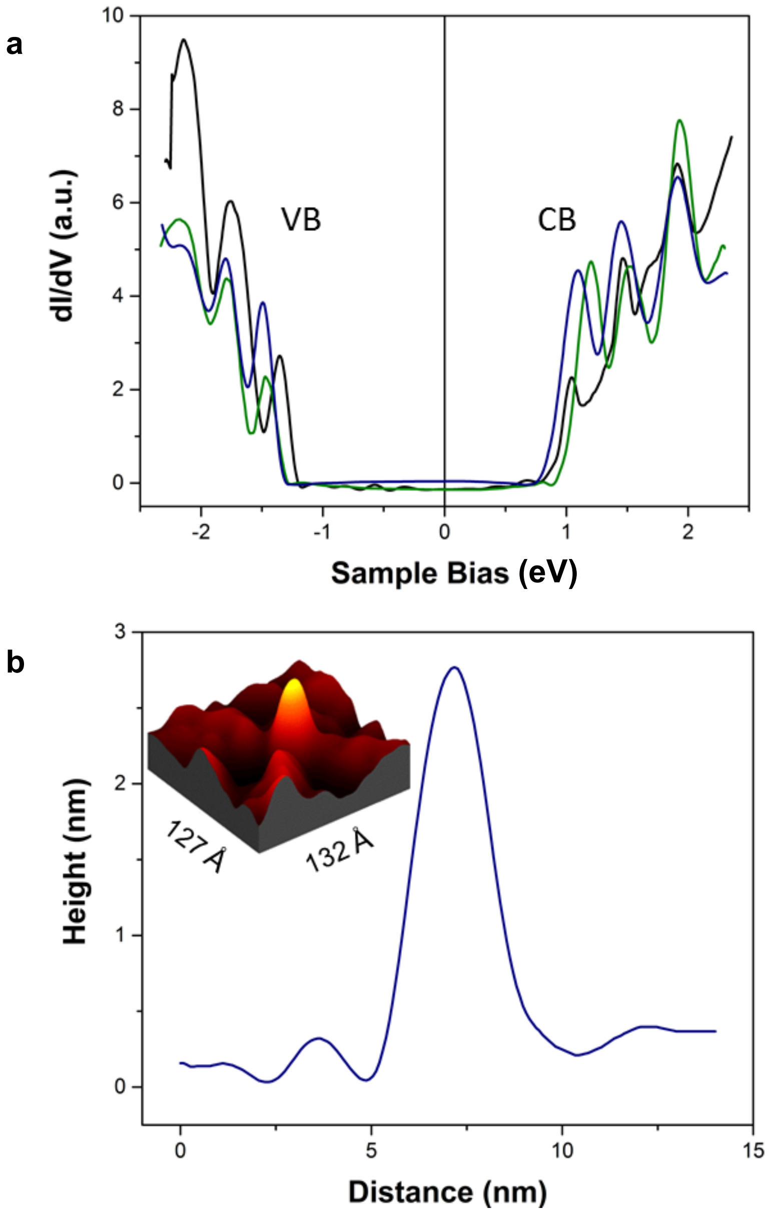

Fig 2.9 (a) Repetitive dI/dV-V tunneling spectra measured on three different FcD-SiNCs. The band gap extracted for these spectra is around 2.30 eV. The navy-blue spectrum in (a) was measured on the NC whose topographic image is presented in the inset of (b), which presents also a topographic cross-section taken along the diagonal of the image. All measurements were performed with sample-bias and current setting of 1.6 V and 0.2 nA.

2.5 Conclusions

SiNCs have been functionalized with a ferrocene group. This is evident by PL quenching of SiNCs. CV results as well as STS confirm electronic interaction between the SiNC and surface group. The mechanism of PL quenching is due to electron transfer from the ferrocene to the SiNC as seen in the irreversible oxidation of ferrocene and the n-type doping evident in the STS measurements.

2.6 References

(1) Tiwari, S.; Rana, F.; Hanafi, H.; Hartstein, A.; Crabbé, E. F.; Chan, K. *Appl. Phys. Lett.* **1996**, *68* (10), 1377.

(2) Gresback, R.; Kramer, N. J.; Ding, Y.; Chen, T.; Kortshagen, U. R.; Nozaki, T. *ACS Nano* **2014**, *8* (6), 5650.

(3) Liu, C.; Holman, Z. C.; Kortshagen, U. R. *Nano Lett.* **2009**, *9* (1), 449.

(4) Lalic, N.; Linnros, J. *J. Lumin.* **1998**, *80* (1), 263.

(5) Puzzo, D. P.; Henderson, E. J.; Helander, M. G.; Wang, Z.; Ozin, G. A.; Lu, Z. *Nano Lett.* **2011**, *11* (4), 1585.

(6) Cheng, K.; Anthony, R.; Kortshagen, U. R.; Holmes, R. J. *Nano Lett.* **2011**, *11* (5), 1952.

(7) Soreni-Harari, M.; Yaacobi-Gross, N.; Steiner, D.; Aharoni, A.; Banin, U.; Millo, O.; Tessler, N. *Nano Lett.* **2008**, *8* (2), 678.

(8) Wolf, O.; Dasog, M.; Yang, Z.; Balberg, I.; Veinot, J. G. C.; Millo, O. *Nano Lett.* **2013**, *13* (6), 2516.

(9) Dunitz, J. D.; Orgel, L. E. *Nature* **1953**, *171* (4342), 121.

(10) Kealy, T. J.; Pauson, P. L. *Nature* **1951**, *168* (4285), 1039.

(11) Ito, N.; Saji, T.; Aoyagui, S. *J. Organomet. Chem.* **1983**, *247* (3), 301.

(12) Chidsey, C. E. D.; Bertozzi, C. R.; Putvinski, T. M.; Mujsce, A. M. *J. Am. Chem. Soc.* **1990**, *112* (11), 4301.

(13) Smalley, J. F.; Feldberg, S. W.; Chidsey, C. E. D.; Linford, M. R.; Newton, M. D.; Liu, Y. P. *J. Phys. Chem.* **1995**, *99* (35), 13141.

(14) Martínez, R.; Ratera, I.; Tárraga, A.; Molina, P.; Veciana, J. *Chem. Commun.* **2006**, No. 36, 3809.

(15) Mulrooney, R. C.; Singh, N.; Kaur, N.; Callan, J. F. *Chem. Commun.* **2009**, No. 6, 686.

(16) Fabre, B. *Acc. Chem. Res.* **2010**, *43* (12), 1509.

(17) Batterjee, S. M.; Marzouk, M. I.; Aazab, M. E.; El-Hashash, M. A. *Appl. Organomet. Chem.* **2003**, *17* (5), 291.

(18) Weber, K.; Hockett, L.; Creager, S. *J. Phys. Chem. B* **1997**, *101* (41), 8286.

(19) Riveros, G.; González, G.; Chornik, B. *J. Braz. Chem. Soc.* **2010**, *21* (1), 25.

(20) Lattimer, J. R. C.; Brunschwig, B. S.; Lewis, N. S.; Gray, H. B. *J. Phys. Chem. C* **2013**, *117* (51), 27012.

(21) Huang, K.; Duclairoir, F.; Pro, T.; Buckley, J.; Marchand, G.; Martinez, E.; Marchon, J.-C.; De Salvo, B.; Delapierre, G.; Vinet, F. *ChemPhysChem* **2009**, *10* (6), 963.

(22) Marrani, A. G.; Dalchiele, E. A.; Zanoni, R.; Decker, F.; Cattaruzza, F.; Bonifazi, D.; Prato, M. *Electrochim. Acta* **2008**, *53* (11), 3903.

(23) Bateman, J. E.; Eagling, R. D.; Worrall, D. R.; Horrocks, B. R.; Houlton, A. *Angew. Chem., Int. Ed.* **1998**, *37* (19), 2683.

(24) Yu, J.; Shapter, J. G.; Johnston, M. R.; Quinton, J. S.; Gooding, J. J. *Electrochim. Acta* **2007**, *52* (21), 6206.

(25) Song, Y.; Kang, X.; Zuckerman, N. B.; Phebus, B.; Konopelski, J. P.; Chen, S. *Nanoscale* **2011**, *3* (5), 1984.

(26) Dorokhin, D.; Tomczak, N.; Reinhoudt, D. N.; Velders, A. H.; Vancso, G. J. *Nanotechnology* **2010**, *21* (28), 285703.

(27) Gagne, R. R.; Koval, C. A.; Lisensky, G. C. *Inorg. Chem.* **1980**, *19* (9), 2854.

(28) Wolkin, M. V.; Jorne, J.; Fauchet, P. M.; Allan, G.; Delerue, C. *Phys. Rev. Lett.* **1999**, *82*

(1), 197.
(29) Holmes, J. D.; Johnston, K. P.; Doty, R. C.; Korgel, B. A. *Science* **2000**, *287* (5457), 1471.
(30) Purkait, T. K.; Iqbal, M.; Wahl, M. H.; Gottschling, K.; Gonzalez, C. M.; Islam, M. A.; Veinot, J. G. C. *J. Am. Chem. Soc.* **2014**, *136* (52), 17914.
(31) Cheng, X.; Lowe, S. B.; Ciampi, S.; Magenau, A.; Gaus, K.; Reece, P. J.; Gooding, J. J. *Langmuir* **2014**, *30* (18), 5209.
(32) Dorokhin, D.; Tomczak, N.; Velders, A. H.; Reinhoudt, D. N.; Vancso, G. J. *J. Phys. Chem. C* **2009**, *113* (43), 18676.
(33) Mobarok, M. H.; Buriak, J. M. *Chem. Mater.* **2014**, *26* (15), 4653.
(34) Avramov, P. V; Fedorov, D. G.; Sorokin, P. B.; Chernozatonskii, L. A.; Gordon, M. S. *arXiv Prepr. arXiv0709.2279* **2007**, 1.
(35) Hua, F.; Swihart, M. T.; Ruckenstein, E. *Langmuir* **2005**, *21* (13), 6054.
(36) Hessel, C. M.; Henderson, E. J.; Veinot, J. G. C. *J. Phys. Chem. C* **2007**, *111* (19), 6956.
(37) Fischer, A. B.; Wrighton, M. S.; Umana, M.; Murray, R. W. *J. Am. Chem. Soc.* **1979**, *101* (13), 3442.
(38) Rehm, J. M.; McLendon, G. L.; Fauchet, P. M. *J. Am. Chem. Soc.* **1996**, *118* (18), 4490.
(39) Huck, L. A.; Buriak, J. M. *J. Am. Chem. Soc.* **2012**, *134* (1), 489.
(40) Swart, I.; Liljeroth, P.; Vanmaekelbergh, D. *Chem. Rev.* **2016**, acs.chemrev.5b00678.
(41) Banin, U.; Cao, Y.; Katz, D.; Millo, O. *Nature* **1999**, *400* (6744), 542.
(42) Banin, U.; Millo, O. *Annu. Rev. Phys. Chem.* **2003**, *54* (1), 465.

Chapter 3 Investigation into the Effect of Surface Chemistry on the Photostability of Silicon Nanocrystals

3.1 Introduction to the Photostability of Silicon Nanocrystals

The PL properties of semiconductor nanoparticles (or QDs) make them an attractive material for many optoelectronic devices[1–3] and imaging applications.[4,5] QDs are an alternative to fluorescent molecules because of their bright, size-dependent photoluminescence and imaging technologies are taking advantage of their use.[4,6] Among QD materials, silicon is a prime candidate for these applications due to its biocompatibility.[5] However, despite the promising application of silicon, there are still some limitations, particularly the long-term stability of SiNC PL.

Imaging with QDs offers numerous benefits over doing so with fluorescent molecules. The long excited state lifetimes of PL can decrease the noise associated with the auto-fluorescence of the surrounding tissues.[7] Size dependent PL and broad absorption profiles make QDs ideal for imaging multiple wavelengths simultaneously.[6] QDs can also be less susceptible to photobleaching than molecular probes.[8] Tailorable surface chemistry increases the versatility of QDs for targeted imaging.[8] Unfortunately, QDs based upon II-VI or III-V semiconductors contain toxic elements and have sparked concern over their toxicity and application in bioimaging.[9] For example, CdSe QDs can be cytotoxic if not capped with a passivating shell such as ZnS; even with this apparent passivation these core-shell materials can still show significant toxicity under intense UV light.[10]

Silicon QDs exhibit many of the same properties as other inorganic quantum dots but with one key advantage - biocompatibility.[11,12] Target molecules can also be attached to SiNC surfaces allowing versatility for different imaging applications.[13] Despite the appeal of SiNCs in bioimaging applications there are still challenges associated with their PL that may limit their use in imaging or other optoelectronic applications.

Despite showing promising optical properties, SiNCs can still suffer from photobleaching (i.e., the decrease in PL intensity that arises as a result of prolonged excitation).[14] For prototypical CdSe and CdS quantum dots it has been proposed that photobleaching results from photo-enhanced oxidation and/or the creation of surface trap states.[15,16] Epitaxial growth (Scheme 3.1a) of an inorganic shell of high band gap material (e.g., ZnS) helps protect the QD core from oxidation and the resulting PL degradation.[15] This shell structure also reduces the Auger recombination process that also contributes to photobleaching of quantum dots.[17] To date no equivalent epitaxial core-shell structure has been realized for silicon nanocrystals.[18] Surface modification of SiNCs has largely been limited to functionalization of organic surface groups.[19]

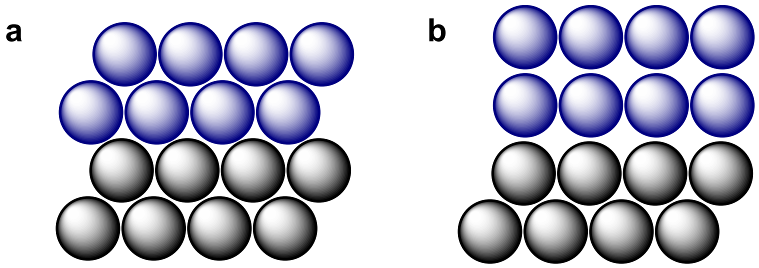

Scheme 3.1 (a) The epitaxial growth of materials with matched interfacial crystal structures and (b) nonepitaxial growth between interfacial crystal structures. Epitaxial growth is the addition of a crystalline layer over another crystalline layer or substrate.

The PL response of SiNCs is complex; quantum confinement,[20,21] surface chemistry,[22] oxidation,[23] and UV exposure[24] all play roles. Controlled manipulation of SiNC PL offered by quantum confinement and surface chemistry is advantageous; however, oxidation[25,26] and extended UV exposure[24,27] are detrimental to SiNC PL stability. Both oxidation[18,28] and UV exposure[29,30] lead to surface trap states that have deleterious affects on SiNC PL. Further understanding of SiNC PL response under degrading conditions such as oxidation and UV exposure will certainly increase the likelihood that SiNC will supplant organic molecules and toxic metal-based QDs in many optical applications.

To that end, the optical response of SiNCs with a series of surface groups was studied under photobleaching conditions. Although not all-inclusive, the functional groups chosen reflect the wide range of functional group tolerance provided by methods used to tailor SiNC surface chemistry. Dependence of SiNC photobleaching response on surface chemistry may provide insight into achieving silicon nanocrystals with increased PL stability.

3.2 Experimental

3.2.1 Reagents and Materials

HSQ was purchased as Fox 18 from DOW Corning. The solvent was removed to give a white solid. Technical grade 48-50% hydrofluoric acid was purchased from Fisher Scientific. Toluene (99.9% HPLC grade, anhydrous dried using solvent system), methanol (99.8% Reagent grade), and acetonitrile (99.9% HPLC grade, dried using solvent system) were purchased from Sigma Aldrich. Ethanol was reagent grade. 1-dodecene (95%) was ordered from Sigma Aldrich. 1-dodecene was passed over activated alumina prior to use. 2-octanone (98% Reagent grade) and 1-pentene (98%) were purchased from Sigma Aldrich. 1H, 1H', 2H-Perfluoro-1-octene (99%)

was purchased from Alfa Aesar. 2-octanone, 1-pentene and 1H, 1H', 2H-Perfluoro-1-octene were also passed over activated alumina prior to use.

3.2.2 Hydride Terminated Freestanding 3 nm Silicon Nanocrystals

Generally, 3.0 g of HSQ was transferred to a quartz boat and processed at 1100 ˚C in a flowing 5%/95% hydrogen/argon atmosphere for one hour at a heating rate of 18 ˚C/min. The resulting brown black solid was ground using an agate mortar and pestle to a brown powder. This powder was shaken in a wrist action shaker with silica beads for approximately 15 hours. The resulting fine powder was suspended in ethanol and transferred to a filter. After filtering, the solid was air dried. The resulting solid was briefly ground again to break up large aggregates prior to etching.

The composite (0.15 g) was placed in a Teflon beaker. Equal volumes of deionized water, ethanol and HF were added and the mixture was stirred for one hour at room temperature. The cloudy, pale yellow mixture was extracted with 15 mL toluene three times. The toluene extract containing hydride terminated SiNCs was centrifuged for 10 minutes at 3000 rpm to afford an orange solid and clear colourless supernatant. The supernatant was discarded and the solid was used in the functionalization procedures noted below.

3.2.3 Silicon Nanocrystal Surface Modification

3.2.3.1 Dodecyl-Terminated Silicon Nanocrystals: Sample 1 (SiNC-D1)

Hydride terminated SiNCs (d ~ 3 nm) were re-dispersed in 5 mL of 1-dodecene. The mixture was mixed over molecular sieves for approximately 1 minute to remove trace moisture and transferred to a Schlenk flask under argon. The Schlenk flask was evacuated and refilled with argon in triplicate. The reaction mixture was stirred under argon at 180 ˚C for 15 hours.

The resulting clear orange solution was transferred equally to two 40 mL (PTFE) centrifuge tubes. Additional toluene (ca. 7 mL) was added to each tube. The particles were precipitated upon adding 5 mL ethanol and 20 mL methanol to each tube to yield a cloudy yellow mixture. Centrifugation at 12000 rpm was performed and the clear colourless supernatant discarded. The solid residue in each centrifuge tube was resuspended in 7 mL toluene and precipitated upon addition of 25 mL methanol followed by centrifugation to provide an orange solid. This solvent/anti-solvent and centrifugation procedure was repeated three times. The final product was resuspended in toluene and filtered through a 0.45 μm PTFE filter into a vial. No effort was made to exclude air during the purification procedures.

3.2.3.2 Dodecyl-Terminated Silicon Nanocrystals: Sample 2 (SiNC-D2)

The preparative method described for SiNC-D1 was employed. No effort was made to exclude air during the purification procedure, but after purification the solvent was removed in vacuo and the sample was immediately transferred to a nitrogen filled glovebox.

3.2.3.3 Dodecyl-Terminated Silicon Nanocrystals: Sample 3 (SiNC-D3)

Approximately 30 mg of 3 nm hydride terminated silicon nanocrystals were transferred to a small Schlenk tube with 5 mL benzene. The flask was submerged in liquid nitrogen. Once the solvent was frozen, the flask was put under vacuum and was then removed from the liquid nitrogen. After the solvent was sublimed, the particles were transferred to a nitrogen filled glovebox and transferred to a vial. 1-dodecene and dry toluene (3 mL each) were added to afford a cloudy yellow suspension. A small amount (less than 10 mg) of XeF_2 initiator was added to the stirring mixture. After approximately 60 seconds a clear orange solution resulted.

The solution was transferred to a small PTFE centrifuge tube in the glove box and 15 mL of dry acetonitrile was added as an anti-solvent. The cloudy orange suspension was sealed in the centrifuge tube, removed from the glove box, and centrifuged for 25 minutes at 12000 rpm. The clear colourless supernatant was decanted in the glove box and the residue was dispersed in toluene (3 mL) and 12 mL of dry acetonitrile was added to induce precipitation. Centrifugation was repeated. This solvent/anti-solvent purification procedure was repeated three times. Finally, the particles were dissolved in a minimal amount of dry toluene and filtered through a 0.2 micrometer PTFE syringe filter into a vial and stored in a nitrogen filled glove box.

3.2.3.4 Alkoxy-Terminated Silicon Nanocrystals (SiNC-A)

The same preparative method outlined for sample SiNC-D3 was employed using 2-octanone in place of 1-dodecene. A clear orange solution resulted after approximately 60 seconds after initiator addition. The solution was centrifuged three times with a 1:4 ratio of dry toluene to dry acetonitrile using the solvent/anti-solvent approach as outlined for the purification of SiNC-D3, filtered and transferred to a vial in a nitrogen filled glovebox.

3.2.3.5 Perfluoro-Terminated Silicon Nanocrystals (SiNC-B)

The method used to prepare SiNC-D3 was employed but 1H,1H',2H perfluoro-1-octene was employed in place of 1-dodecene. A clear orange solution results. No purification was performed due to limited solvent compatibility.

3.2.3.6 Pentyl-Terminated Silicon Nanocrystals (SiNC-C)

The preparative method used to SiNC-D3 was employed, but the particles were functionalized with 1-pentene in place of 1-dodecene. A clear orange solution results. No purification was performed.

3.3 Materials Characterization

3.3.1 Fourier Transform Infrared Spectroscopy

FTIR was performed using a Thermo Nicolet 8700 FTIR Spectrometer and Continuum FTIR Microscope. Samples were prepared in a nitrogen filled glove box by drop casting a thin film from toluene onto a silicon wafer, residual solvent was removed and the samples were sealed in vials. Samples were removed for the glove box and the FTIR spectra were recorded immediately.

3.3.1.1 FTIR Study of Surface Chemistry Changes

SiNC samples were prepared and analyzed as outlined in Section 3.3.1. An initial baseline spectrum was recorded at time zero. The samples were exposed to UV radiation from the same UV LED used for photobleaching studies below and the FTIR spectra were rerecorded at predetermined times.

3.3.2 X-ray Photoelectron Spectroscopy

XPS experiments where performed at room temperature using a Kratos Axis spectrometer with monochromatized Al Kα (hυ = 1486.71 eV). The pressure of the chamber was maintained at or below 5×10^{-10} Torr. Samples were drop cast from solution onto a copper foil. A hemispherical electron-energy analyzer working at the pass energy of 20 eV was used to collect core-level spectra while survey spectra within a range of binding energies from 0 to 1100 eV were collected at an analyzer pass energy of 160 eV. All spectra were calibrated to the adventitious carbon 1s peak at 248.8 eV.

3.3.3 Transmission Electron Microscopy

Bright field TEM images were recorded with a JOEL2011TEM equipped with a LaB_6 filament using an accelerating voltage of 200 kV. TEM samples were prepared by depositing a droplet of dilute functionalized SiNC toluene suspensions onto a holey carbon coated copper grid and the solvent was removed under vacuum. The size distribution of each sample of particles was determined using Imagej software on over 200 particles.

3.3.4 Photobleaching of Silicon Nanocrystals

100 microliters of approximately 3 mg/mL SiNC solutions where drop cast onto quartz wafers in a nitrogen filled glovebox. After the wafers were dry, they were placed under vacuum for 20 minutes and sealed under nitrogen prior to removal from the glovebox. The samples were loaded into a chamber with an optical window for photoluminescence measurements. A Varian Turbo Dry 70 vacuum pump with a Varian BA2C senTorr gauge controller were used for inert atmosphere measurements. A pressure of at least 1.0×10^{-4} Torr was reached before starting the photobleaching experiments. Excitation of the SiNCs was achieved with a 365 nm LED purchased from Prizmatixs. The excitation power of the LED was 245 mW/cm^2. PL was collected by optic fiber and recorded using an Ocean Optics spectrometer and Spectra Suite software. All spectra were corrected to a blackbody radiator. PL spectra were collected every 3

seconds for a minimum of 60 minutes. A minimum of two replicate photobleaching experiments were performed for each sample in inert conditions and air with the exception of experiments involving SiNC-D1 which were only recorded once in air. Spectra were processed using a custom program modified from Ross Lockwood. To determine peak wavelengths and shifts the PL spectra where fit using a skew normal distribution.

3.3.5 Radiative Decay measurements of Silicon Nanocrystals

PL lifetime decay measurements were performed using a Coherent Enterprise laser operated at 351 nm and a power of 20 mW. An acousto-optic modulator operating at 200 Hz with a 50% duty cycle was used to modulate the excitation source. A Hamamatsu H7422 photomultiplier tube was used as the collector. The decay was first measured in vacuum (less than 1.0×10^{-4} Torr). After the initial measurement air was introduced into the apparatus and the lifetime was rerecorded. The lifetimes were fit using a log normal distribution analysis in Matlab.

3.4 Results

3.4.1 Silicon Nanocrystal Characterization

A series of SiNCs bearing different surface groups was prepared in order to investigate the effect of surface chemistry on photobleaching. Characterization of the NCs by FTIR revealed expected features related to the target surface groups. The FTIR spectra of all the samples are shown in Fig 3.1. Surface hydride and oxide are present in all SiNC samples. For the dodecyl-terminated particles, SiNC-D1, SiNC-D2, and SiNC-D3, the FTIR spectra indicate the presence of long chain alkyl groups at approximately 3000 to 2800 cm^{-1}. Residual Si-H on all the particles is indicated by the peak between 2000 and 2100 cm^{-1}. Si-O stretching between 1000 and 1100

cm^{-1} is present in all dodecyl functionalized SiNC FTIR spectra as well. SiND-D3 functionalized via XeF_2 in inert atmosphere still shows the presence of oxygen despite efforts to minimize exposure. However, the Si-O feature for the SiND-D3 sample is less intense relative to C-H stretch of the dodecyl group. SiNC-C functionalized with pentene using the same XeF_2 preparative method inside the glove box also shows a substantial amount of oxide. Confirmation of functionalization with 1-pentene is observed by the C-H stretches shown in the FTIR at 2962 to 2849 cm^{-1}.

The FTIR spectrum of perfluoro functionalized SiNCs, SiNC-B, shows an alkyl stretching feature between 2924 and 2853 cm^{-1}. An unsaturated $–CH_2$ stretching feature is also observed at 3309 cm^{-1} suggesting the presence of unreacted ligand. The feature at 2110 cm^{-1} is attributed to residual silicon hydride bonds. The broad peak between 1300 and 1050 cm^{-1} is consistent with the presence of C-F bonds.[31] Surface oxide cannot be discounted as the absorption may be obscured by the board nature of the C-F peak.

Alkoxy functionalized SiNCs (i.e., SiNC-A) show features typical of alkyl surface groups. Evidence of residual hydride is also present. There is also a relatively weak, broad absorption at approximately 1083 cm^{-1} and is likely a combination of Si-O due the surface bond as well as partial surface oxidation.

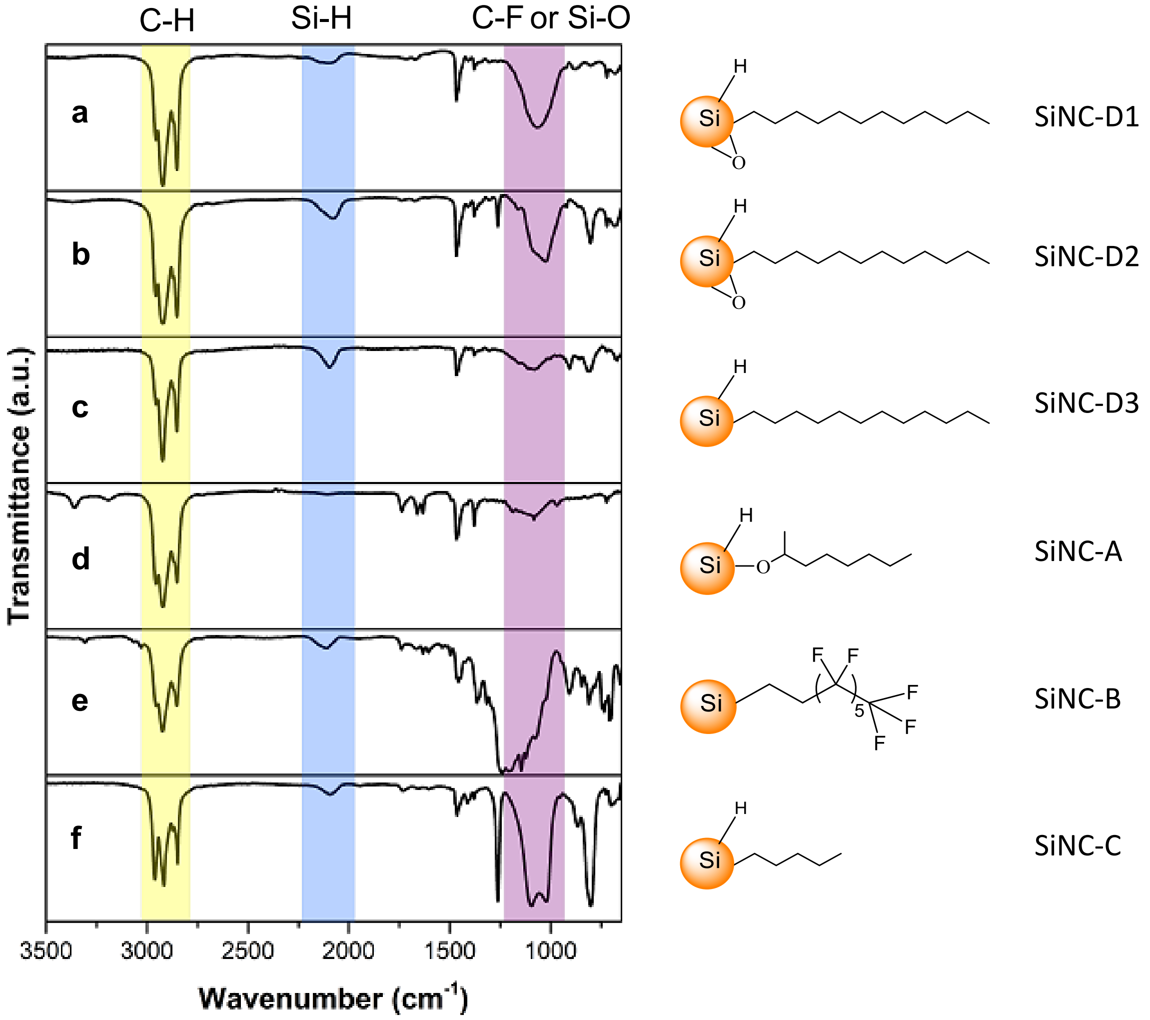

Fig 3.1 FTIR spectra with the corresponding nanocrystal structure and sample numbers.

XPS is useful in evaluating the oxidation states of the SiNCs. Survey scans of the SiNCs are shown in Fig 3.2. XPS of the particles indicates that functionalized NCs retain a Si (0) core typical of binding energies close to 99.3 eV (Fig 3.3). Higher binding energy components are also evident and are a result of Si-C bonds (approximately 102 eV)[32] as well as sub-oxides (103.5 - 104 eV).[20,32,33]

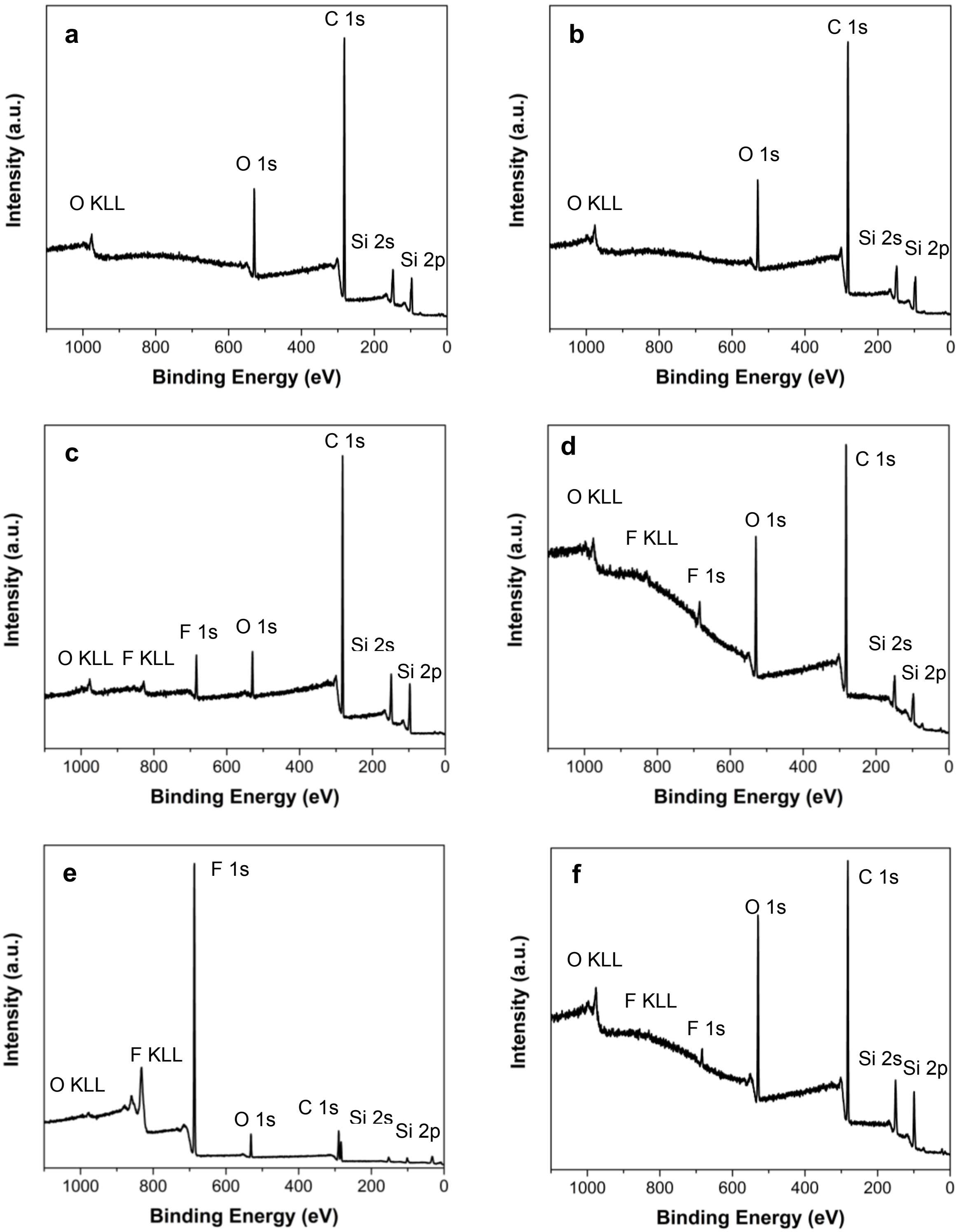

Fig 3.2 XPS survey scans of functionalized SiNCs (a) SiND-D1, (b) SiNC-D2, (c) SiNC-D3, (d) SiNC-A, (e) SiNC-B, and (f) SiNC-C.

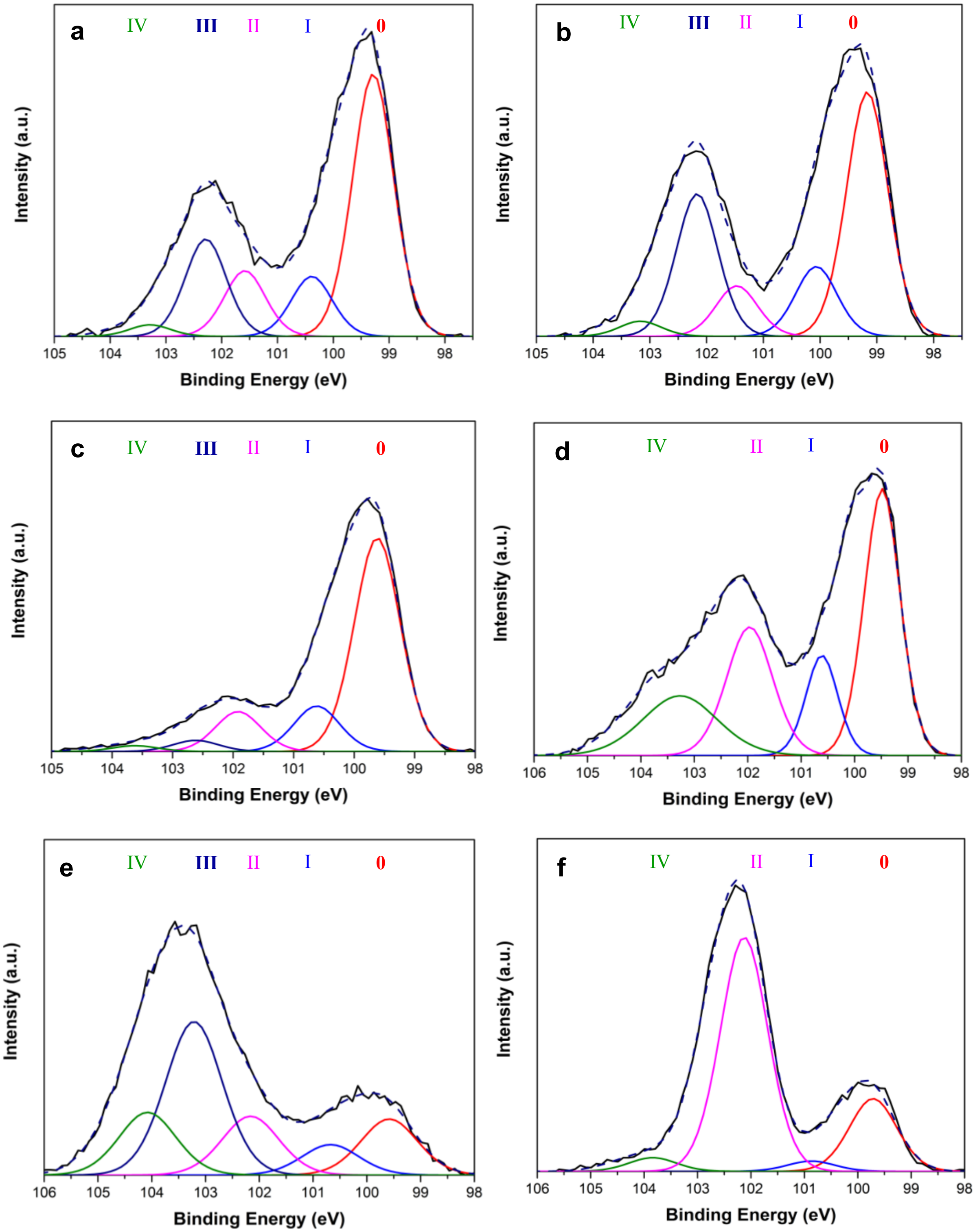

Fig 3.3 XP spectra of the silicon 2p region of functionalized SiNCs, (a) SiND-D1, (b) SiNC-D2, (c) SiNC-D3, (d) SiNC-A, (e) SiNC-B, and (f) SiNC-C. The Si 2p½ fitting features have been omitted for clarity. The oxidation states of Si correspond to the roman numerals. The colour of the oxidation states also corresponds to the colours of the roman numerals.

Transmission electron microscopy (TEM) indicates the presence of particles in all samples (Fig 3.4). Dodecyl modified SiNCs (i.e., SiNC-D1, SiNC-D2, and SiNC-D3) had size distributions of 3.0 ± 0.7 (Fig 3.5a), 3.5 ± 0.8 (Fig 3.5b), and 2.3 ± 0.6 nm (Fig 3.5c) respectively. SiNC-A (i.e., the alkoxy functionalized SiNCs) had a size distribution of 3.1 ± 0.6 nm (Fig 3.5d). Pentyl functionalized SiNC-C had a size distribution of 2.7 ± 0.6 nm (Fig 3.5f). Perfluoro-modified SiNC-B had a larger than expected average size of 5.0 ± 1.0 nm (Fig 3.5e) and largest standard deviation. The origin of the larger size of the SiNC-B is unclear, but may result from the mistaken use of a precursor composite initially containing larger sized particles (i.e., processed at a higher temperature).

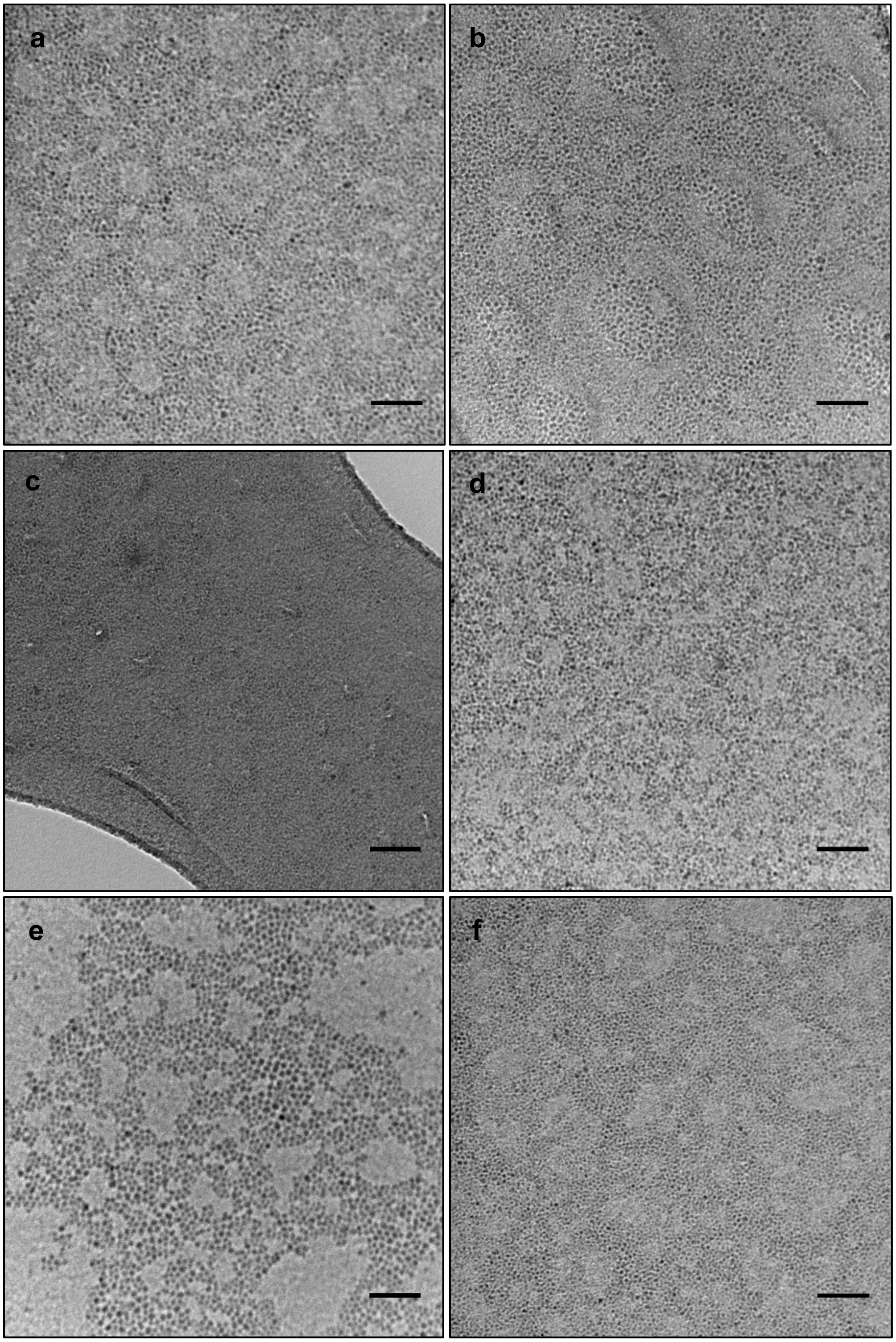

Fig 3.4 TEM images of (a) SiN-D1, (b) SiNC-D2, (c) SiNC-D3, (d) SiNC-A, (e) SiNC-B and (f) SiNC-C. All scale bars are 50 nm.

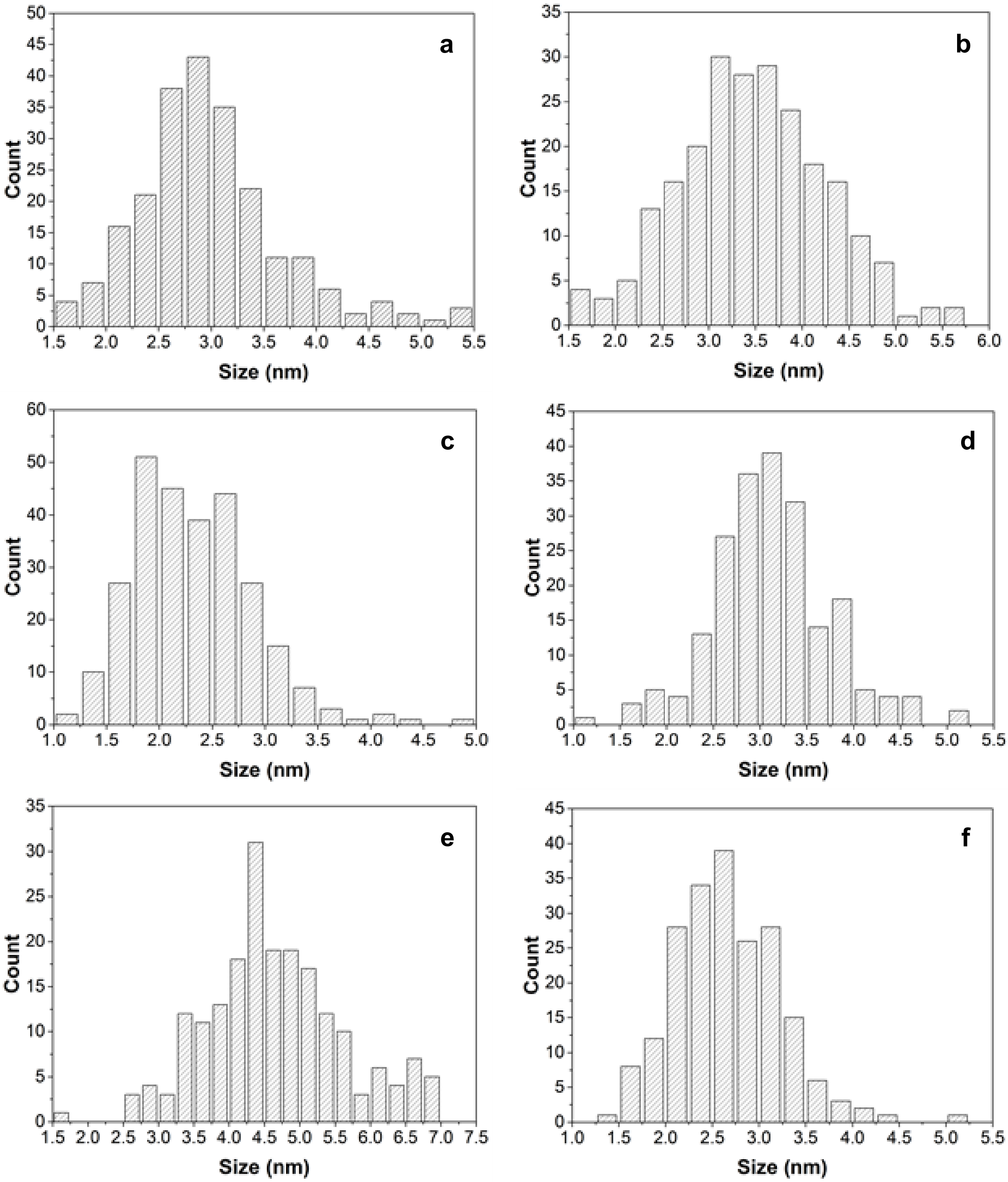

Fig 3.5 Particle size distributions of SiNCs (a) SiN-D1, (b) SiNC-D2, (c) SiNC-D3, (d) SiNC-A, (e) SiNC-B and (f) SiNC-C. Over 200 particles were used for each individual distribution.

3.4.2 Photobleaching Studies of Silicon Nanocrystals

Samples were drop cast onto quartz wafers in a nitrogen filled glovebox. While this was found to be the most consistent method of deposition, particle agglomeration could not be avoided. Spin casting of the wafers was also investigated, however, it could only be performed outside the glovebox and resulted in poor substrate coating.

Photobleaching studies were conducted under ambient and high vacuum conditions. High vacuum conditions where used to minimize the effect of air and oxygen during photobleaching. Despite all efforts, very limited exposure to air could not be eliminated; wafers were exposed to air briefly (less than 5 minutes) when transferring from the sealed vial to the vacuum apparatus. It is expected that surface passivation of the SiNC minimizes (even eliminates) the impact of this brief exposure.

3.4.2.1 Photobleaching in Ambient Conditions

The alkyl surface treatments, SiNC-C (Fig 3.10) and SiNC-D1 (Fig 3.6) showed the most resistance to photobleaching in ambient conditions. The first photobleaching trial of pentyl functionalized SiNC-C showed a decrease to 76 and 46% of the initial PL intensity after 5 and 60 minutes, respectively. The second trial showed a larger decrease to 42% in 5 minutes and 22% of the initial intensity after 60 minutes of photobleaching. The SiNC-D1 sample (i.e., oxidized dodecyl functionalized SiNCs) reached an intensity of 64% after 5 minutes and 37% after 60 minutes of photobleaching in ambient conditions. These NCs possess the greatest surface oxide as evidenced by the Si-O region of the FTIR spectrum, however close examination of the Si-O features suggests the oxide species differ for these two samples. This difference in the nature of the oxide may account for the differences observed in PL response between the pentyl (i.e., SiNC-C) and oxidized dodecyl system. Interestingly, dodecyl capped SiNCs prepared while attempting to limit surface oxidation (i.e., SiNC-D2, Fig 3.7; SiNC-D3, Fig 3.8) were not as resistant to photobleaching in air as SiNC-D1. After 60 minutes, SiNC-D2 and SiNC-D3 had intensities of between 4 and 15% for all experimental replicates.

Perfluoro-functionalized SiNC-B (Fig 3.9) did not show any increased resistivity to photobleaching in ambient conditions. They showed a decrease to 7% for both trials after 60 minutes. It is reasonable that the perfluoro functionalization renders the surface hydrophobic which would limit surface access of atmospheric water that would reasonably oxidize SiNCs upon photoexcitation.[31]

The PL response of alkoxy functionalized SiNC-A decreased dramatically within the first 5 minutes of light exposure to 11% of the initial PL intensity. After 60 mintues 6% PL intensity remained (Fig 3.11). This observation is consistent with the observations that the nature of the Si-O species and ability of water to access the SiNC surface impact the SiNC PL. It is reasonable that the Si-OR species will evolve with light exposure and the H-bonding acceptor properties of the Si-OR moieties will promote water-surface interaction leading to surface oxidation.

The maximum wavelength of the PL spectra was resolved as a way to quantify changes throughout the photobleaching process. Wavelength shifts have been previously associated with the creation of surface states affecting SiNC PL.[18] The peak wavelength profiles for all the nanocrystals and for each trial are shown in Appendix II. Within the first 5 minutes all of the samples except for SiNC-D1 (the oxidized dodecyl SiNCs) shown an initial blue-shift of the peak wavelength maximum. However, it was often observed that the initial decrease in PL maxima was followed by a gradual increase (red-shift) in PL wavelength maxima. Examples of this behavior are seen in Fig 3.9f and Fig 3.11f. The initial blue-shift seen in air for the majority of the samples could be due to oxidation of silicon nanocrystals causing a decrease in crystalline core size.[34,35]

There is also some variation in wavelength shifts between successive experimental replicate profiles of the same sample in ambient conditions. Pentyl functionalized SiNC-B initially showed a blue-shift from 628 to 580 nm after 60 minutes. The subsequent replicate of SiNC-B showed a blue-shift from 648 to 630 nm within the first 5 minutes, followed by a red-shift to 634 nm after 60 minutes. The alkoxy functionalized sample, SiNC-A, showed only a blue-shift from 651 to 644 nm after 60 minutes. For SiNC-A only one experiment was carried out to 60 minutes. Both SiNC-D2 (partially oxidized dodecyl functionalized SiNCs) and SiNC-D3 (minimally oxidized dodecyl functionalized SiNCs) showed the same behavior for all experimental replicates - an initial decrease of wavelength over the first 5 minutes followed by a gradual increase over 60 minutes. Shifts from 696 to 693 nm and then to over 693 nm was observed for SiNC-D2. SiNC-D2 also shifted from 693 to 691 nm then to 692 nm. SiNC-D3 blue-shifted from 635 to 622 nm then to 625 nm. The second replicate for SiNC-D3 shifted from 641 to 623 nm then above 623 nm in 60 minutes. SiNC-D1, also with only one experimental trial, showed a red-shift from 690 to 695 nm over 60 minutes.

3.4.2.2 Photobleaching of Silicon Nanocrystals in Vacuum Conditions

In inert atmosphere conditions the amount of photobleaching is lessened for all surface chemistries. It is assumed that there is little or no free oxygen or water present that can facilitate the photobleaching. UV irradiation is presumed to be the dominate source of photobleaching.[29]

Significant variations in photobleaching responses between SiNC samples was observed under inert atmosphere.

The PL spectrum of the oxidized dodecyl functionalized SiNC-D1 under UV irradiation in vacuum shows a moderate amount of photobleaching as see in Fig 3.6a and c. The majority of the photobleaching (approximately 10% of the initial intensity) occurs within the first 10 minutes of exposure to UV radiation. After 60 minutes a final intensity between 80 and 90% is observed for all three replicates. The wavelength of the PL initially shows a small red-shift in PL maxima followed by a slow decrease in wavelength (Fig 3.6e). The profile of the wavelength shift (a small red-shift followed by slow blue-shift) was consistent between all three sample replicates in inert atmosphere. The red-shift in all cases was approximately 1 nm followed by a blue-shift to, or near to, the starting wavelength. The initial starting wavelength shifted from 695 nm to 681 nm over the period of time required to complete three photobleaching measurements for SiNC-D1 (approximately one month).

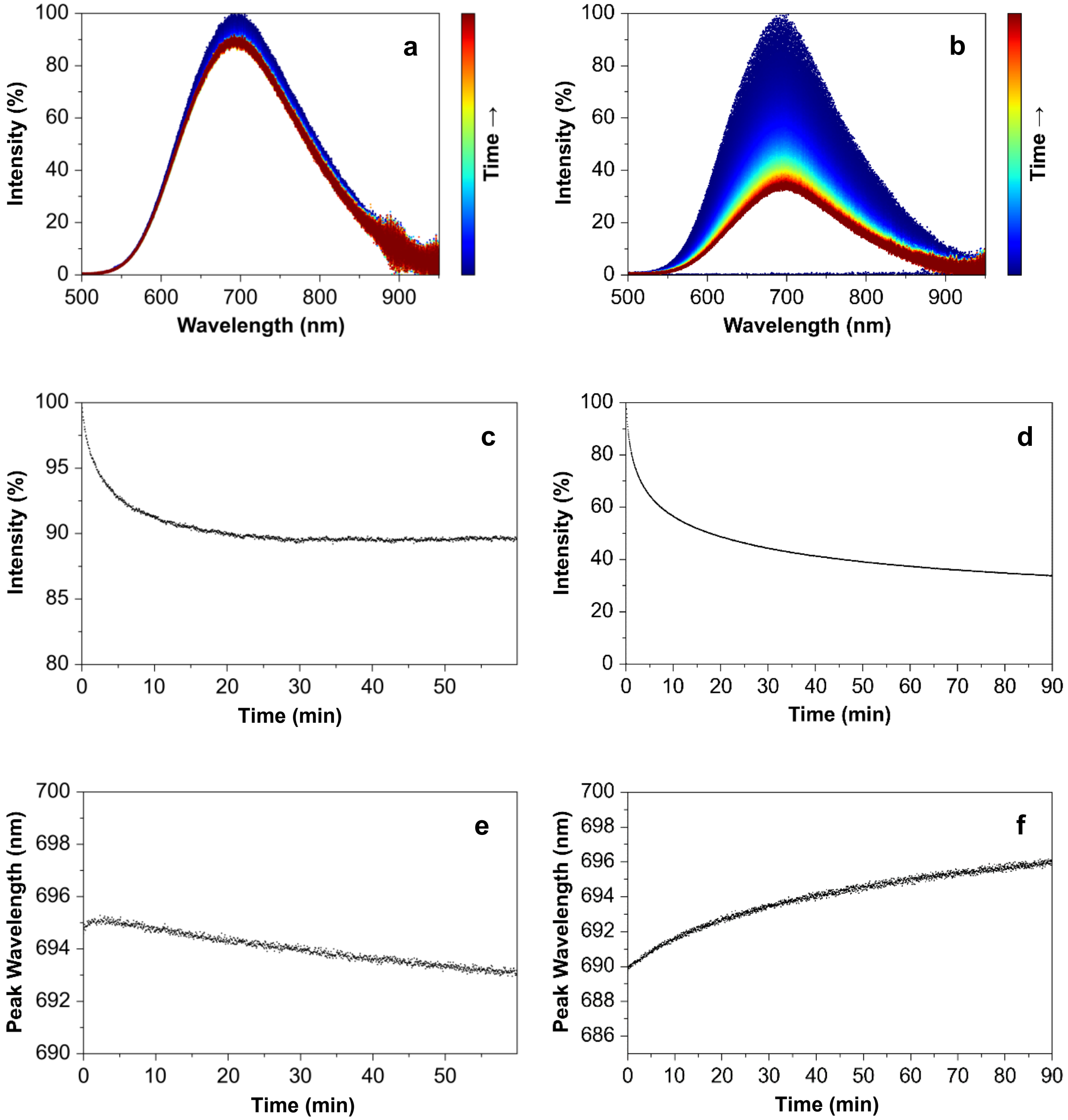

Fig 3.6 Photobleaching profiles for SiNC-D1, oxidized dodecyl functionalized silicon nanocrystals. The (a) PL spectra of the sample as a function of time, (c) PL intensity profile and (e) the approximate peak wavelength under continuous UV illumination in inert atmosphere are shown. The (b) PL spectra (d) PL intensity and (f) approximate peak wavelength of the sample are also shown under normal atmospheric conditions as a function of time.

The PL spectra SiNC-D2 (partially oxidized dodecyl functionalized SiNCs) shows a small degree of photobleaching for all of the experimental replicates. The PL intensity plots show a small initial decrease in PL intensity following the first 2 minutes of exposure to the UV irradiation. However, there was variation between all three photobleaching experiments after 5 minutes of exposure for sample SiNC-D2. The first experiment showed a decrease in PL intensity followed by a plateauing of the photobleaching at approximately 93% after about 60 minutes of exposure. In the following two replicate experiments, a small initial decrease in PL intensity to approximately 96% was observed in the first 5 minutes but was followed by an increase to approximately 98% of the original PL intensity as seen in Fig 3.7c within 60 minutes. The photobleaching profiles for all the replicates of SiNC-D2 in vacuum are shown in Appendix II.

The PL photobleaching profiles were fairly consistent between experiments and showed a blue-shift in PL maxima of 1 to 2 nm during 60 minutes of UV exposure. Over the course of approximately one month required to complete the experimental replicates, there was a small blue-shift of the starting PL maxima from approximately 691 to 687 nm. This was similar to the behavior observed for SiNC-D1.

The photobleaching of the minimally oxidized dodecyl functionalized SiNCs (SiNC-D3) showed an interesting trend. Initial exposure to UV light caused the PL intensity to increase. After reaching a maximum the PL began to gradually decrease to about 80 to 85% of the maximum intensity reached in 60 minutes (Fig 3.8a and c). A slight blue-shift in the PL of approximately 3 nm was observed for all sample replicates. It was also observed for SiNC-D3 that the starting wavelength maxima red-shifted from 640 to 644 nm during the time required for collection of all sample replicates.

The alkyl functionalized particles were expected to all have similar photobleaching responses. However, the photobleaching profiles of the dodecyl samples SiNC-D1, SiNC-D2 and SiNC-D3 were all remarkably different in inert conditions. It is therefore not possible to rule out variations between SiNC samples despite having the same surface group. Prior surface oxidation is the likely cause of variation between photobleaching responses of the same surface group.

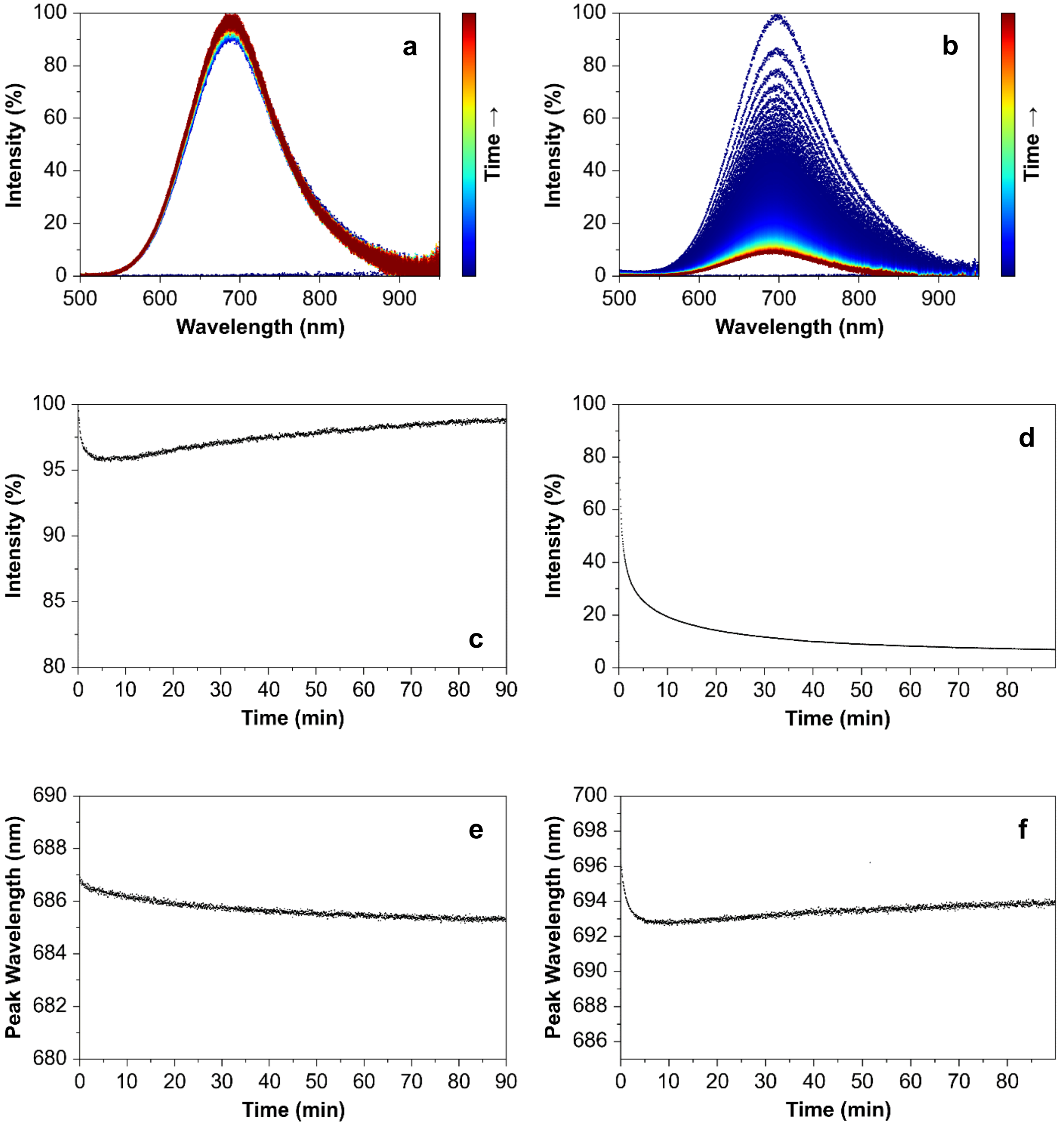

Fig 3.7 Photobleaching profiles for SiNC-D2, partially oxidized dodecyl functionalized silicon nanocrystals. The (a) PL spectra of the sample as a function of time, (c) PL intensity profile and (e) the approximate peak wavelength under continuous UV illumination in inert atmosphere are shown. The (b) PL spectra (d) PL intensity and (f) approximate peak wavelength of the sample are also shown under normal atmospheric conditions as a function of time.

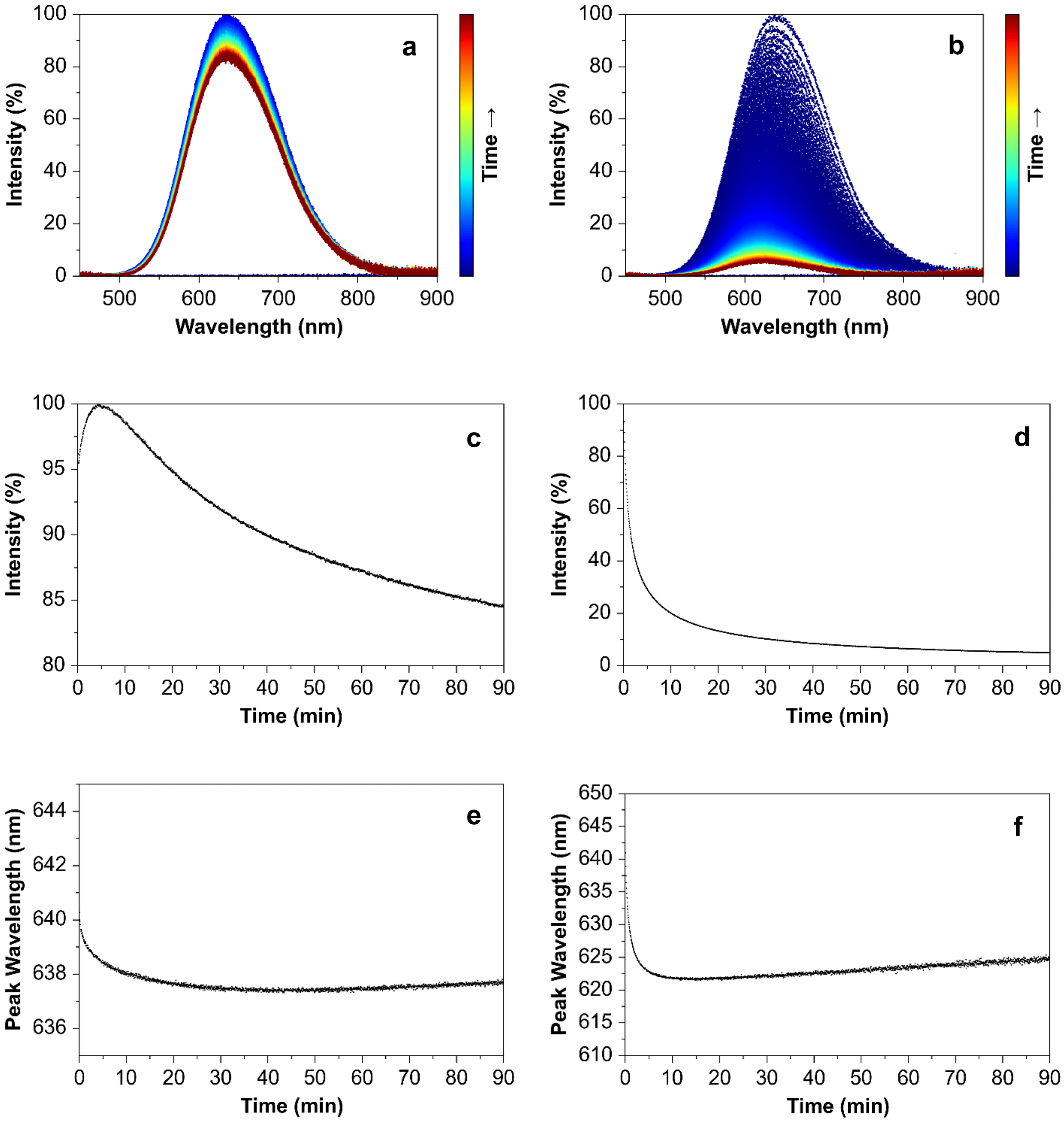

Fig 3.8 Photobleaching profiles for SiNC-D3, minimally oxidized dodecyl functionalized silicon nanocrystals. The (a) PL spectra of the sample as a function of time, (c) PL intensity profile and (e) the approximate peak wavelength under continuous UV illumination in inert atmosphere are shown. The (b) PL spectra (d) PL intensity and (f) approximate peak wavelength of the sample are also shown under normal atmospheric conditions as a function of time

Photobleaching experiments of the perfluoro functionalized NCs (SiNC-B) showed an interesting response. Exposure to the UV caused a very brief decrease in PL during the first minutes of the experiment (Fig 3.9a). A steady rise in the PL intensity is then observed for the remainder of the UV exposure. The initial PL intensity was approximately 85 -90% of the final intensity reached during the photobleaching experiments. The PL wavelength maximum also shows a steady red-shift throughout the experiment from 622 to 627 nm. The initial and final wavelengths were the same among all replicates of the sample. The increase or photo-enhancement of the PL from the perflouro-functionalized particles points to a passivation mechanism of UV-induced defects states that would otherwise decrease the PL intensity. Lockwood *et al*. observed an increase in PL intensity for hydride terminated particles irradiated with an argon laser.[35] However, the increase in PL intensity was only observed in ambient air and not under inert atmosphere conditions. [35] Previous observations of silicon nanocrystals photobleached in humid argon increased in PL intensity, suggesting passivation of surface dangling bonds by water molecules.[36] Given the inert atmosphere and hydrophobic surface group it is unlikely that water molecules would be able to passivate the surface and cause the increase in PL intensity. SiNC-B particles were also larger relative to the other samples. As a result, size variation cannot be ruled out as a compounding factor effecting the photobleaching of the particles.

The pentyl functionalized silicon nanocrystals (Fig 3.10) display a similar trend in photobleaching to the aforementioned oxidized dodecyl functionalized nanocrystals (SiND-D1) with respect to the amount of overall photobleaching. There is a slight variation between the intensity profiles for experimental replicates, however a decrease to 87% is observed in 60 minutes for both replicates. The overall wavelength shift was inconsistent between sample replicates. The first photobleaching experiment showed a blue-shift from 650 to 648 nm over 60 minutes. The second replicate showed a blue-shift from 648 to 647 nm in the first 5 minutes followed by a red-shift to 647 nm in 60 minutes.

The alkoxy functionalized silicon nanocrystals showed the largest amount of photobleaching under inert conditions. After 60 minutes of exposure the intensity varied from 65 to 50% of the initial intensity for the sample replicates. A typical spectra and photobleaching profile are shown in Fig 3.11a and c. A red-shift of the PL maxima was also observed for the duration of UV exposure for the first two replicates. A shift of 624 to 633 nm over 60 minutes was observed for the first trial and a shift from 625 to 637 nm was observed for the second replicate experiment. The third replicate experiment showed a blue-shift for the first 5 minutes of photobleaching from 630 nm to approximately 624 nm followed by a gradual red-shift of the wavelength maximum to 628 nm at 60 minutes. Given the presence of oxygen in the functional group, it is likely surface functionalized oxygen (Si-OR) is contributing to the photobleaching of the SiNCs. Polarization of the silicon atom bonded to the oxygen may inductively weaken other silicon-silicon surface bonds increasing the amount of photobleaching when exposed to UV under inert conditions. The polarization may facilitate a process similar to the Cabrera-Mott effect in which surface adsorbed water molecules polarize and weaken the Si-Si bond facilitating bond breakage.[37] A resulting dangling bond could act as a radiative trap decreasing the PL intensity.[29]

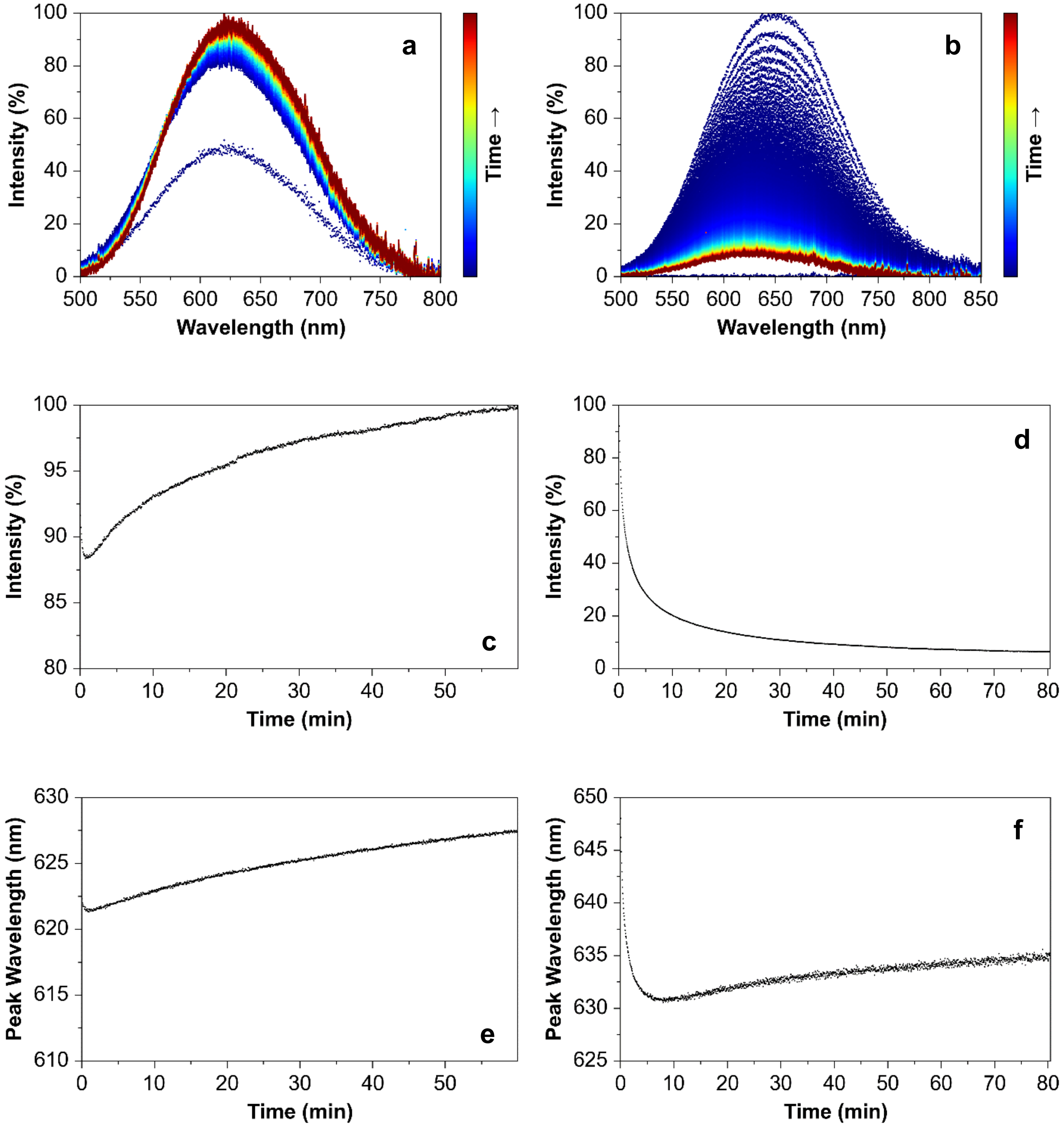

Fig 3.9 Photobleaching profiles for SiNC-B, perfluoro functionalized silicon nanocrystals. The (a) PL spectra of the sample as a function of time, (c) PL intensity profile and (e) the approximate peak wavelength under continuous UV illumination in inert atmosphere are shown. The (b) PL spectra (d) PL intensity and (f) approximate peak wavelength of the sample are also shown under normal atmospheric conditions as a function of time. The spectra in the middle of (a) is an artifact of the PL spectrum collection process.

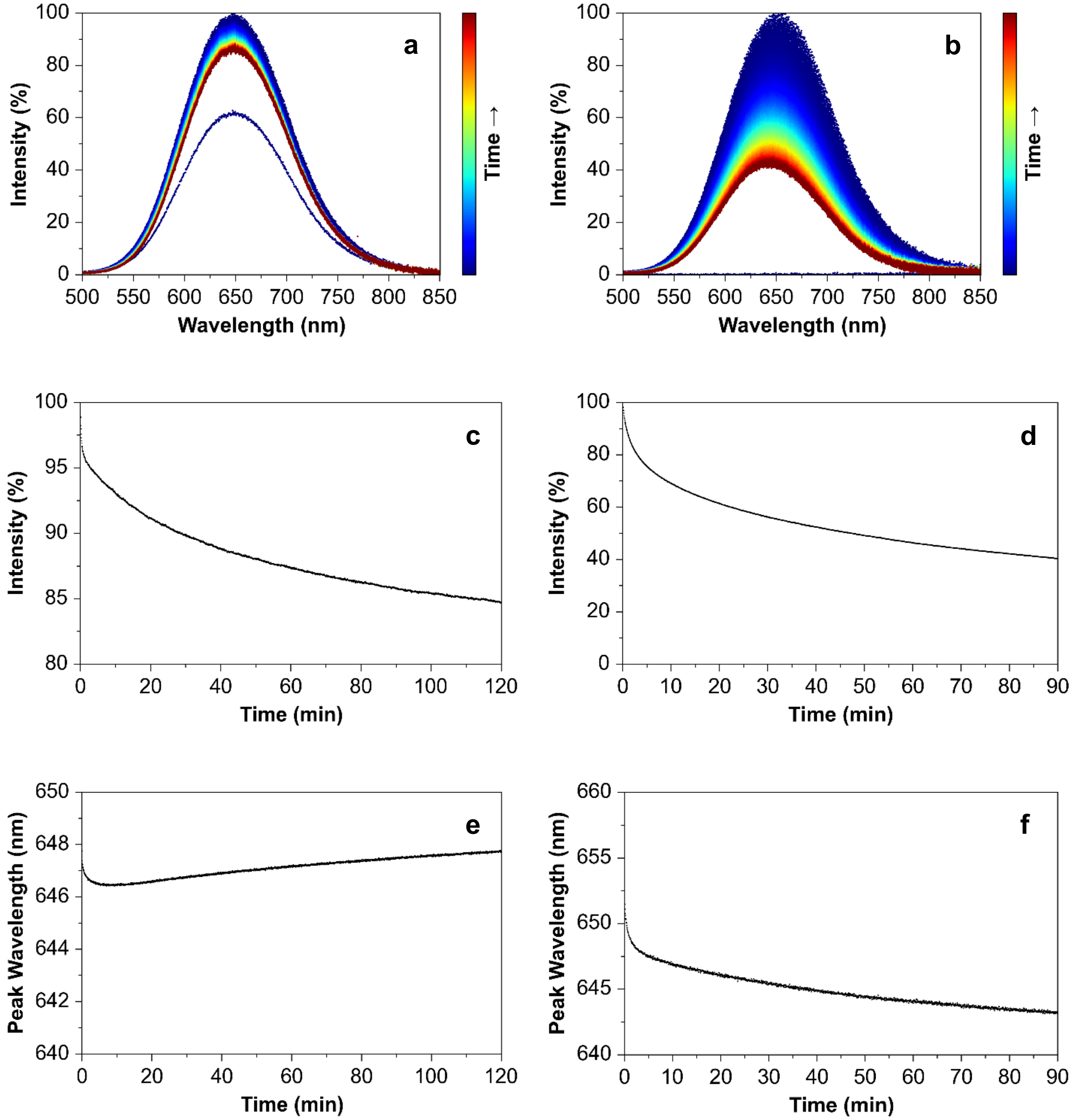

Fig 3.10 Photobleaching profiles for SiNC-C, pentyl functionalized silicon nanocrystals. The (a) PL spectra of the sample as a function of time, (c) PL intensity profile and (e) the approximate peak wavelength under continuous UV illumination in inert atmosphere are shown. The (b) PL spectra (d) PL intensity and (f) approximate peak wavelength of the sample are also shown under normal atmospheric conditions as a function of time. The individual spectra at approximately 60 % in (a) is an artifact of the PL spectrum collection process.

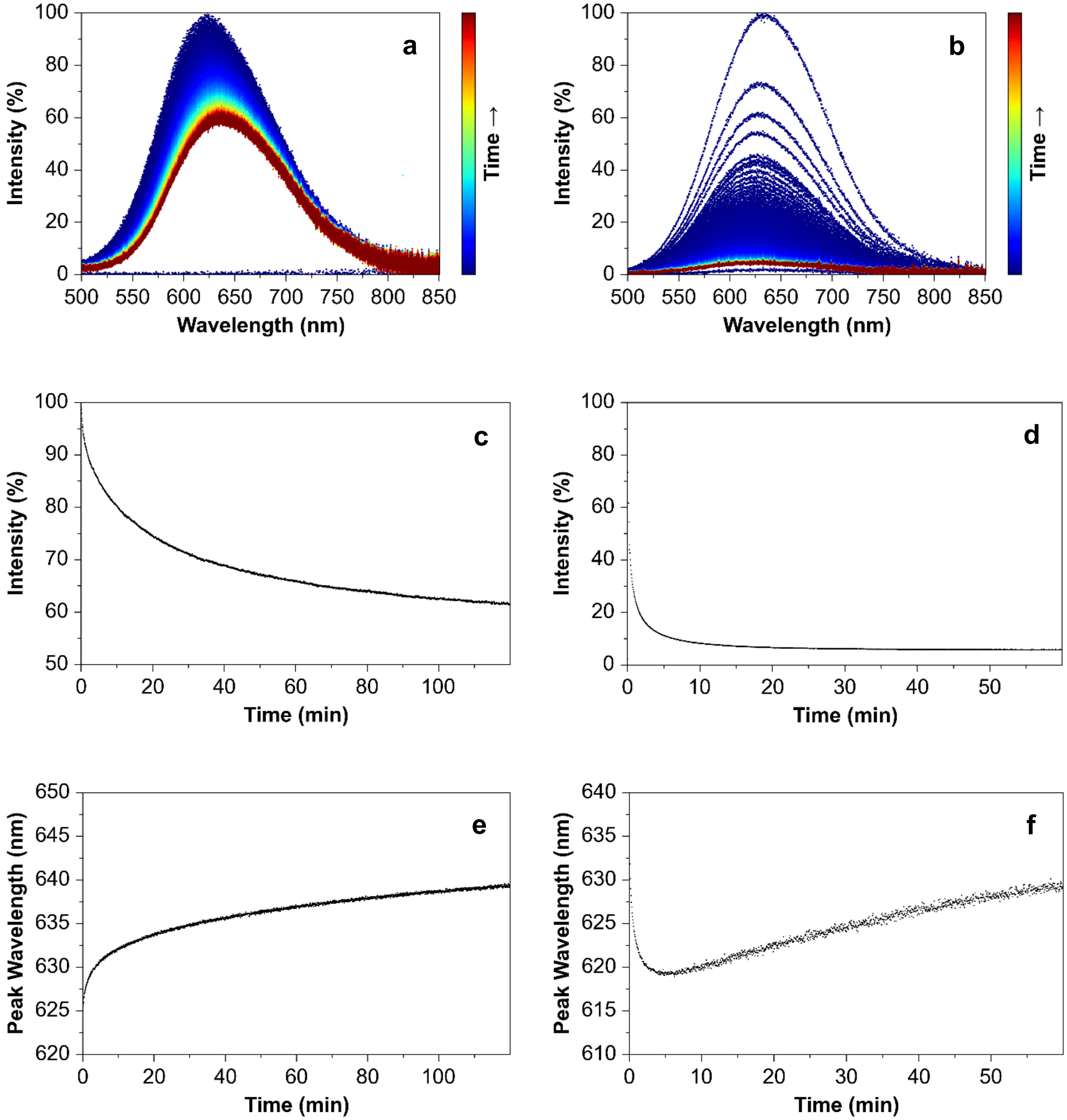

Fig 3.11 Photobleaching profiles for SiNC-A, alkoxy functionalized silicon nanocrystals. The (a) PL spectra of the sample as a function of time, (c) PL intensity profile and (e) the approximate peak wavelength under continuous UV illumination in inert atmosphere are shown. The (b) PL spectra (d) PL intensity and (f) approximate peak wavelength of the sample are also shown under normal atmospheric conditions as a function of time.

The peak decay frequency of silicon nanocrystal PL can provide insight into the mechanism of PL decay. The decay of the particles was first recorded under inert conditions in order to minimize photobleaching associated with the laser excitation source. An initial decay measurement prior to any photobleaching could not be obtained due to the nature of the measurement itself. It was assumed that the initial photobleaching of the laser combined with the introduction of air would approximate the photobleaching behavior of the SiNC samples in air. The decay measurements are summarized in Table 3.1 and Table 3.2.

A log normal distribution is an alternative model to the stretched exponential decay model for fitting PL decay curves from SiNCs.[38,39] The PL decay curves were fit to a log normal probability distribution of decay frequencies (Eqn. 3.1) to give the peak decay frequency, Γ_o. The width of the distribution at 1/e is Δ. A is a normalization constant (Eqn.3.2). The mean log lifetime of the silicon nanocrystal decay can be determined from the decay frequency using the mean log equation (Eqn. 3.3).

$$f(\Gamma) = \mathrm{A}\exp^{-\left(\frac{\ln\Gamma - \ln\Gamma_0}{\operatorname{arcsinh}\frac{\Delta}{\Gamma_0}}\right)^2} \qquad \text{Eqn 3.1}$$

$$\mathrm{A} = \left(\sqrt{\pi}\,\Gamma_0 \operatorname{arcsinh}\left(\frac{\Delta}{2\,\Gamma_0}\right)\exp\left(\frac{\operatorname{arcsinh}\frac{\Delta}{2\,\Gamma_0}}{4}\right)^2\right) \qquad \text{Eqn 3.2}$$

$$\text{Log mean } \tau = \left(\frac{1}{\exp^{\ln(\Gamma_0)+\frac{1}{2}\left(\operatorname{arcsinh}\left(\frac{\Delta}{2\,\Gamma_0}\right)/\sqrt{2}\right)^2}}\right) \qquad \text{Eqn 3.3}$$

Sample	Vacuum Measurements		
	Δ	Γ_o	Log Mean τ
	s^{-1}	s^{-1}	μs
SiNC-D1	30060	11460	65
SiNC-D2	24100	9873	78
SiNC-D3	32010	20250	43
SiNC-A	54100	22540	34
SiNC-B	25970	15830	55
SiNC-C	44230	26810	32

Table 3.1 Peak decay frequency parameters and log mean lifetime of silicon nanocrystal samples under vacuum conditions.

Sample	Air Measurements		
	Δ	Γ_o	Log Mean τ
	s^{-1}	s^{-1}	μs
SiNC-D1	40920	11930	55
SiNC-D2	37750	12010	57
SiNC-D3	72390	37400	22
SiNC-A	86400	24820	26
SiNC-B	74440	22510	30
SiNC-C	64480	27940	28

Table 3.2 Peak decay frequency parameters and log mean lifetime of silicon nanocrystal samples after the introduction of air into the measurement chamber.

Lifetime measurements provide insight into the decay mechanism of silicon nanocrystals. The PL decay lifetime can be described by $1/\tau_{PL}=1/\tau_{NR}+1/\tau_{R}$ and is equivalent to the sum of the radiative and non-radiative decay times.[40] The log mean lifetimes of the silicon nanocrystals are 10s of microseconds long and indicate band gap emission from freestanding SiNCs.[41] In all cases after in introduction of air, the log mean lifetime, τ, was observed to decrease. The decrease in PL lifetime indicates a shorter PL decay pathway. UV exposure and oxidation of the nanocrystals and the introduction of radiative trap surface states with faster relaxation times may account of the decrease in lifetimes.[42]

Photobleaching in ambient air was studied by FTIR to establish chemical changes to the NC surface. An FTIR spectrum was recorded prior to photobleaching in air. The particles were exposed to UV in air and the FTIR spectra was rerecorded to establish qualitative changes in surface chemistry. The FTIR spectra are shown in Fig 3.12. Photobleaching in air for the partially oxidized dodecyl functionalized sample SiNC-D2 and minimally oxidized dodecyl functionalized SiNC-D3 was accompanied by an increase in Si-O stretching at 1100 cm^{-1} with a simultaneous decrease in Si-H intensity at approximately 2100 cm^{-1}. Sample SiNC-D2 also showed a slight increase in –OH absorbance at 3300 cm^{-1} likely due to an increase in silanol on the surface. The oxidized dodecyl functionalized sample SiNC-D1 also showed a decrease in the Si-H absorbance but no conclusive change in Si-O could be discerned. The shorted chain pentene sample SiNC-C showed a decrease in Si-H but an increase in Si-O absorbance was not clearly observed. SiNC-D1 and SiNC-C originally had the largest Si-O absorbances. Perfluoro functionalized SiNC-B shows decrease in Si-H but a negligible increase in Si-O in the FTIR spectra. Alkoxy functionalized SiNC-A showed an increase in Si-O and a decrease in the Si-H absorption. The decrease in Si-H absorbance points to breaking of Si-H bonds resulting in dangling bond trap states. Other researchers have also observed a decrease in the Si-H stretch in FTIR of SiNCs when exposed to oxygen.[29,35] Changes in the Si-O may not occur in inert atmosphere but the breaking of Si-H bonds is still expected to occur with UV light exposure in inert atmosphere.

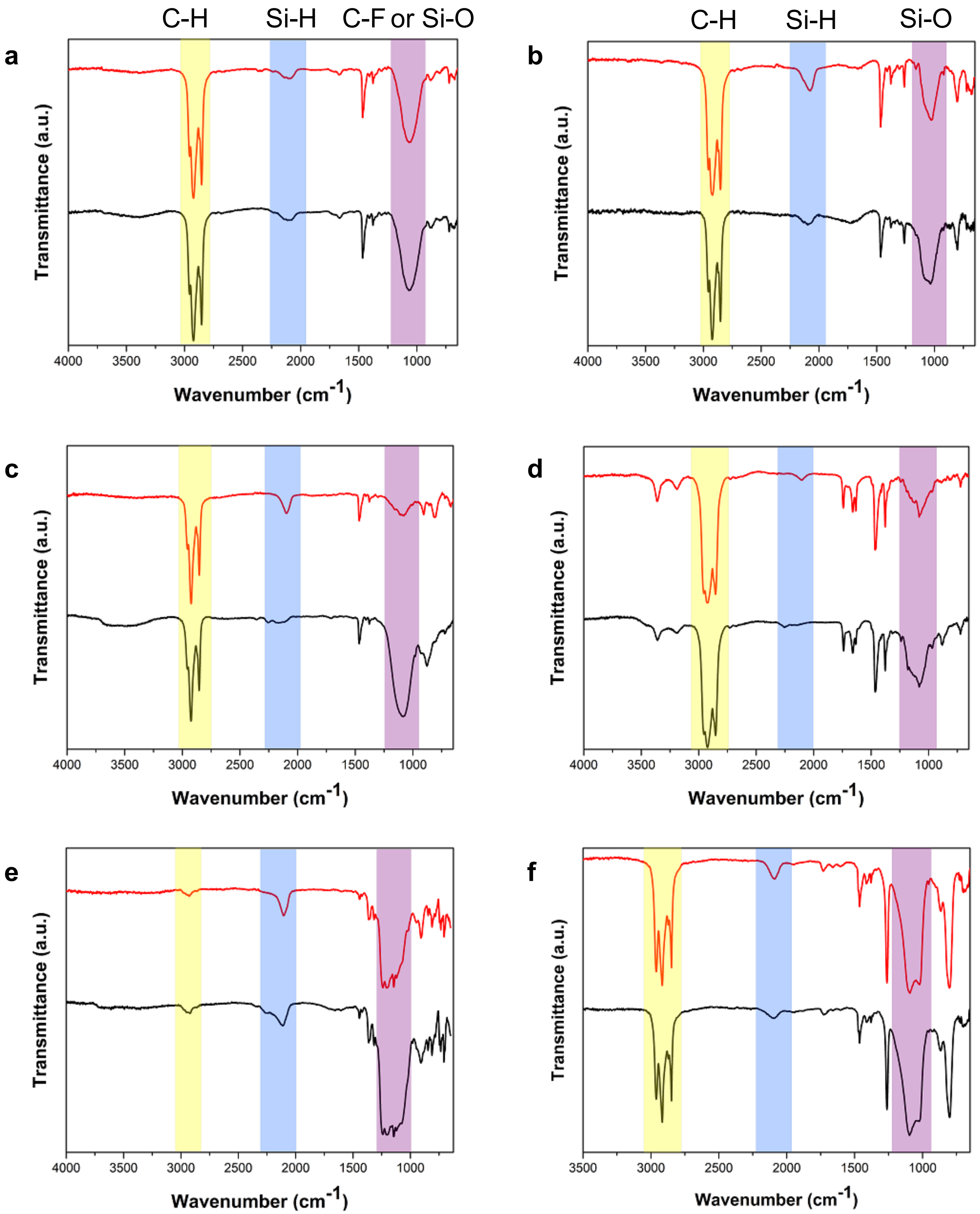

Fig 3.12 FTIR spectra of (a) SiNC-D1, (b) SiNC-D2, (c) SiNC-D3, (d) SiNC-A, (e) SiNC-B and (f) SiNC-C initially (red curve) and after of exposure to UV irradiation (black curve). The black curve for SiNC-D1 (a) was recorded after 60 minutes. All other spectra were recorded after 90 minutes of UV irradiation.

3.5 Conclusions

The role of surface chemistry was investigated using four different surface groups functionalized on silicon nanocrystals. Photobleaching was greatest for all surface groups in ambient conditions. In inert conditions, all dodecyl functionalized samples groups were expected to have similar photobleaching responses. This was not observed. The photobleaching response showed variation between dodecyl functionalized samples and is concluded to be due to differing amounts of prior surface oxidation of the SiNCs. The ketone displays the greatest degree of photobleaching of the all the NCs in inert conditions. Polarization of the Si-Si surface bonds by the direct Si-O linkage is concluded to facilitate the UV induced bond breakage resulting in an increase in photobleaching. It is concluded that the amount of oxidation and type of oxidation of the NCs plays a stronger role in the photobleaching response of SiNCs than the ligand type.

3.6 References

(1) Kamat, P. V. *J. Phys. Chem. C* **2008**, *112* (48), 18737.

(2) Anikeeva, P. O.; Halpert, J. E.; Bawendi, M. G.; Bulović, V. *Nano Lett.* **2009**, *9* (7), 2532.

(3) Park, N.-M.; Kim, T.-S.; Park, S.-J. *Appl. Phys. Lett.* **2001**, *78* (17), 2575.

(4) Michalet, X.; Pinaud, F. F.; Bentolila, L. A.; Tsay, J. M.; Doose, S.; Li, J. J.; Sundaresan, G.; Wu, A. M.; Gambhir, S. S.; Weiss, S. *Science* **2005**, *307* (5709), 538.

(5) Cheng, X.; Lowe, S. B.; Reece, P. J.; Gooding, J. J. *Chem. Soc. Rev.* **2014**, *43* (8), 2680.

(6) Alivisatos, A. P.; Gu, W.; Larabell, C. *Annu. Rev. Biomed. Eng.* **2005**, *7* (1), 55.

(7) Dahan, M.; Laurence, T.; Pinaud, F.; Chemla, D. S.; Alivisatos, A. P.; Sauer, M.; Weiss, S. *Opt. Lett.* **2001**, *26* (11), 825.

(8) Chan, W. C. W.; Nie, S. *Science* **1998**, *281* (5385), 2016.

(9) Lewinski, N.; Colvin, V.; Drezek, R. *Small* **2008**, *4* (1), 26.

(10) Derfus, A. M.; Chan, W. C. W.; Bhatia, S. N. *Nano Lett.* **2004**, *4* (1), 11.

(11) Bayliss, S. C.; Heald, R.; Fletcher, D. I.; Buckberry, L. D. *Adv. Mater.* **1999**, *11* (4), 318.

(12) T., S. M. *ACS Nano* **2008**, *2* (5), 873.

(13) Zhai, Y.; Dasog, M.; Snitynsky, R. B.; Purkait, T. K.; Aghajamali, M.; Hahn, A. H.; Sturdy, C. B.; Lowary, L.; Veinot, J. G. C. *J. Mater. Chem. B Mater. Biol. Med.* **2014**, *2* (47), 8427.

(14) English, D. S.; Pell, L. E.; Yu, Z.; Barbara, P. F.; Korgel, B. A. *Nano Lett.* **2002**, *2* (7), 681.

(15) Sark, W. van; Frederix, P. *J.* **2001**.

(16) Xu, L.; Huang, X.; Zhu, J.; Chen, H.; Chen, K. *J. Mater. Sci.* **2000**, *35* (6), 1375.

(17) García-Santamaría, F.; Chen, Y.; Vela, J.; Schaller, R. D.; Hollingsworth, J. A.; Klimov, V. I. *Nano Lett.* **2009**, *9* (10), 3482.

(18) Wolkin, M. V.; Jorne, J.; Fauchet, P. M.; Allan, G.; Delerue, C. *Phys. Rev. Lett.* **1999**, *82* (1), 197.

(19) Veinot, J. G. C. *Chem. Commun. (Cambridge, United Kingdom)* **2006**, No. 40, 4160.

(20) Hessel, C. M.; Henderson, E. J.; Veinot, J. G. C. *J. Phys. Chem. C* **2007**, *111* (19), 6956.

(21) Colin M. Hessel; Eric J. Henderson, and; Veinot, J. G. C. **2006**.

(22) Dasog, M.; De los Reyes, G. B.; Titova, L. V; Hegmann, F. A.; Veinot, J. G. C. *ACS Nano* **2014**, *8* (9), 9636.

(23) Hua, F.; Erogbogbo, F.; Swihart, M. T.; Ruckenstein, E. *Langmuir* **2006**, *22* (9), 4363.

(24) Hua, F.; Swihart, M. T.; Ruckenstein, E. *Langmuir* **2005**, *21*, 6054.

(25) Harper, J.; Sailor, M. J. *Langmuir* **1997**, *13* (17), 4652.

(26) Tischler, M. A.; Collins, R. T.; Stathis, J. H.; Tsang, J. C. *Appl. Phys. Lett.* **1992**, *60* (5), 639.

(27) Yang, J.; Liptak, R.; Rowe, D.; Wu, J.; Casey, J.; Witker, D.; Campbell, S. A.; Kortshagen, U. *Appl. Surf. Sci.* **2014**, *323*, 54.

(28) Puzder, A.; Williamson, A. J.; Grossman, J. C.; Galli, G. *Phys. Rev. Lett.* **2002**, *88* (9), 097401.

(29) Wu, J. J.; Kortshagen, U. *RSC Adv.* **2015**.

(30) Godefroo, S.; Hayne, M.; Jivanescu, M.; Stesmans, A.; Zacharias, M.; Lebedev, O. I.; Van Tendeloo, G.; Moshchalkov, V. V. *Nat Nano* **2008**, *3* (3), 174.

(31) Qian, C.; Sun, W.; Wang, L.; Chen, C.; Liao, K.; Wang, W.; Jia, J.; Hatton, B. D.; Casillas, G.; Kurylowicz, M.; Yip, C. M.; Mastronardi, M. L.; Ozin, G. A. *J. Am. Chem.*

Soc. **2014**, *136* (45), 15849.
(32) Avila, A.; Montero, I.; Galán, L.; Ripalda, J. M.; Levy, R. *J. Appl. Phys.* **2001**, *89* (1), 212.
(33) Hessel, C. M.; Rasch, M. R.; Hueso, J. L.; Goodfellow, B. W.; Akhavan, V. A.; Puvanakrishnan, P.; Tunnel, J. W.; Korgel, B. A. *Small* **2010**, *6* (18), 2026.
(34) Ledoux, G.; Gong, J.; Huisken, F. *Appl. Phys. Lett.* **2001**, *79* (24), 4028.
(35) Lockwood, R.; McFarlane, S.; Rodríguez Núñez, J. R.; Wang, X. Y.; Veinot, J. G. C.; Meldrum, A. *J. Lumin.* **2011**, *131* (7), 1530.
(36) Mastronardi, M. L.; Chen, K. K.; Liao, K.; Casillas, G.; Ozin, G. A. *J. Phys. Chem. C* **2015**, *119* (1), 826.
(37) Cerofolini, G. F.; Mascolo, D.; Vlad, M. O. *J. Appl. Phys.* **2006**, *100* (5), 054308.
(38) van Driel, A. F.; Nikolaev, I. S.; Vergeer, P.; Lodahl, P.; Vanmaekelbergh, D.; Vos, W. L. *Phys. Rev. B* **2007**, *75* (3), 035329.
(39) Nguyen, A.; Gonzalez, C. M.; Sinelnikov, R.; Newman, W.; Sun, S.; Lockwood, R.; C Veinot, J. G.; Meldrum, A. **2016**.
(40) Kanemitsu, Y. *Phys. Rev. B* **1996**, *53* (20), 13515.
(41) Wilson, W. L.; Szajowski, P. F.; Brus, L. E. *Science* **1993**, *262* (5137), 1242.
(42) Mastronardi, M. L.; Maier-Flaig, F.; Faulkner, D.; Henderson, E. J.; Kübel, C.; Lemmer, U.; Ozin, G. A. **2011**.

Chapter 4 Conclusions and Future Work

The effect of surface chemistry on the optoelectronic properties of silicon nanocrystals was investigated. Specifically, the electronic properties and photostability of SiNCs were investigated as a function of surface chemistry. The conclusions are summarized along with ideas for future work.

4.1 Surface Functionalization of Silicon Nanocrystals with Electroactive End Groups

4.1.1 Conclusions

Surface functionalization of SiNC with a ferrocene moiety was successful. Surface characterization techniques including FTIR, NMR and XPS confirmed the presence of ferrocene functionalized to SiNC. The PL response of the SiNCs was modified as a result of the electronic interactions between the nanocrystal and the electroactive surface group. Investigation into the interaction as probed by CV revealed a change in the ferrocene electrochemical response from electrochemically reversible to irreversible. STS measurements show a shift in the SiNC valence band to more negative values typical of n-type doping.[1] Electron transfer from the ferrocene to the silicon nanocrystal accounts for the observations.

4.1.2 Future Work

Bulk silicon is limited in optical technologies due to its poor luminescent properties; however, SiNCs show promise in such technologies due to their PL. The functionalization of ferrocene to the surface of SiNCs leads to loss of PL in the ferrocene functionalized material. Studies on bulk silicon have revealed that electron transfer to the silicon electrode from an external redox couple can be controlled provided a sufficiently thick insulting monolayer on the bulk silicon.[2] A longer alkyl chain used to tether the ferrocene moiety to the SiNC may provide sufficient isolation of the systems to render a luminescent, electroactive hybrid material. Ferrocene molecules with longer alkyl chains could be synthesized via a number of routes: lithiation of ferrocene followed by reaction with halide terminated long chain alkenes,[3] or click reactions.[4] Tailoring of the electroactive ligand and selection of a species that would not undergo electron transfer with the SiNCs may also lead to the formation of a luminescent electroactive hybrid material.

4.2 Photostability of Surface Functionalized Silicon Nanocrystals

4.2.1 Conclusions

The photostability of SiNCs functionalized with a series of surface groups was investigated in air and inert atmosphere in chapter 3. Samples exposed to UV light in air showed a dramatic decrease in PL intensity. Only two samples, the oxidized dodecyl (SiNC-D1) and pentyl (SiNC-C) functionalized SiNCs, showed increased resistance to photobleaching after 60 minutes relative to the other samples. SiND-1 showed a decrease to 37 % of the initial intensity while SiNC-C showed a decrease to 46 and 22 % after 60 minutes. The remainder of the samples showed decreases in intensity to near or below 15 % after 60 minutes of UV exposure in air. Larger variations in the photobleaching response occurred in inert atmosphere. The variation between surface groups is concluded to be more pronounced in inert atmosphere due to the exclusion of water and oxygen. PL intensity of the perfluoro functionalized SiNC increased under UV exposure. As well the minimally oxidized dodecyl functionalized SiNC showed an increase in PL intensity followed by a decrease to between 80 and 85 % of the initial intensity.

The two other dodecyl samples did not show the same behavior during inert UV exposure. The variation is concluded to be due to prior surface oxidation of the particles rather than the surface ligand. Alkoxy functionalized SiNCs showed the largest amount of photobleaching reaching approximately 6 and 50 % in atmospheric and inert conditions respectively. Polarization of the SiNC surface by the direct Si-O linkage is concluded to increase the photo-instability of the SiNC.

4.2.2 Future Work

More efficient surface passivation techniques are required to more thoroughly determine the influence of surface ligands on photostability of SiNC PL while limiting the effect of SiNC oxidation. Photostable SiNC have been reported via a double hydrosilylation process.[5] Using the double hydrosilylation technique it may be possible to produce SiNC that are even less susceptible to oxidation. By limiting the effect of oxidation, the effect of surface chemistry on photostability could be more easily interrogated.

Different surface functionalities may also be explored. The surface groups studied here were hydrophobic in nature. Hydrophilic groups could also be investigated. Hydrophilic functionalization of SiNCs is often necessary for targeted cell and imaging studies.[6] It was determined from the lifetime measurements that the SiNCs investigated in this work emit via recombination in the band gap. Surface state emission may be more susceptible to photobleaching.[7] Investigation into the photostability of surface state emitting particles may provide more insight into achieving photostable SiNCs.

4.3 References

(1) Wolf, O.; Dasog, M.; Yang, Z.; Balberg, I.; Veinot, J. G. C.; Millo, O. *Nano Lett.* **2013**, *13* (6), 2516.

(2) Barrelet, C. J.; Robinson, D. B.; Cheng, J.; Hunt, T. P.; Quate, C. F.; Chidsey, C. E. D. *Langmuir* **2001**, *17* (11), 3460.

(3) Riveros, G.; Meneses, S.; Escobar, S.; Garin, C.; Chornik, B. *J. Chil. Chem. Soc.* **2010**, *55* (1), 61.

(4) Marrani, A. G.; Dalchiele, E. A.; Zanoni, R.; Decker, F.; Cattaruzza, F.; Bonifazi, D.; Prato, M. *Electrochim. Acta* **2008**, *53* (11), 3903.

(5) Wu, J. J.; Kortshagen, U. R. *RSC Adv.* **2015**, *5* (126), 103822.

(6) Zhai, Y.; Dasog, M.; Snitynsky, R. B.; Purkait, T. K.; Aghajamali, M.; Hahn, A. H.; Sturdy, C. B.; Lowary, T. L.; Veinot, J. G. C. *J. Mater. Chem. B* **2014**, *2* (47), 8427.

(7) Dasog, M.; De los Reyes, G. B.; Titova, L. V; Hegmann, F. A.; Veinot, J. G. C. *ACS Nano* **2014**, *8* (9), 9636.

Bibliography

(1) Daniel, M. C.; Astruc, D. *Chem. Rev.* **2004**, *104* (1), 293.
(2) Eustis, S.; El-Sayed, M. A. *Chem. Soc. Rev.* **2006**, *35* (3), 209.
(3) Thostenson, E. T.; Ren, Z.; Chou, T. *Compos. Sci. Technol.* **2001**, *61* (13), 1899.
(4) Baughman, R. H.; Zakhidov, A. A.; de Heer, W. A. *Science* **2002**, *297* (5582), 787.
(5) Lu, A.; Salabas, E. L.; Schüth, F. *Angew. Chem. Int. Ed.* **2007**, *46* (8), 1222.
(6) Lee, C.; Wei, X.; Kysar, J. W.; Hone, J. *Science* **2008**, *321* (5887), 385.
(7) Anikeeva, P. O.; Halpert, J. E.; Bawendi, M. G.; Bulović, V. *Nano Lett.* **2009**, *9* (7), 2532.
(8) Duan, X.; Niu, C.; Sahi, V.; Chen, J.; Parce, J. W.; Empedocles, S.; Goldman, J. L. *Nature* **2003**, *425* (6955), 274.
(9) Grätzel, M. *J. Photochem. Photobiol. A Chem.* **2004**, *164* (1), 3.
(10) West, J. L.; Halas, N. J. *Annu. Rev. Biomed. Eng.* **2003**, *5* (1), 285.
(11) Huang, X.; El-Sayed, I. H.; Qian, W.; El-Sayed, M. A. *J. Am. Chem. Soc.* **2006**, *128* (6), 2115.
(12) Alivisatos, A. P.; Gu, W.; Larabell, C. *Annu. Rev. Biomed. Eng.* **2005**, *7* (1), 55.
(13) Murray, C. B.; Norris, D. J.; Bawendi, M. G. *J. Am. Chem. Soc.* **1993**, *115* (19), 8706.
(14) Micic, O. I.; Curtis, C. J.; Jones, K. M.; Sprague, J. R.; Nozik, A. J. *J. Phys. Chem.* **1994**, *98* (19), 4966.
(15) Olshavsky, M. A.; Goldstein, A. N.; Alivisatos, A. P. *J. Am. Chem. Soc.* **1990**, *112* (25), 9438.
(16) Ishii, H.; Sugiyama, K.; Ito, E.; Seki, K. *Adv. Mater.* **1999**, *11* (8), 605.
(17) Hessel, C. M.; Reid, D.; Panthani, M. G.; Rasch, M. R.; Goodfellow, B. W.; Wei, J.; Fujii, H.; Akhavan, V.; Korgel, B. A. *Chem. Mater.* **2012**, *24* (2), 393.
(18) Murray, C. B.; Sun, S.; Gaschler, W.; Doyle, H.; Betley, T. A.; Kagan, C. R. *IBM J. Res. Dev.* **2001**, *45* (1), 47.
(19) Moreels, I.; Justo, Y.; De Geyter, B.; Haustraete, K.; Martins, J. C.; Hens, Z. *ACS Nano* **2012**, *5* (3), 2004.
(20) Hirayama, H.; Tanaka, S.; Ramvall, P.; Aoyagi, Y. *Appl. Phys. Lett.* **1998**, *72* (14), 1736.
(21) Uematsu, T.; Doi, T.; Torimoto, T.; Kuwabata, S. *J. Phys. Chem. Lett.* **2010**, *1* (22), 3283.
(22) Kamat, P. V. *J. Phys. Chem. C* **2008**, *112* (48), 18737.
(23) Talapin, D. V; Murray, C. B. *Science* **2005**, *310* (5745), 86.
(24) Chan, W. C. W.; Nie, S. *Science* **1998**, *281* (5385), 2016.
(25) Murphy, C. J. Anal. Chem. **2002**, 74 (19), 520 A.
(26) Alivisatos, A. P. *Science* **1996**, *271* (5251), 933.
(27) Brus, L. E. *J. Chem. Phys.* **1983**, *79* (11), 5566.
(28) Brus, L. E. *J. Chem. Phys.* **1984**, *80* (9), 4403.
(29) Alivisatos, A. P. *J. Phys. Chem.* **1996**, *100* (31), 13226.
(30) Ekimov, A. I.; Efros, A. L.; Onushchenko, A. A. *Solid State Commun.* **1985**, *56* (11), 921.
(31) Kayanuma, Y. *Phys. Rev. B* **1988**, *38* (14), 9797.
(32) Trwoga, P. F.; Kenyon, A. J.; Pitt, C. W. *J. Appl. Phys.* **1998**, *83* (7), 3789.
(33) Wilson, W. L.; Szajowski, P. F.; Brus, L. E. *Science* **1993**, *262* (5137), 1242.
(34) Ledoux, G.; Gong, J.; Huisken, F.; Guillois, O.; Reynaud, C. *Appl. Phys. Lett.* **2002**, *80* (25), 4834.
(35) Bayliss, S. C.; Heald, R.; Fletcher, D. I.; Buckberry, L. D. *Adv. Mater.* **1999**, *11* (4), 318.
(36) Stewart, M. P.; Buriak, J. M. *Adv. Mater.* **2000**, *12* (12), 859.

(37) Erogbogbo, F.; Yong, K.-T.; Roy, I.; Xu, G.; Prasad, P. N.; Swihart, M. T. *ACS Nano* **2008**, *2* (5), 873.
(38) Cheng, K.; Anthony, R.; Kortshagen, U. R.; Holmes, R. J. *Nano Lett.* **2011**, *11* (5), 1952.
(39) Lalic, N.; Linnros, J. *J. Lumin.* **1998**, *80* (1), 263.
(40) Puzzo, D. P.; Henderson, E. J.; Helander, M. G.; Wang, Z.; Ozin, G. A.; Lu, Z. *Nano Lett.* **2011**, *11* (4), 1585.
(41) Liu, C.; Holman, Z. C.; Kortshagen, U. R. *Nano Lett.* **2009**, *9* (1), 449.
(42) Park, J.-H.; Gu, L.; von Maltzahn, G.; Ruoslahti, E.; Bhatia, S. N.; Sailor, M. J. *Nat. Mater.* **2009**, *8* (4), 331.
(43) Content, S.; Trogler, W. C.; Sailor, M. J. *Chem. - A Eur. J.* **2000**, *6* (12), 2205.
(44) Germanenko, I. N.; Li, S.; El-Shall, M. S. *J. Phys. Chem. B* **2001**, *105* (1), 59.
(45) Graetz, J.; Ahn, C. C.; Yazami, R.; Fultz, B. *Electrochem. Solid-State Lett.* **2003**, *6* (9), A194.
(46) Islam, M. A.; Purkait, T. K.; Veinot, J. G. C. *J. Am. Chem. Soc.* **2014**, *136* (43), 15130.
(47) Canham, L. T. *Appl. Phys. Lett.* **1990**, *57* (10), 1046.
(48) Cullis, A. G.; Canham, L. T. *Nature* **1991**, *353* (6342), 335.
(49) Fahlman, B. D. *Materials Chemistry*; Springer Netherlands: Dordrecht, 2011.
(50) Kasap, S. O. *Optoelectronics and photonics : principles and practices*; Prentice Hall, 2013.
(51) Yoffe, A. D. *Adv. Phys.* **1993**, *42* (2), 173.
(52) Heintz, B. A. S.; Fink, M. J.; Mitchell, B. S. *Adv. Mater.* **2007**, *19* (22), 3984.
(53) Sailor, M. J. *Porous silicon in practice preparation, characterization and applications*; Weinheim :, 2012.
(54) Long, Y.; Zhao, Q.; Zhang, Z.; Tian, Z.; Pang, D. *Analyst* **2012**, *137* (4), 805.
(55) Heinrich, J. L.; Curtis, C. L.; Credo, G. M.; Kavanagh, K. L.; Sailor, M. J. *Science* **1992**, *255* (5040), 66.
(56) Bley, R. A.; Kauzlarich, S. M.; Davis, J. E.; Lee, H. W. H. *Chem. Mater.* **1996**, *8* (8), 1881.
(57) Heath, J. R. *Science* **1992**, *258* (5085), 1131.
(58) Arul Dhas, N.; Raj, C. P.; Gedanken, A. *Chem. Mater.* **1998**, *10* (11), 3278.
(59) Baldwin, R. K.; Pettigrew, K. A.; Ratai, E.; Augustine, M. P.; Kauzlarich, S. M. *Chem. Commun.* **2002**, *23* (17), 1822.
(60) Tilley, R. D.; Warner, J. H.; Yamamoto, K.; Matsui, I.; Fujimori, H. *Chem. Commun.* **2005**, *115* (14), 1833.
(61) Bley, R. A.; Kauzlarich, S. M. *J. Am. Chem. Soc.* **1996**, *118* (49), 12461.
(62) Yang, C.; Bley, R. A.; Kauzlarich, S. M.; Lee, H. W. H.; Delgado, G. R. *J. Am. Chem. Soc.* **1999**, *121* (22), 5191.
(63) Pettigrew, K. A.; Liu, Q.; Power, P. P.; Kauzlarich, S. M. *Chem. Mater.* **2003**, *15* (21), 4005.
(64) Neiner, D.; Chiu, H. W.; Kauzlarich, S. M. *J. Am. Chem. Soc.* **2006**, *128* (34), 11016.
(65) Cheng, X.; Lowe, S. B.; Reece, P. J.; Gooding, J. J. *Chem. Soc. Rev.* **2014**, *43* (8), 2680.
(66) Holmes, J. D.; Ziegler, K. J.; Doty, R. C.; Pell, L. E.; Johnston, K. P.; Korgel, B. A. *J. Am. Chem. Soc.* **2001**, *123* (16), 3743.
(67) Murthy, T. U. M. S.; Miyamoto, N.; Shimbo, M.; Nishizawa, J. *J. Cryst. Growth* **1976**, *33* (1), 1.
(68) Littau, K. A.; Szajowski, P. J.; Muller, A. J.; Kortan, A. R.; Brus, L. E. *J. Phys. Chem.*

1993, *97* (6), 1224.
(69) Li, X.; He, Y.; Talukdar, S. S.; Swihart, M. T. *Langmuir* **2003**, *19* (20), 8490.
(70) Mangolini, L.; Thimsen, E.; Kortshagen, U. *Nano Lett.* **2005**, *5* (4), 655.
(71) Mangolini, L.; Kortshagen, U. *Adv. Mater.* **2007**, *19* (18), 2513.
(72) Liu, S.-M.; Sato, S.; Kimura, K. *Langmuir* **2005**, *21* (14), 6324.
(73) Hessel, C. M.; Henderson, E. J.; Veinot, J. G. C. *Chem. Mater.* **2006**, *18* (138), 36139.
(74) Hessel, C. M.; Henderson, E. J.; Veinot, J. G. C. *J. Phys. Chem. C* **2007**, *111* (19), 6956.
(75) Fujii, M.; Yamaguchi, Y.; Takase, Y.; Ninomiya, K.; Hayashi, S. *Appl. Phys. Lett.* **2004**, *85* (7), 1158.
(76) Fukuda, M.; Fujii, M.; Sugimoto, H.; Imakita, K.; Hayashi, S. *Opt. Lett.* **2011**, *36* (20), 4026.
(77) Sugimoto, H.; Fujii, M.; Imakita, K.; Hayashi, S.; Akamatsu, K. **2012**, *116* (33), 17969.
(78) Gupta, A.; Swihart, M. T.; Wiggers, H. *Adv. Funct. Mater.* **2009**, *19* (5), 696.
(79) Veinot, J. G. C. *Chem. Commun.* **2006**, No. 40, 4160.
(80) Dasog, M.; Kehrle, J.; Rieger, B.; Veinot, J. G. C. *Angew. Chem. Int. Ed.* **2016**, *55* (7), 2322.
(81) Buriak, J. M. *Chem. Rev.* **2002**, *102* (5), 1271.
(82) Bateman, J. E.; Eagling, R. D.; Worrall, D. R.; Horrocks, B. R.; Houlton, A. *Angew. Chem. Int. Ed.* **1998**, *37* (19), 2683.
(83) Hua, F.; Swihart, M. T.; Ruckenstein, E. *Langmuir* **2005**, *21* (13), 6054.
(84) J. M. Schmeltzer; Lon A. Porter, J.; Michael P. Stewart; Buriak, J. M. **2002**, *18* (8), 2971.
(85) Warner, J. H.; Hoshino, A.; Yamamoto, K.; Tilley, R. D. *Angew. Chemie* **2005**, *117* (29), 4626.
(86) Purkait, T. K.; Iqbal, M.; Wahl, M. H.; Gottschling, K.; Gonzalez, C. M.; Islam, M. A.; Veinot, J. G. C. *J. Am. Chem. Soc.* **2014**, *136* (52), 17914.
(87) Höhlein, I. M. D.; Kehrle, J.; Helbich, T.; Yang, Z.; Veinot, J. G. C.; Rieger, B. *Chem. - A Eur. J.* **2014**, *20* (15), 4212.
(88) Dasog, M.; Yang, Z.; Regli, S.; Atkins, T. M.; Faramus, A.; Singh, M. P.; Muthuswamy, E.; Kauzlarich, S. M.; Tilley, R. D.; Veinot, J. G. C. *ACS Nano* **2013**, *7* (3), 2676.
(89) Dasog, M.; De los Reyes, G. B.; Titova, L. V; Hegmann, F. A.; Veinot, J. G. C. *ACS Nano* **2014**, *8* (9), 9636.
(90) Höhlein, I. M. D.; Angı, A.; Sinelnikov, R.; Veinot, J. G. C.; Rieger, B. *Chem. - A Eur. J.* **2015**, *21* (7), 2755.
(91) Dasog, M.; Bader, K.; Veinot, J. G. C. *Chem. Mater.* **2015**, *27* (4), 1153.
(92) Delerue, C.; Allan, G.; Lannoo, M. *Phys. Rev. B* **1993**, *48* (15), 11024.
(93) Rodríguez, J. A.; Vásquez-Agustín, M. A.; Morales-Sánchez, A.; Aceves-Mijares, M. *J. Nanomater.* **2014**, *2014*, 1.
(94) Kanemitsu, Y.; Ogawa, T.; Shiraishi, K.; Takeda, K. *Phys. Rev. B* **1993**, *48* (7), 4883.
(95) Koch, F.; Petrova-Koch, V.; Muschik, T. *J. Lumin.* **1993**, *57* (1), 271.
(96) Wolkin, M. V.; Jorne, J.; Fauchet, P. M.; Allan, G.; Delerue, C. *Phys. Rev. Lett.* **1999**, *82* (1), 197.
(97) Filippou, A. C.; Baars, B.; Chernov, O.; Lebedev, Y. N.; Schnakenburg, G. *Angew. Chem. Int. Ed.* **2014**, *53* (2), 565.
(98) Puzder, A.; Williamson, A. J.; Grossman, J. C.; Galli, G. *Phys. Rev. Lett.* **2002**, *88* (9), 097401.
(99) Kocevski, V.; Eriksson, O.; Rusz, J. *Phys. Rev. B* **2015**, *91* (12), 125402.

(100) Pi, X. D.; Liptak, R. W.; Deneen Nowak, J.; Wells, N. P.; Carter, C. B.; Campbell, S. A.; Kortshagen, U. R. *Nanotechnology* **2008**, *19* (24), 245603.
(101) Hua, F.; Erogbogbo, F.; Swihart, M. T.; Ruckenstein, E. *Langmuir* **2006**, *22* (9), 4363.
(102) Islam, M. A.; Purkait, T. K.; Mobarok, M. H.; Hoehlein, I. M. D.; Sinelnikov, R.; Iqbal, M.; Azulay, D.; Balberg, I.; Millo, O.; Rieger, B.; Veinot, J. G. C. *Angew. Chemie Int. Ed.* **2016**, *55* (26), 7393.
(103) Angı, A.; Sinelnikov, R.; Meldrum, A.; Veinot, J. G. C.; Balberg, I.; Azulay, D.; Millo, O.; Rieger, B. *Nanoscale* **2016**, *8* (15), 7849.
(104) Fabre, B. *Chem. Rev.* **2016**, *116* (8), 4808.
(105) Fabre, B. *Acc. Chem. Res.* **2010**, *43* (12), 1509.
(106) Rehm, J. M.; McLendon, G. L.; Fauchet, P. M. *J. Am. Chem. Soc.* **1996**, *118* (18), 4490.
(107) Dorokhin, D.; Tomczak, N.; Reinhoudt, D. N.; Velders, A. H.; Vancso, G. J. *Nanotechnology* **2010**, *21* (28), 285703.
(108) Song, Y.; Kang, X.; Zuckerman, N. B.; Phebus, B.; Konopelski, J. P.; Chen, S. *Nanoscale* **2011**, *3* (5), 1984.
(109) Guldi, D. M.; Marcaccio, M.; Paolucci, D.; Paolucci, F.; Tagmatarchis, N.; Tasis, D.; Vázquez, E.; Prato, M. *Angew. Chemie* **2003**, *115* (35), 4338.
(110) Wu, J. J.; Kortshagen, U. R. *RSC Adv.* **2015**, *5* (126), 103822.
(111) Jurbergs, D.; Rogojina, E.; Mangolini, L.; Kortshagen, U. *Appl. Phys. Lett.* **2006**, *88* (23), 233116.
(112) Ledoux, G.; Guillois, O.; Porterat, D.; Reynaud, C.; Huisken, F.; Kohn, B.; Paillard, V. *Phys. Rev. B* **2000**, *62* (23), 15942.
(113) Pereira, R. N.; Rowe, D. J.; Anthony, R. J.; Kortshagen, U. *Phys. Rev. B* **2011**, *83* (15), 155327.
(114) Cerofolini, G. F.; Mascolo, D.; Vlad, M. O. *J. Appl. Phys.* **2006**, *100* (5), 054308.
(115) Tischler, M. A.; Collins, R. T.; Stathis, J. H.; Tsang, J. C. *Appl. Phys. Lett.* **1992**, *60* (5), 639.
(116) Harper, J.; Sailor, M. J. *Langmuir* **1997**, *13* (17), 4652.
(117) Yang, J.; Liptak, R.; Rowe, D.; Wu, J.; Casey, J.; Witker, D.; Campbell, S. A.; Kortshagen, U. *Appl. Surf. Sci.* **2014**, *323*, 54.
(118) English, D. S.; Pell, L. E.; Yu, Z.; Barbara, P. F.; Korgel, B. A. *Nano Lett.* **2002**, *2* (7), 681.
(119) Godefroo, S.; Hayne, M.; Jivanescu, M.; Stesmans, A.; Zacharias, M.; Lebedev, O. I.; Van Tendeloo, G.; Moshchalkov, V. V. *Nat. Nanotechnol.* **2008**, *3* (3), 174.
(120) Buriak, J. M. *Chem. Mater.* **2014**, *26* (1), 763.
(121) Huck, L. A.; Buriak, J. M. *Langmuir* **2012**, *28* (47), 16285.
(122) Staebler, D. L.; Wronski, C. R. *Appl. Phys. Lett.* **1977**, *31* (4), 292.
(123) Tiwari, S.; Rana, F.; Hanafi, H.; Hartstein, A.; Crabbé, E. F.; Chan, K. *Appl. Phys. Lett.* **1996**, *68* (10), 1377.
(124) Gresback, R.; Kramer, N. J.; Ding, Y.; Chen, T.; Kortshagen, U. R.; Nozaki, T. *ACS Nano* **2014**, *8* (6), 5650.
(125) Soreni-Harari, M.; Yaacobi-Gross, N.; Steiner, D.; Aharoni, A.; Banin, U.; Millo, O.; Tessler, N. *Nano Lett.* **2008**, *8* (2), 678.
(126) Wolf, O.; Dasog, M.; Yang, Z.; Balberg, I.; Veinot, J. G. C.; Millo, O. *Nano Lett.* **2013**, *13* (6), 2516.
(127) Dunitz, J. D.; Orgel, L. E. *Nature* **1953**, *171* (4342), 121.

(128) Kealy, T. J.; Pauson, P. L. *Nature* **1951**, *168* (4285), 1039.
(129) Ito, N.; Saji, T.; Aoyagui, S. *J. Organomet. Chem.* **1983**, *247* (3), 301.
(130) Chidsey, C. E. D.; Bertozzi, C. R.; Putvinski, T. M.; Mujsce, A. M. *J. Am. Chem. Soc.* **1990**, *112* (11), 4301.
(131) Smalley, J. F.; Feldberg, S. W.; Chidsey, C. E. D.; Linford, M. R.; Newton, M. D.; Liu, Y. P. *J. Phys. Chem.* **1995**, *99* (35), 13141.
(132) Martínez, R.; Ratera, I.; Tárraga, A.; Molina, P.; Veciana, J. *Chem. Commun.* **2006**, No. 36, 3809.
(133) Mulrooney, R. C.; Singh, N.; Kaur, N.; Callan, J. F. *Chem. Commun.* **2009**, No. 6, 686.
(134) Batterjee, S. M.; Marzouk, M. I.; Aazab, M. E.; El-Hashash, M. A. *Appl. Organomet. Chem.* **2003**, *17* (5), 291.
(135) Weber, K.; Hockett, L.; Creager, S. *J. Phys. Chem. B* **1997**, *101* (41), 8286.
(136) Riveros, G.; González, G.; Chornik, B. *J. Braz. Chem. Soc.* **2010**, *21* (1), 25.
(137) Lattimer, J. R. C.; Brunschwig, B. S.; Lewis, N. S.; Gray, H. B. *J. Phys. Chem. C* **2013**, *117* (51), 27012.
(138) Huang, K.; Duclairoir, F.; Pro, T.; Buckley, J.; Marchand, G.; Martinez, E.; Marchon, J.-C.; De Salvo, B.; Delapierre, G.; Vinet, F. *ChemPhysChem* **2009**, *10* (6), 963.
(139) Marrani, A. G.; Dalchiele, E. A.; Zanoni, R.; Decker, F.; Cattaruzza, F.; Bonifazi, D.; Prato, M. *Electrochim. Acta* **2008**, *53* (11), 3903.
(140) Yu, J.; Shapter, J. G.; Johnston, M. R.; Quinton, J. S.; Gooding, J. J. *Electrochim. Acta* **2007**, *52* (21), 6206.
(141) Gagne, R. R.; Koval, C. A.; Lisensky, G. C. *Inorg. Chem.* **1980**, *19* (9), 2854.
(142) Holmes, J. D.; Johnston, K. P.; Doty, R. C.; Korgel, B. A. *Science* **2000**, *287* (5457), 1471.
(143) Cheng, X.; Lowe, S. B.; Ciampi, S.; Magenau, A.; Gaus, K.; Reece, P. J.; Gooding, J. J. *Langmuir* **2014**, *30* (18), 5209.
(144) Dorokhin, D.; Tomczak, N.; Velders, A. H.; Reinhoudt, D. N.; Vancso, G. J. *J. Phys. Chem. C* **2009**, *113* (43), 18676.
(145) Mobarok, M. H.; Buriak, J. M. *Chem. Mater.* **2014**, *26* (15), 4653.
(146) Avramov, P. V; Fedorov, D. G.; Sorokin, P. B.; Chernozatonskii, L. A.; Gordon, M. S. *arXiv Prepr. arXiv0709.2279* **2007**, 1.
(147) Fischer, A. B.; Wrighton, M. S.; Umana, M.; Murray, R. W. *J. Am. Chem. Soc.* **1979**, *101* (13), 3442.
(148) Huck, L. A.; Buriak, J. M. *J. Am. Chem. Soc.* **2012**, *134* (1), 489.
(149) Swart, I.; Liljeroth, P.; Vanmaekelbergh, D. *Chem. Rev.* **2016**, acs.chemrev.5b00678.
(150) Banin, U.; Cao, Y.; Katz, D.; Millo, O. *Nature* **1999**, *400* (6744), 542.
(151) Banin, U.; Millo, O. *Annu. Rev. Phys. Chem.* **2003**, *54* (1), 465.
(152) Park, N.-M.; Kim, T.-S.; Park, S.-J. *Appl. Phys. Lett.* **2001**, *78* (17), 2575.
(153) Michalet, X.; Pinaud, F. F.; Bentolila, L. A.; Tsay, J. M.; Doose, S.; Li, J. J.; Sundaresan, G.; Wu, A. M.; Gambhir, S. S.; Weiss, S. *Science* **2005**, *307* (5709), 538.
(154) Dahan, M.; Laurence, T.; Pinaud, F.; Chemla, D. S.; Alivisatos, A. P.; Sauer, M.; Weiss, S. *Opt. Lett.* **2001**, *26* (11), 825.
(155) Lewinski, N.; Colvin, V.; Drezek, R. *Small* **2008**, *4* (1), 26.
(156) Derfus, A. M.; Chan, W. C. W.; Bhatia, S. N. *Nano Lett.* **2004**, *4* (1), 11.
(157) Zhai, Y.; Dasog, M.; Snitynsky, R. B.; Purkait, T. K.; Aghajamali, M.; Hahn, A. H.; Sturdy, C. B.; Lowary, L.; Veinot, J. G. C. *J. Mater. Chem. B Mater. Biol. Med.* **2014**, *2*

(47), 8427.
(158) Sark, W. van; Frederix, P. *J.* **2001**.
(159) Xu, L.; Huang, X.; Zhu, J.; Chen, H.; Chen, K. *J. Mater. Sci.* **2000**, *35* (6), 1375.
(160) García-Santamaría, F.; Chen, Y.; Vela, J.; Schaller, R. D.; Hollingsworth, J. A.; Klimov, V. I. *Nano Lett.* **2009**, *9* (10), 3482.
(161) Qian, C.; Sun, W.; Wang, L.; Chen, C.; Liao, K.; Wang, W.; Jia, J.; Hatton, B. D.; Casillas, G.; Kurylowicz, M.; Yip, C. M.; Mastronardi, M. L.; Ozin, G. A. *J. Am. Chem. Soc.* **2014**, *136* (45), 15849.
(162) Avila, A.; Montero, I.; Galán, L.; Ripalda, J. M.; Levy, R. *J. Appl. Phys.* **2001**, *89* (1), 212.
(163) Hessel, C. M.; Rasch, M. R.; Hueso, J. L.; Goodfellow, B. W.; Akhavan, V. A.; Puvanakrishnan, P.; Tunnel, J. W.; Korgel, B. A. *Small* **2010**, *6* (18), 2026.
(164) Ledoux, G.; Gong, J.; Huisken, F. *Appl. Phys. Lett.* **2001**, *79* (24), 4028.
(165) Lockwood, R.; McFarlane, S.; Rodríguez Núñez, J. R.; Wang, X. Y.; Veinot, J. G. C.; Meldrum, A. *J. Lumin.* **2011**, *131* (7), 1530.
(166) Mastronardi, M. L.; Chen, K. K.; Liao, K.; Casillas, G.; Ozin, G. A. *J. Phys. Chem. C* **2015**, *119* (1), 826.
(167) van Driel, A. F.; Nikolaev, I. S.; Vergeer, P.; Lodahl, P.; Vanmaekelbergh, D.; Vos, W. L. *Phys. Rev. B* **2007**, *75* (3), 035329.
(168) Nguyen, A.; Gonzalez, C. M.; Sinelnikov, R.; Newman, W.; Sun, S.; Lockwood, R.; C Veinot, J. G.; Meldrum, A. **2016**.
(169) Kanemitsu, Y. *Phys. Rev. B* **1996**, *53* (20), 13515.
(170) Mastronardi, M. L.; Maier-Flaig, F.; Faulkner, D.; Henderson, E. J.; Kübel, C.; Lemmer, U.; Ozin, G. A. **2011**.
(171) Barrelet, C. J.; Robinson, D. B.; Cheng, J.; Hunt, T. P.; Quate, C. F.; Chidsey, C. E. D. *Langmuir* **2001**, *17* (11), 3460.
(172) Riveros, G.; Meneses, S.; Escobar, S.; Garin, C.; Chornik, B. *J. Chil. Chem. Soc.* **2010**, *55* (1), 61.
(173) Zhai, Y.; Dasog, M.; Snitynsky, R. B.; Purkait, T. K.; Aghajamali, M.; Hahn, A. H.; Sturdy, C. B.; Lowary, T. L.; Veinot, J. G. C. *J. Mater. Chem. B* **2014**, *2* (47), 8427.
(174) Wolfe, J. P. *Phys. Today* **1982**, *35* (3), 46.

Appendix I

AI.1 Surface Coverage Determination from NMR for FcD-SiNC

AI.1.1 Theoretical Outline

Theoretical number of surface hydrides $= \frac{mass\ of\ sample}{(\text{Volume SiNC})(\text{density Si})}\frac{\#\ surface\ hydride}{SiNC}$

Total # of nanocrystals in sample= $\frac{mass\ of\ sample}{(\text{Volume SiNC})(\text{density Si})}$

# of Ligands Determined from NMR

moles of TMS in XmL of CdCl3 with 0.03%TMS Std $= \frac{(Volume\ Std\ used)\left(\frac{0.03}{100}\right)(density\ TMS)}{\text{MW}_{TMS}}$

TMS H in sample $= (moles\ TMS)NA\left(\frac{12H}{TMS\ molecule}\right)$

ligand Hs in sample $= \#\ TMS\ H\left(\frac{Integrated\ Area\ of\ ligand\ \ H\ in\ NMR}{Integrated\ Area\ \ of\ TMS\ H\ in\ NMR}\right)$

ligands in sample $= \frac{\#\ ligand\ H}{\left(\frac{number\ of\ protons}{ligand\ area\ in\ NMR}\right)}$

of surface ligands per nanocrystals $= \left(\frac{Total\ number\ of\ ligands}{Total\ number\ of\ SiNC}\right)$

Surface Coverage $= \frac{number\ of\ surface\ ligands\ per\ nanocrystal}{theoretical\ number\ of\ surface\ hydrides}$

AI.1.2 Sample Calculation Number of Ligands Determined from NMR

Theoretical Number of surface hydrides $= \frac{4mg}{(\frac{4}{3}\pi 1.4nm^3)(2.328g/cm^3)} \frac{200\ surface\ hydride}{2.8nm\ SiNC}$

$$= 2.99 \times 10^{19}$$

moles of TMS in XmL of CdCl3 with 0.03%TMS Std $= \frac{(Volume\ Std\ used)\left(\frac{0.03}{100}\right)(density\ TMS)}{\mathrm{MW}_{TMS}}$

$$= \frac{(0.6mL)\left(\frac{0.03}{100}\right)(0.648g/mL)}{88.23g/mol} = 1.32 \times 10^{-6} mol$$

TMS H in sample $= (moles\ TMS)NA(\frac{12H}{TMS}) = 9.55 \times 10^{18}$Hs

dodecyl Hs in sample $= \#\ TMS\ H\ \left(\frac{Integrated\ area\ of\ ligand\ \ H\ in\ NMR}{Integrated\ area\ \ of\ TMS\ H\ in\ NMR}\right) = 9.55 \times 10^{18}\left(\frac{25}{1}\right)$

$$= 2.39 \times 10^{20}\text{Hs}$$

dodecyl ligands in sample$= \frac{\#\ ligand\ H}{\left(\frac{number\ of\ protons\ integrated}{ligand\ molecule}\right)} = \frac{2.39\times 10^{20}}{\left(\frac{25}{dodecyl\ ligand}\right)}$

$$= 9.55 \times 10^{18} \text{ dodecyl ligands}$$

ferrocenyl Hs in sample $= \#\ TMS\ H\left(\frac{Area\ of\ ligand\ \ H\ in\ NMR}{Area\ \ of\ TMS\ H\ in\ NMR}\right) = 9.55 \times 10^{18}\left(\frac{5}{1}\right)$

$$= 4.78 \times 10^{19} \text{ Hs}$$

#ferrocenyl ligands in sample $= \frac{\#\ ligand\ H}{\left(\frac{number\ of\ protons\ integrated}{ligand\ molecule}\right)} = \frac{9.55\times 10^{18}}{\left(\frac{9}{ferrocenyl\ ligand}\right)}$

$$= 5.31 \times 10^{18} \text{ ferrocenyl ligands}$$

# of surface ligands per nanocrystals $= \left(\frac{Total\ number\ of\ ligands}{Total\ number\ of\ SiNC}\right)$

Total # of nanocrystals in sample= $\frac{4mg}{(\frac{4}{3}\pi 1.4nm^3)(2.328g/cm^3)}$

$$= 1.49 \times 10^{17}\text{SiNC in 4mg sample}$$

# of dodecyl ligands per nanocrystal = $\left(\frac{9.55\times10^{18}\ ligands}{1.49\times10^{17}\ SiNC}\right) = 65$

# of ferrocenyl ligands per nanocrystals $= \left(\frac{5.31\times10^{18}\ ligands}{1.49\times10^{17}\ SiNC}\right) = 34$

Surface Coverage $= \frac{number\ of\ surface\ ligands\ per\ nanocrystal}{theoretical\ number\ of\ surface\ hydride}$

$$= \frac{(9.55 \times 10^{18} + 5.31 \times 10^{18})}{2.99 \times 10^{19}} \times 100 = 50\%$$

AI.2 Surface Coverage Determination by TGA for FcD-SiNC

AI.2.1 Theoretical Outline

Total Weight% (Wt%) Loss = 49.3%

Mole Ratio $\frac{A}{B}$ (calculated from NMR Integration) $= \left(\dfrac{\frac{integratoin\ area\ of\ ligand\ A\ H\ in\ NMR}{number\ of\ protons/ligand\ A}}{\frac{integration\ area\ of\ ligand\ B\ H\ in\ NMR}{number\ of\ protons/ligand\ B}} \right)$

Wt% of ligand$\frac{A}{B} = \frac{WtA}{WtB} = \left(mole\ ratio\ \frac{A}{B} \times \frac{MWA}{MWB} \right)$

$Wt_A + Wt_B = 1$

$Wt_A = Wt_B \frac{WtA}{WtB}$

$Wt_B = \frac{1}{(1 + \frac{WtA}{WtB})}$

$Wt_A = \frac{1}{(1 + \frac{WtA}{WtB})} \frac{WtA}{WtB}$

Wt% Loss of ligand A $= Wt\%\ of\ ligand\ A \times Total\ Wt\%\ Loss$

Wt% Loss of ligand B $= Wt\%\ ligand\ B \times Total\ Wt\%\ Loss$

Mole% of ligand A $= \dfrac{\left(\frac{Wt\%\ lossA}{MWA}\right)}{\left(\frac{Wt\%\ lossA}{MWA} + \frac{Wt\%\ lossB}{MWB} + \frac{100 - Total\ Wt\%loss}{MWSi}\right)} \times 100$

Mole% of ligand B $= \dfrac{\left(\frac{Wt\%\ lossB}{MWB}\right)}{\left(\frac{Wt\%\ lossA}{MWA} + \frac{Wt\%\ lossB}{MWB} + \frac{100 - Total\ Wt\%loss}{MWSi}\right)} \times 100$

Mole% Silicon $= \dfrac{\left(\frac{100 - Total\ Wt\%loss}{MWSi}\right)}{\left(\frac{Wt\%\ lossA}{MWA} + \frac{Wt\%\ lossB}{MWB} + \frac{100 - Total\ Wt\%loss}{MWSi}\right)} \times 100$

$$\# \text{ of ligands per nanocrystals} = \frac{\text{mole \% ligand}}{\text{mole \% Si}} \times \text{number of silicon atoms/ nanocrystal}$$

$$\% \text{ Surface Coverage} = \frac{Total\ number\ of\ ligands}{Number\ of\ surface\ hydrides/nanocrystal} \times 100$$

AI.2.2 Sample Calculation

Wt% of ligand$\frac{F}{D} = \frac{WtF}{WtD} = \left(mole\ ratio\ \frac{F}{D} \times \frac{MW_F}{MW_D}\right) = \left(\frac{\frac{5\ H\ in\ NMR}{9\ H\ per\ ferrrocene}}{\frac{25\ H\ in\ NMR}{25\ H\ per\ dodceyl}}\right) \times \frac{217g/mol}{168g/mol} = 0.718$

$Wt_F + Wt_D = 1$ $\qquad$ $\frac{WtF}{WtD} = 0.718$

$Wt_F = Wt_D\ 0.718$

$Wt_D\ 0.718 + Wt_D = 1$

$Wt_D\ (0.718+1) = 1$

$Wt_D = \frac{1}{(1+0.718)} = 0.582$

$Wt_F = \frac{1}{(1+0.718)} \times 0.718 = \frac{0.718}{(1.718)} = 0.418$

Wt% Loss of ferrocenyl ligand$= 0.418\ \times 49.3\% = 20.6\%$

Wt% Loss of dodecyl ligand$= 0.582 \times 49.3\% = 28.7\%$

Mole% of ferrocenyl ligand $= \frac{\left(\frac{20.6}{217g/mol}\right)}{\left(\frac{20.6}{217g/mol}+\frac{28.7}{168g/mol}+\frac{100-49.3}{28g/mol}\right)} = 0.045\times100 = 4.6\%$

Mole% of dodecyl ligand $= \frac{\left(\frac{28.7}{168g/mol}\right)}{\left(\frac{20.6}{217g/mol}+\frac{28.7}{168g/mol}+\frac{100-49.3}{28g/mol}\right)} = 0.082\times100 = 8.2\%$

Mole% Silicon $= \frac{\left(\frac{100-49.3}{168g/mol}\right)}{\left(\frac{20.6}{217g/mol}+\frac{28.7}{168g/mol}+\frac{100-49.3}{28g/mol}\right)}\times100 = 0.872\times100 = 87.2\%$

# of ferrocenyl ligands per nanocrystals $=\frac{4.6\%}{87.2\%} \times 600 = 32$ ferrocenyl ligands/nanocrystal

# of dodecyl ligands per nanocrystals $=\frac{8.2\%}{87.2\%} \times 600 = 57$ dodecyl ligands/nanocrystal

% Surface Coverage $= \frac{32+57}{200} \times 100 = 44\%$

Appendix II

AII.1 Photobleaching Wavelength Shifts

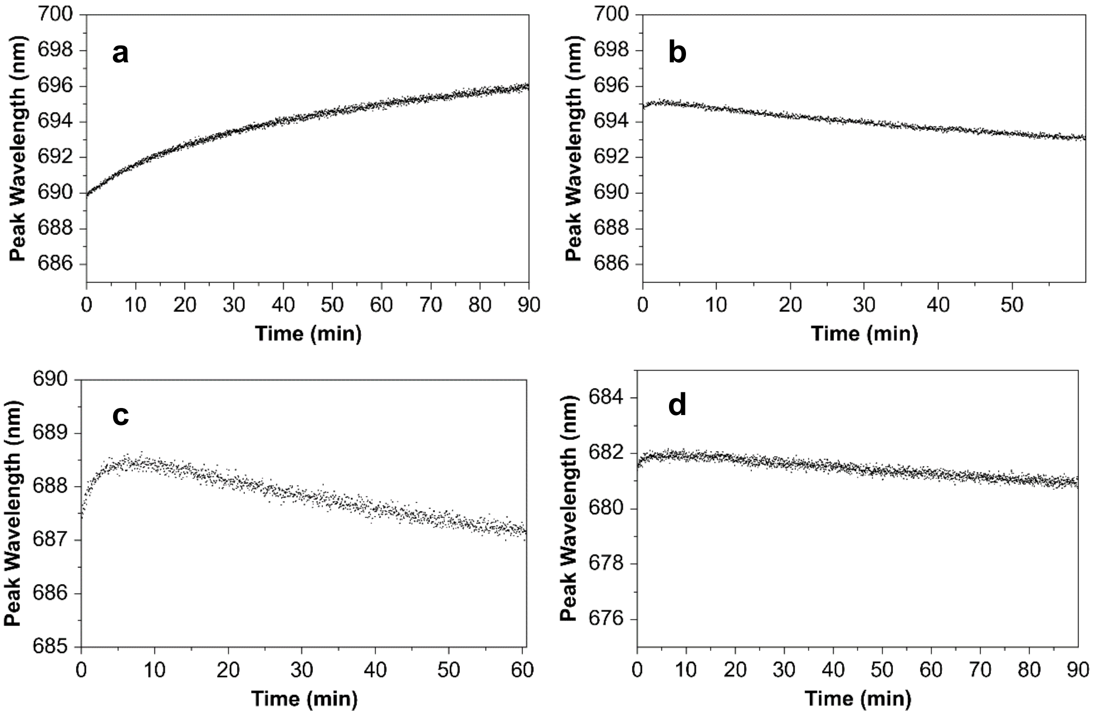

Fig AII.1 Wavelength peak shifts for SiNC-D1 in (a) air and (b), (c) and (d) vacuum.

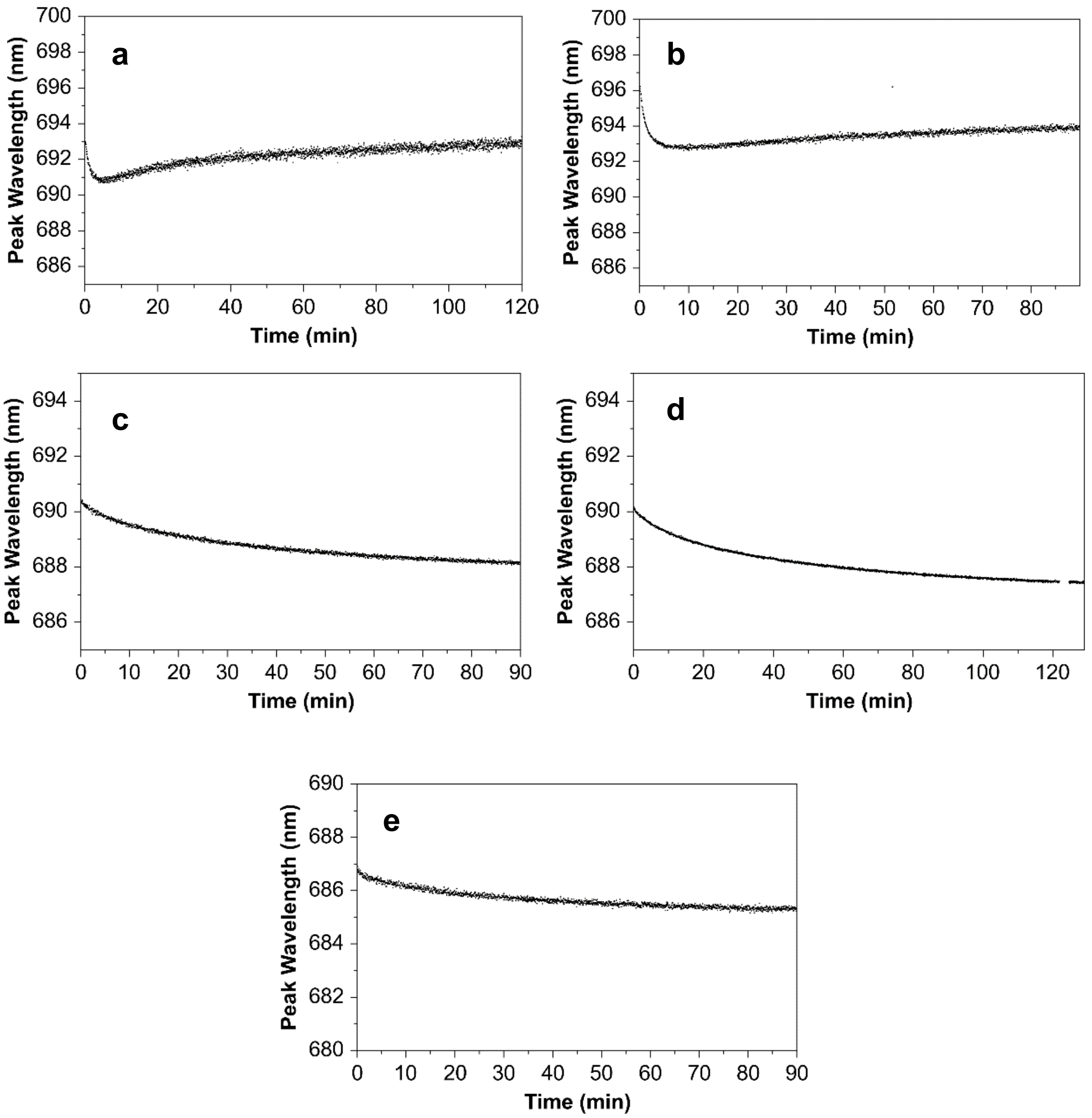

Fig AII.2 Wavelength peak shifts for SiNC-D2 in (a) and (b) air and (c), (d) and (e) vacuum.

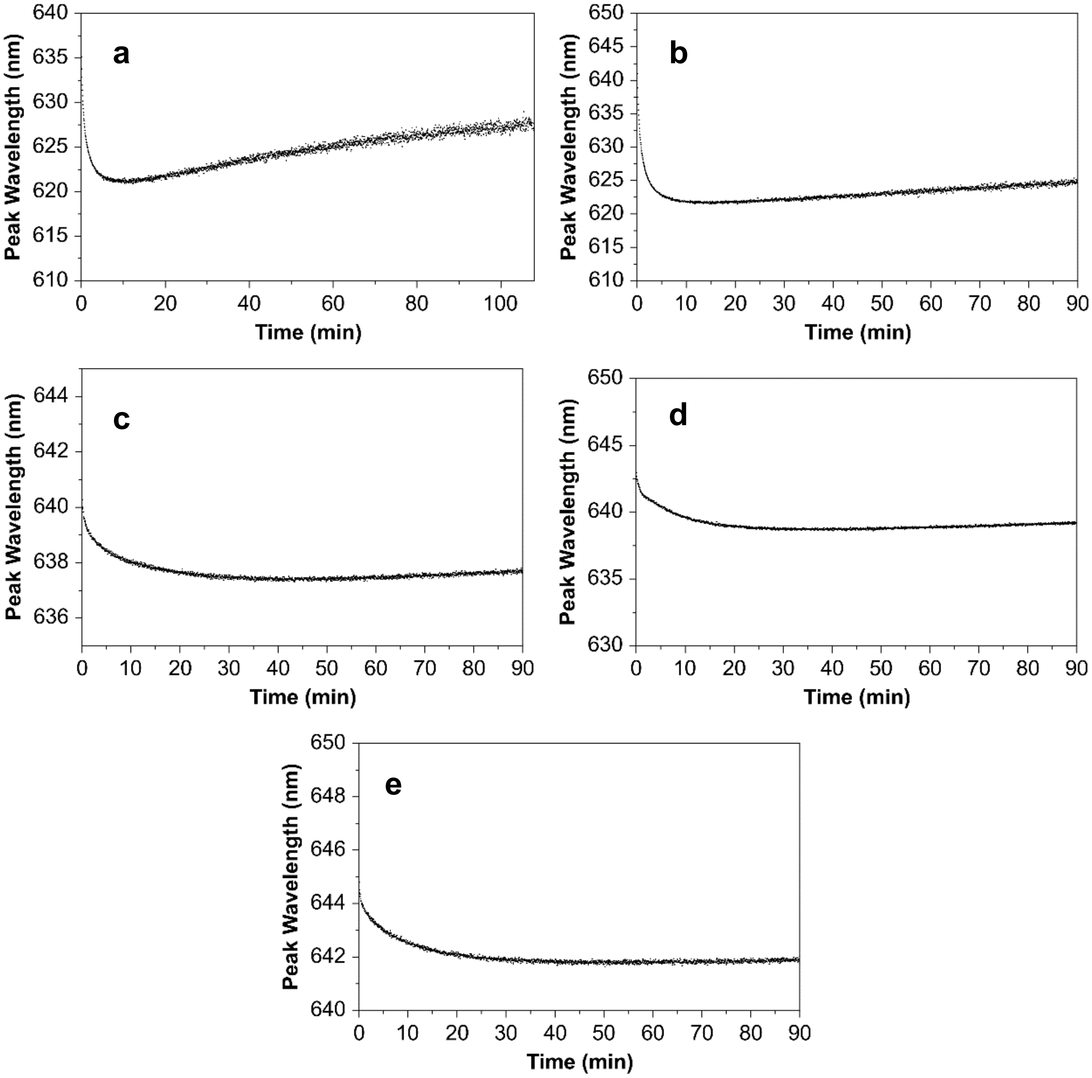

Fig AII.3 Wavelength peak shifts for SiNC-D3 in (a) and (b) air and (c), (d) and (e) vacuum.

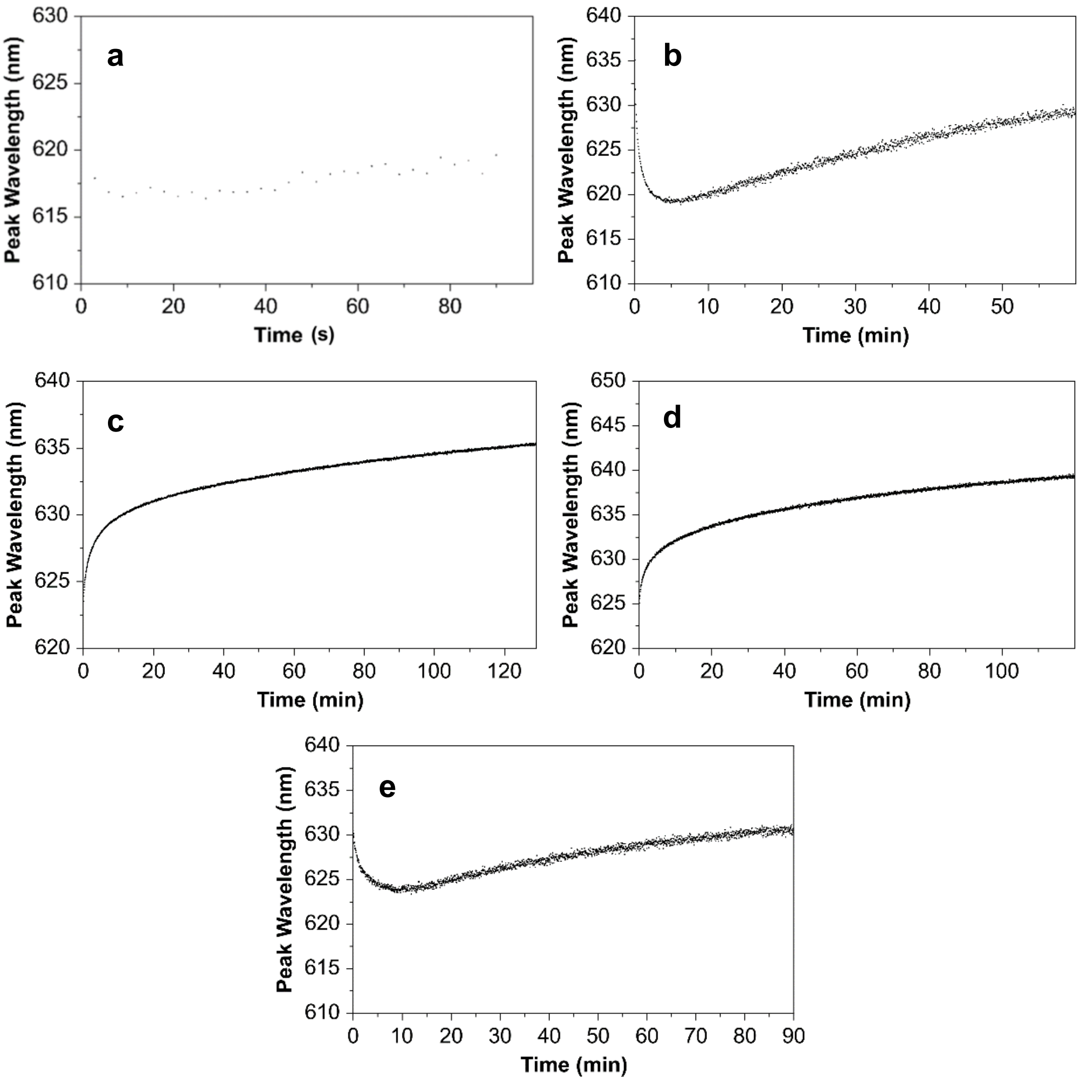

Fig AII.4 Wavelength peak shifts for SiNC-A in (a) and (b) air and (c), (d) and (e) vacuum. The first air measurement was recorded for only 3 minutes. The results of the measurement were included in the analysis.

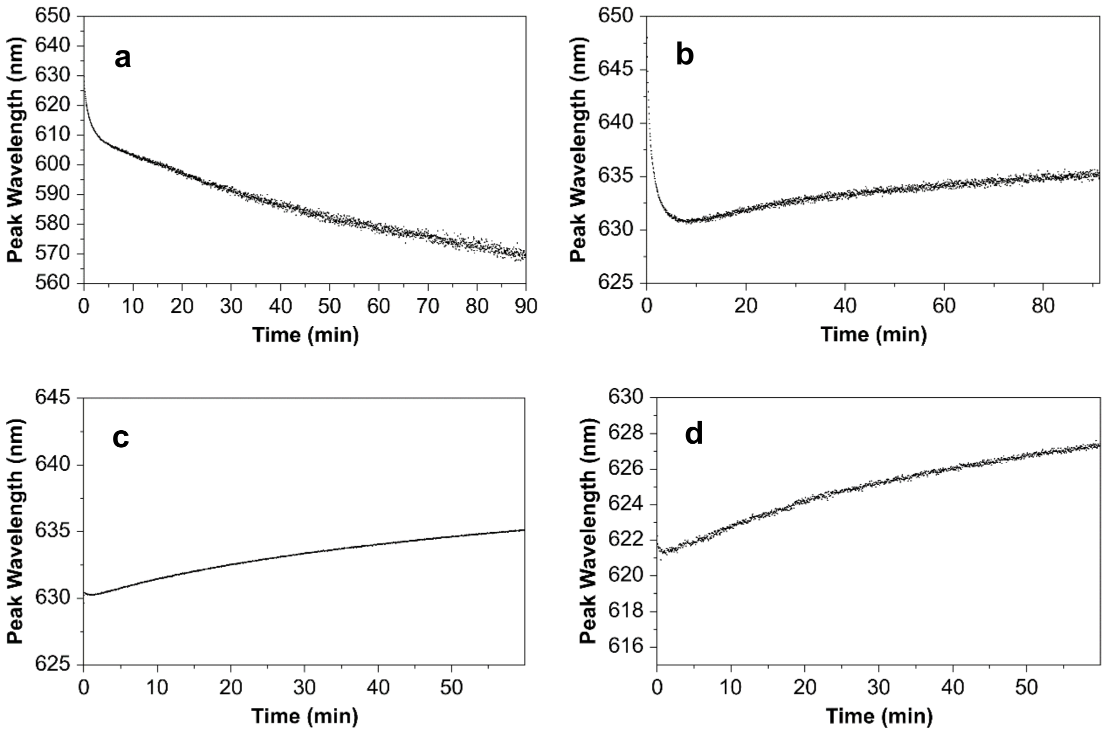

Fig AII.5 Wavelength peak shift for SiNC-B in (a) and (b) air and (c) and (d) vacuum.

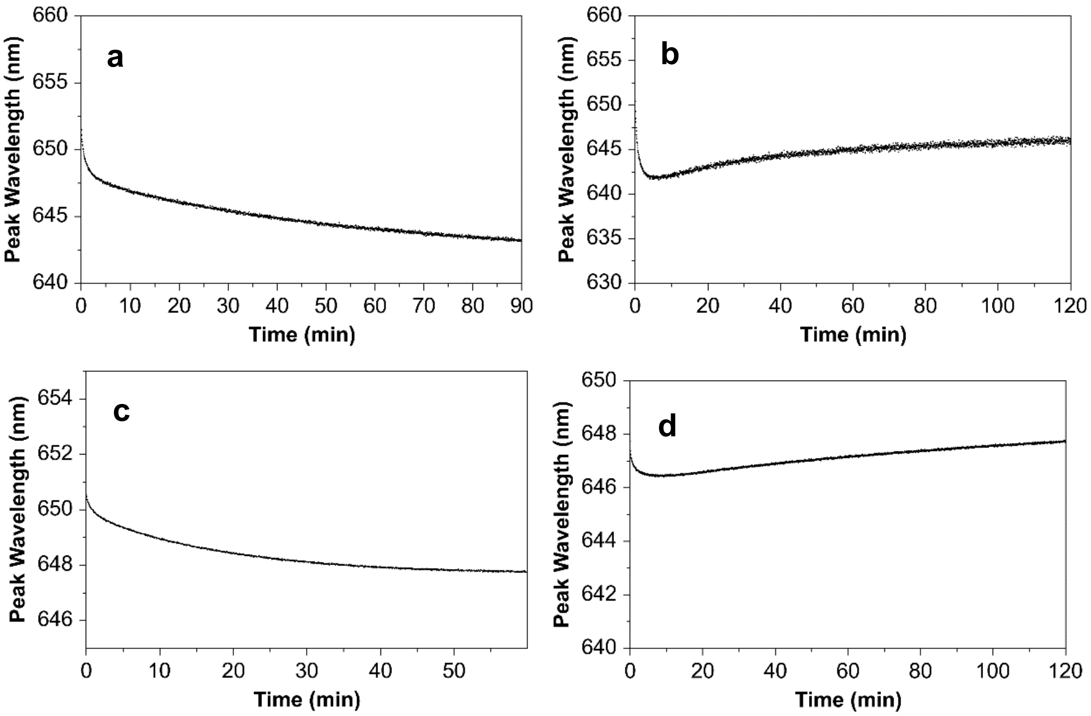

Fig AII.6 Wavelength peak shift for SiNC-C in (a) and (b) air and (c) and (d) vacuum.

AII.2 Photobleaching Intensity Profiles

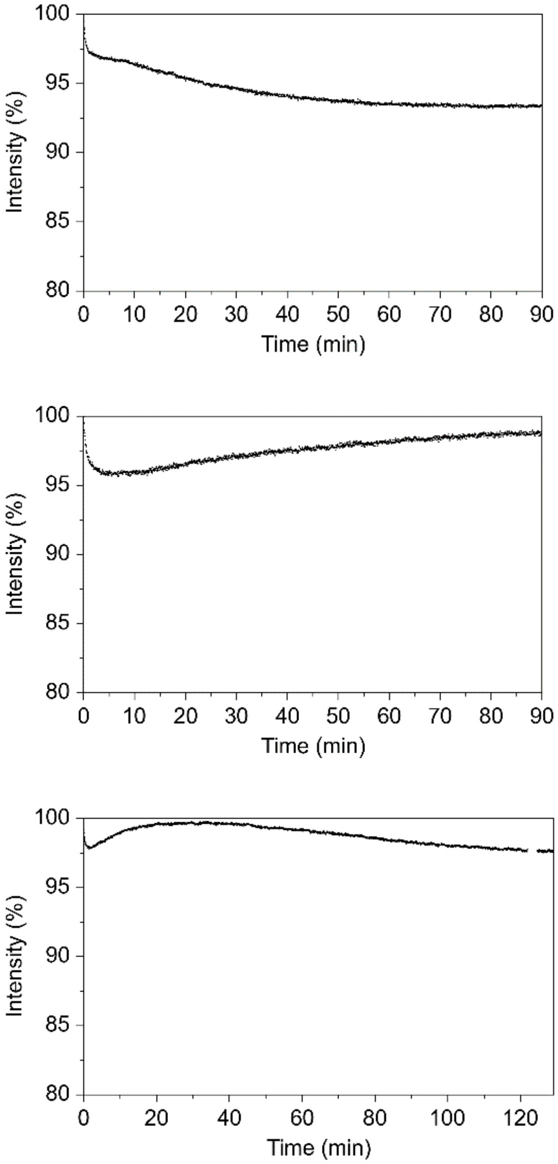

Fig AII.7 Photobleaching intensity profiles of SiNC-D2 in vacuum.